MEASUREMENT OF THE REACTION $\bar{\pi}p \to \bar{\pi}\bar{\pi}^{+}n$ AT 17.2 GeV USING A TRANSVERSELY POLARIZED TARGET

JGH DE GROOT

UNIVERSITEIT VAN AMSTERDAM
ZEEMAN LABORATORIUM

MEASUREMENT OF THE REACTION $\pi^- p \to \pi^- \pi^+ n$ AT 17.2 GeV USING A TRANSVERSELY POLARIZED TARGET

ACADEMISCH PROEFSCHRIFT

ter verkrijging van de graad van doctor in de wiskunde en natuurwetenschappen aan de Universiteit van Amsterdam, op gezag van de Rector Magnificus Dr. G. den Boef, hoogleraar in de faculteit der wiskunde en natuurwetenschappen, in het openbaar te verdedigen in de aula der Universiteit (tijdelijk in de Lutherse Kerk, ingang Singel 411, hoek Spui) op woensdag 19 april 1978, des namiddags om 13.30 uur

door

Johannes Gerardus Hendrikus de Groot
geboren te Waalwijk

promotor : Prof. Dr. A.G. Tenner
copromotor : Dr. G. Lutz
coreferent : Dr. W. Hoogland

The work described in this thesis has been performed at CERN, the European Organization for Nuclear Research. The author was supported by the joint research programs of the "Stichting voor Fundamenteel Onderzoek der Materie" (FOM) and the "Nederlandse Organizatie voor Zuiver Wetenschappelijk Onderzoek" (ZWO).

aan mijn ouders
and to Rose

MEASUREMENT OF THE REACTION $\pi^- p \to \pi^- \pi^+ n$ AT 17.2 GeV USING A TRANSVERSELY POLARIZED TARGET

Contents:

CHAPTER I INTRODUCTION

In this thesis, the measurement and analysis are described of the reaction

$$\pi^- p \to \pi^- \pi^+ n \qquad \text{--- I-1}$$

at 17.2 GeV beam momentum, using a transversely polarized target. The experiment was the last in a series of measurements performed with the CERN-Munich(MPI) spectrometer, which has been in operation at the CERN PS from 1970 to 1975. The spectrometer was designed to study quasi two-body processes at low momentum transfer to the final state nucleon. At various beam momenta, the following reactions have been studied[1,2,3,4,5]:

$$\pi^- p \to \pi^- \pi^+ n$$

$$\pi^+ p \to \pi^+ \pi^+ n$$

$$\pi^- p \to K^+ K^- n$$

$$\pi^- p \to p \bar{p} n$$

$$\pi^- p \to K^- K^0 n$$

The main interest of these reactions is the study of the low momentum transfer production of $\pi\pi$, $K\bar{K}$ and $p\bar{p}$ states. Therefore, no lower limit was imposed by the apparatus on the momentum transfer to the nucleon, i.e. no attempt was made to detect the recoil nucleon.

In the first section of this chapter the physics interest in the reaction I-1 is discussed. In section I-2, a brief review is given, based on an earlier measurment by the same group, of the previous knowledge about the reaction I-1. It is stressed that all $\pi\pi$ phase shift analyses which were based on measurements of the reaction I-1 relied to a certain extent on model dependent assumptions. In chapter V it will be shown that, when a transversely polarized target is used, a model independent amplitude analysis becomes possible. In section 3 of this chapter, the kinematical variables which will be used throughout this work are defined. The quantum numbers of the virtual particles which can be exchanged in the reacion I-1 are determined. In the fourth and last section of this chapter a brief outline is given of the analysis.

I-1 Physics Interest

Measurements of the reaction

$$\pi^- p \rightarrow \pi^- \pi^+ n$$

and some other processes like for instance

$$\pi^+ p \rightarrow \pi^- \pi^+ \Delta^{++}$$

have long been a source of information on the $\pi\pi$ interaction. Direct measurements of the $\pi\pi$ and $K\pi$ interactions are at present impossible because of the non-availability of meson targets. The $\pi\pi$ interaction, however, is of considerable theoretical interest, since it constitutes the simplest hadronic interaction of two spinless particles.

Following a technique which was originally proposed by Goebel[6] and later developed by Chew and Low[7] it is possible to extract information on the $\pi\pi$ interaction from a measurement of the reaction I-1. This information becomes available in the form of the $\pi^+\pi^-$ angular distribution which can be represented by means of the $\pi\pi$ phase shifts. At low values of the momentum transfer squared t (definitions of kinematical variables are given in section I-3) it is usual to view the production process of the reaction I-1 in terms of a one particle exchange model[8]. For the reaction I-1 it is known[1] that at low t and at 17 GeV beam momentum, the dominant contribution to the cross section is One Pion Exchange (OPE). This is drawn symbolically in the following diagram:

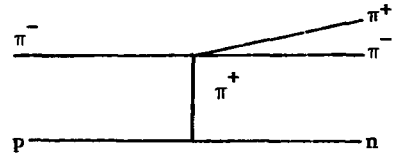

In the Chew and Low formalism (commonly referred to as Chew-Low extrapolation) the invariant four momentum transfer squared t is identified with the square of the mass of the virtual pion which is exchanged between the two vertices in the above diagram (the exchanged pion is said to be off-shell). In order to determine the on-shell $\pi^+\pi^-$ angular distribution, the measured angular distribution of the $\pi^+\pi^-$ must be extrapolated to the unphysical value of t where t equals the square of the pion mass. If OPE is not the only contributing process, this procedure will lead to a

distortion of the resulting angular distribution. The OPE signal must therefore be isolated from the background prior to extrapolation.

The physics interest in the reaction I-1 lies mainly in the possibility to study the $\pi\pi$ interaction. In order to be able to use the Chew-Low formalism, the production mechanism of the reaction I-1 has to be studied in some detail. Quite apart from this, the study of the production mechanism is interesting in itself. A measurement of the reaction I-1 at fixed beam momentum allows the study of its production mechanism as a function of t for different $\pi^+\pi^-$ mass states.

I-2 Previous Knowledge

Reaction I-1 has been the subject of study of many experiments during past years. Several high statistics experiments have led to a good understanding of the production mechanism, and $\pi\pi$ phase shifts up to a $\pi^+\pi^-$ invariant mass of 1.8 GeV have been determined based on these measurements[9]. One of these experiments will be discussed here briefly. We do so for two reasons, firstly to sketch what was previously known about reaction I-1 and secondly because the present work is a logical extension of that experiment.

The experiment[1] was carried out in 1970-1971 by the CERN-Munich(MPI) collaboration using essentially the same spectrometer as the one used for the present experiment. A sample of 300,000 events of the reaction I-1 was recorded at an incident momentum of 17.2 GeV using an (unpolarized) liquid hydrogen target. The $\pi^+\pi^-$ angular distribution as a function of invariant mass and momentum transfer was measured. From the analysis of the t dependence of the $\pi^+\pi^-$ angular distribution it was concluded that at low t OPE dominates the reaction, while at higher values of t, A_2 exchange is the dominant contribution[1]. But apart from pion and A_2 exchange, other effects contribute. In the t-channel $\pi^+\pi^-$ rest frame (Gottfried Jackson frame) OPE couples only to dipion states with helicity $m = 0$. As a consequence, no t-channel states with $m \neq 0$ should be observed for pure OPE. Significant evidence was found however for t-channel $m \neq 0$ states down to the lowest values of t. This was explained successfully in terms of P.K. Williams' "Poor Man's Absorption Model"[10]. In an absorption model[11], the reaction is thought to occur in three stages as pictured by the following diagram:

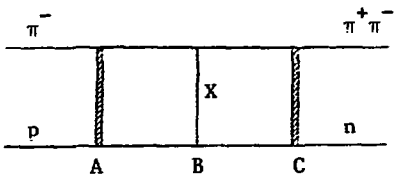

At A the incident particles interact, distorting the incident waves. At B an interaction takes place involving the exchange of the virtual particle X. Finally the outgoing $\pi^+\pi^-$ system and the neutron interact, thereby distorting the outgoing waves. While the details of the interactions A and C are not known, the assumption can be made that these interactions have a simple diffraction behaviour. The data of this previous experiment are generally well described in terms of a model which includes pion and A_2 exchange when absorption effects are taken into account.

Once the production mechanism of the reaction I-1 has been established, the next step in the analysis is an attempt to extract information on the $\pi\pi$ interaction, i.e. a determination of the $\pi\pi$ phase shifts. For this purpose many analyses have been carried out by various authors[12]. In all these analyses model dependent assumptions have to be made at some stage. This is perhaps most clearly demonstrated by an analysis which was performed by Estabrooks and Martin[13]. They proposed a method to determine the production amplitudes in the $\pi^+\pi^-$ inavriant mass region of the ρ meson. As will be described in chapter V, 8 (complex) amplitudes can contribute to the reaction I-1 in the rho region. A measurement of the reaction I-1 with a hydrogen target however yields 6 independently measured quantities. In order to arrive at a soluble set of equations, Estabrooks and Martin made the assumption that the exchange with the quantum numbers of the A_1 does not contribute to the reaction. Other analyses involved even more restrictive assumptions, but the basic problem remains that the number of independently measured quantities is insufficient to perform a model independent analysis.

The only way to obtain substantially more information on the reaction I-1 is to do a measurement of the reaction using a polarized target. In chapter V (Amplitude Analysis) it will be proved that, when the measurement is done using a transversely polarized target, a model independent amplitude

analysis of the reaction I-1 is possible. The motivation for the present experiment is the study of the production mechanism of the reaction I-1 in a model independent way and thus to test the validity of the assumptions which have been made in previous phase shift analyses.

The terms "model independent" and "model dependent" need perhaps some clarification. We will call an analysis model dependent if it involves restrictive physical assumptions about the reaction (like for instance the assumption on the A_1 exchange amplitudes). In this sense the proposed amplitude analysis is model independent, as no assumptions are made about the behaviour of the amplitudes.

I-3 Definitions, Quantum Numbers of the Exchanged Particle

The kinematics of the reaction I-1 is completely determined by the knowledge of the four momenta of the five reacting particles, i.e. 20 quantities. At fixed beam momentum, with the target proton at rest and all reacting particles identified, there are only five independent kinematical quantities left. These five variables are conveniently chosen to be the following (the q_i denote the four momenta):

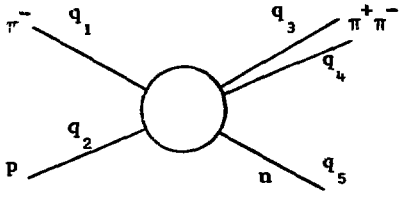

1 $m_{\pi\pi}$, The invariant mass of the $\pi^+\pi^-$ system

$$m^2_{\pi\pi} = (q_3 + q_4)^2$$

We will use the metric $q^2 = q_0^2 - |\vec{q}|^2$

2 t, The four momentum transfer to the nucleon squared

$$t = (q_5 - q_2)^2 = (q_3 + q_4 - q_1)^2$$

Using the metric defined above, t is negative in the physical region.

3,4 θ,ϕ The polar angles of the π^- in the $\pi^+\pi^-$ rest frame.
The polar angles θ and ϕ of the negative pion are defined in the rest frame of the pion pair. For the $\pi^+\pi^-$ rest frame, either the t-channel or the s-channel helicity frame is used (the latter is shown in fig. I-1).

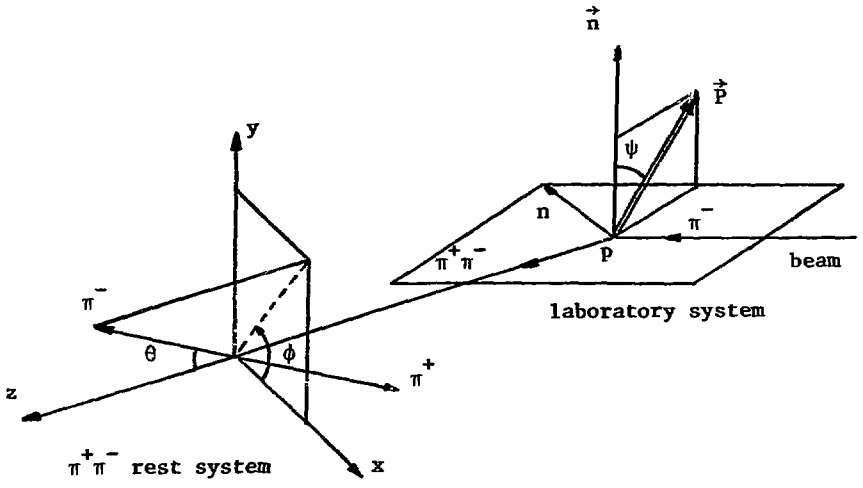

Fig. I-1 Laboratory System and $\pi^+\pi^-$ Rest Frame

In case of the s-channel helicity frame, the z-axis points in the negative neutron direction. For the t-channel helicity frame ("Gottfried Jackson frame") the z-axis is along the direction of the incident π^-. In both cases, the y-axis is parallel to the normal to the production plane (fig. I-1). The s- and t-channel helicity frames are related by a rotation around the y-axis over an angle ω, the Wigner rotation angle (see fig. I-2)

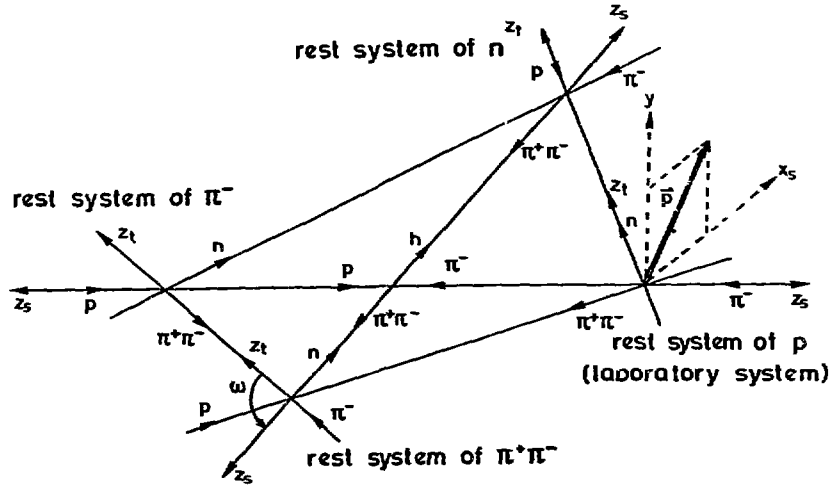

fig. I-2 s- and t-channel helicity frames

5 ψ, the polarization angle.

ψ is defined (fig. I-1) as the angle between the normal to the production plane and the polarization vector $\vec{P}$. When the measurement is performed using an (unpolarized) hydrogen target, the angle ψ is redundant because of rotational symmetry around the beam direction. By the conditions imposed by the apparatus, the polarization vector $\vec{P}$ was perpendicular to the beam direction. The polarization vector $\vec{P}$ lies therefore in the x-y plane if the s-channel helicity frame is used for the proton, which means that in the s-channel frame for the proton helicity $\vec{P}$ has no longitudinal polarization component. This is no longer true in the t-channel proton rest frame, where the z-axis is along the direction of the outgoing neutron. The different s- and t-channel reference frames are drawn schematically in fig. I-2.

As mentioned in section I-1, it is usual to describe processes of the type studied here, where production occurs at small momentum transfer, in terms of a one particle exchange model. It is therefore useful to determine the quantum numbers of the particles which can be exchanged in the reaction I-1. Before we do so we observe that the quantum numbers of the $\pi^+\pi^-$ system are restricted by G-parity, parity and angular momentum conservation. G-parity conservation requires the G-parity of the dipion to be positive. The spin and parity of the $\pi^+\pi^-$ system are restricted to natural spin-parity (i.e. $J^P = 0^+, 1^-, 2^+$ etc.). The only well-known objects with mass below 2 GeV which are allowed as $\pi^+\pi^-$ resonances are ρ, f and g.

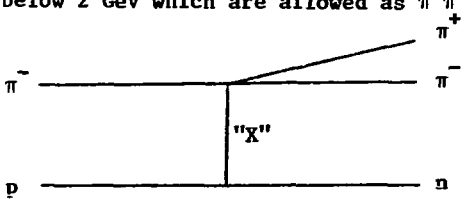

The assignment of the quantum numbers of the exchanged particle ("X") follows from conservation laws applied at both vertices in the above diagram. Because the analysis of the rho region will be the main subject of this thesis, we will restrict ourselves to the case where only dipion S and P waves contribute. Obviously $B = S = 0$ and $Q = +1$. From isospin conservation at the lower vertex it follows that the isospin of X is 0 or 1. Since the secondary pions have both negative G-parity, the G-parity of the X is also negative. From angular momentum and parity conservation

applied at the meson vertex, it follows that, when the dipion system is in an S-wave state only unnatural parity (i.e. $0^-,1^+,2^-$ etc.) can be exchanged[14]. When the dipion system is in a P-wave state, both natural and unnatural parity can be exchanged. For the latter case it follows that the m = 0 P-wave can only be produced by unnatural parity exchange, while the m = ±1 can be formed by both natural and unnatural parity exchange. The objects with the lowest mass which can be exchanged in the reaction I-1 are therefore π,A_1 and A_2[15]. Both the π and A_1 have unnatural, the A_2 natural parity. We will not enter the discussion whether the A_1 is established as a true resonance or not. We will refer to "exchange with the quantum numbers of the A_1" as A_1 exchange in this work.

From conservation laws applied at the baryon vertex it follows that in the t-channel reference frame for the nucleon helicities, pion exchange leads to nucleon spin flip, while A_1exchange gives t-channel nucleon spin noflip. The crossing matrix for the unnatural parity exchange amplitudes transforms t-channel flip in s-channel noflip (also noflip →flip), except for a very small interval in t close to t_{min}[9]). The latter can be understood by recalling that at t_{min} the s- and t-channel reference frames are identical (see fig. I-2). The application of the conservation laws at the baryon vertex furthermore leads to the conclusion that A_2 exchange can give nucleon spin flip and noflip in both the s- and t-channel reference frames.

I-4 Outline of the Analysis

The identification of all reacting particles in the reaction I-1 and the measurement of the momenta and trajectories of the beam particle and the two secondary pions, allows the determination of the kinematical quantities $m_{\pi\pi}$,t,θ,ϕ and ψ. The measurement therefore consists essentially of a measurement of the mass- and t-dependence of the $\pi^+\pi^-$ angular distribution. Because of the finite range of the strong interaction, the amplitudes which describe the reaction can be expanded in a series of spherical harmonic functions $Y_\ell^m(\cos\theta,\phi)$ with a limited number of terms. The $\pi^+\pi^-$ decay angular distribution can then also be expanded in a series of spherical harmonic functions. It is convenient to present the experimental results in the form of the mass- and t-dependence of the coefficients

in the latter expansion. These coefficients are commonly called the spherical harmonic moments of the $\pi^+\pi^-$ decay angular distribution. From a measurement with a hydrogen target one obtains the mass- and t-dependence of a set of moments $\langle \mathrm{Re}Y_\ell^m(\cos\theta,\phi)\rangle$, where ℓ equals twice the highest spin contribution and $0 \leq m \leq \ell$. With a transversely polarized target however, extra independent information is obtained in the form of the two sets of moments $\langle \mathrm{Re}Y_\ell^m(\cos\theta,\phi)\cos\psi\rangle$ and $\langle \mathrm{Im}Y_\ell^m(\cos\theta,\phi)\sin\psi\rangle$. For the case of S- and P-wave contributions, i.e. rho production, one obtains 15 moments from a measurement with a polarized target, whereas a measurement using a hydrogen target yields only 6 moments.

The outline of the analysis is therefore as follows. After geometrical reconstruction and the kinematic fit (described in chapter III) the quantities $m_{\pi\pi}, t, \theta, \phi$ and ψ are determined. The moments of the $\pi^+\pi^-$ angular distribution are calculated, taking into account the limited geometrical acceptance of the spectrometer. The method of acceptance correction (a generalization of the method of moments[1]) is described in some detail in chapter IV. In chapter V a set of relations is derived between the amplitudes and the moments. Based on these relations an amplitude analysis is carried out to determine, in a model independent way, the amplitudes which contribute to the reaction I-1.

REFERENCES (Chapter I)

1) G.Grayer, B.Hyams, C.Jones, P.Schlein, P.Weilhammer, W.Blum, H.Dietl, W.Koch, E.Lorenz, G.Lütjens, W.Männer, J.Meissburger, W.Ochs and U.Stierlin, Nucl. Physics B75, (1974) 189.

2) G.Hentschel, Ph.D. Thesis, University of Munich.
MPI report, MPI-PAE/Exp.EL.56. September 1976.
and
H.Becker, W.Blum, V.Chabaud, H.Dietl, G.Grayer, G.Hentschel, B.Hyams, C.Jones, E.Lorenz, G.Lütjens, G.Lutz, W.Männer, J.Meissburger, D.Notz, R.Richter, K.Rybicki, U.Stierlin and P.Weilhammer: Paper submitted to the 18th Int. Conf. on High Energy Physics, Tbilisi 1976.

3) J.Meissburger, Ph.D. Thesis, University of Munich.
MPI report, MPI-PAE/Exp.EL.48. September 1974.
and
B.Hyams, C.Jones, P.Weilhammer, W.Blum, H.Dietl, G.Grayer, W.Koch, E.Lorenz, G.Lütjens, W.Männer, J.Meissburger and U.Stierlin, Nucl. Physics B73, (1973) 202.

4) W.Hoogland, S.Peters, G.Grayer, B.Hyams, P.Weilhammer, W.Blum, H.Dietl, G.Hentschel, W.Koch, E.Lorenz, G.Lütjens, G.Lutz, W.Männer, R.Richter and U.Stierlin, Nucl. Physics B126, (1977) 109.

5) G.Grayer, B.Hyams, C.Jones, P.Schlein, W.Blum, H.Dietl, W.Koch, H.Lippmann, E.Lorenz, G.Lütjens, W.Männer, J.Meissburger, U.Stierlin and P.Weilhammer, Phys. Letters 34B, (1971) 333.

6) F.J. Dyson, Phys. Rev. 99, (1955) 1037.

7) C.J. Goebel, Phys. Rev. Letters 1, (1958) 337.

8) G.F. Chew and F.E. Low, Phys. Rev. 113, (1959) 1640.

9) B.R. Martin, D.Morgan and G.Shaw, "Pion Pion Interaction in Particle Physics", Academic Press, New York, 1976.
and
J.L. Petersen:"The $\pi\pi$ Interaction", CERN Yellow Report, 77-04.

10) P.K. Williams, Phys. Rev. D1, (1970) 1312
and
G.C. Fox, Proc. Cal. Tech. Conference on Phenomenology in Particle Physics, Pasadena, (1971).

11) K.Gottfried and J.D. Jackson, Nuovo Cim. 34, (1974) 735.

12) W.Ochs: Die Bestimmung von $\pi\pi$ Streuphasen auf der Grundlage einer Amplitudenanalyse der Reaktion $\pi^- p \to \pi^-\pi^+ n$ bei 17 GeV/c Primärimpuls, Ph.D. Thesis, University of Munich, 1973.
and
B.Hyams, C.Jones, P.Weilhammer, W.Blum, H.Dietl, G.Grayer, W.Koch, E.Lorenz, G.Lütjens, W.Männer, J.Meissburger, W.Ochs and U.Stierlin, Nucl. Physics B100, (1975) 205.
and
P.Estabrooks and A.D. Martin, $\pi\pi$ Partial Waves from 0.6 to 1.8 GeV, University of Durham Preprint.
See also refs. 1 and 9.

13) P.Estabrooks and A.D. Martin, Phys. Letters 41B, (1972) 350
and
P.Estabrooks, A.D. Martin, G.Grayer, B. Hyams, C.Jones, P.Weilhammer, W.Blum, H.Dietl, W.Koch, E.Lorenz, G.Lütjens, W.Männer, J.Meissburger and U.Stierlin, Int. Conf. on $\pi\pi$ Scattering and Associated Topics, Tallahassee, 1973. (eds. P.K. Williams and V.Hagopian) AIP Conf. Proc. 13 New York, (1973) p.37.

14) N. Schmitz, CERN Yellow Report 65-24 Vol. I.

15) Particle Data Group: "Review of Particle Properties" 1976.

CHAPTER II THE APPARATUS

II-a The Spectrometer

In this chapter we describe briefly the CERN-Munich(MPI) spectrometer, in particular as it was modified for use with a Polarized Target. In its previous application to experiments with a hydrogen target, the spectrometer has been reported on elsewhere[1,2,3].

A schematic top view of the experimental setup is shown in fig.II-1. The beam is incident from the left. The beam pions are identified by the threshold Cerenkov counter C_1, before entering the beam spectrometer. The beam spectrometer consists of two 2 m CERN standard bending magnets (M in fig.II-1), and two packs of wire spark chambers which measured the beam direction before and after deflection.

The charged secondary particles, produced in the polarized target are momentum analysed using the spectrometer magnet (AEG), and two sets of wire spark chambers before and after the magnet. The particles are identified by two large Cerenkov hodoscopes C_2 and C_3.

In the following text, the sets of spark chambers will be referred to as Arm I to V, as shown in fig.II-1.

In the following sections, the different elements of the spectrometer are described in more detail.

II-a-1 The Beam

The experiment was carried out in the p_{14} beam in the East Experimental Hall of the CERN Proton Synchrotron. This unseparated beam was set to negative polarity and was tuned to a momentum of 17.2 GeV. Some typical beam parameters are given in table II-1. It must be noted however, that these parameters are taken from one particular experimental period. The experiment was carried out during several periods of typically 2-3 weeks. Between different periods ("runs") the parameters of the beam varied slightly.

The useful dimensions of the beam were limited by the scintillation counter B_4, a counter with an 18 mm circular hole in it.

Since the beam was unseparated, it contained not only pions, but also kaons, antiprotons, muons and electrons. The kaon and antiproton content of the beam would give rise to unwanted background reactions,

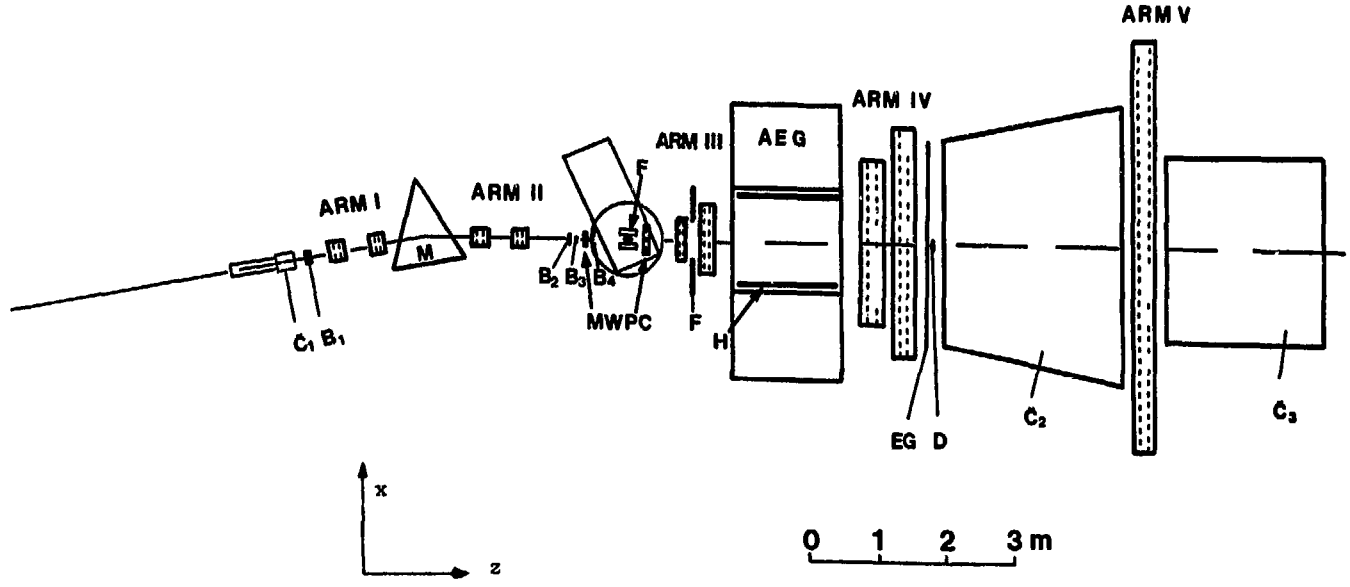

Fig. II-1 Top view of the CERN-Munich(MPI) Spectrometer.

therefore kaons and antiprotons were filtered out using signals of a CERN standard threshold Cerenkov counter. In practice two such counters were put in the beam, the second was not used in the trigger described hereafter, but its signals were recorded on magnetic tape and were used later in the off line analysis.

PS burst length	350 ms.
Production angle	5 mrad
Momentum	17.2 GeV
Spot size at target x	3.9 mm
y	3.7 mm
Beam divergence x	1.4 mrad
at target y	1.8 mrad
Total negative particles per PS burst	100,000
Negative pions through B_4 hole	60,000
Antiproton contents	0.04%
Kaon content	0.60%
Muon content	2.40%
Electron content	< 0.40%

Table II-1. Parameters of the p_{14} Beam

II-a-2 The Spark Chambers

The spark chambers used in this experiment were wire spark chambers with magnetostrictive readout. The chambers were designed and built by the Max Planck Institut für Physik und Astrophysik in Munich[4]).

The high voltage pulses to the chambers were obtained by discharging a set of condensers over spark gaps[5]). The signals from the magnetostrictive readout lines were preamplified and fed into a 30 MHz S.E.N. Spadac digitizer via zero-crossing discriminators[6]).

The spatial resolution of the chambers, as measured with beam tracks traversing the whole spectrometer, amounted to an average of 0.3 mm.

Table II-2 gives some of the characteristics of the spark chambers used in this experiment.

	number of chambers	sensitive area (cm)	gap width (mm)	wire orientation
Arm I and II	16	25 × 25	8	0^o,90^o, $\pm 45^o$
Arm III-a	6	45 × 75	10	0^o,90^o, $\pm 45^o$
Arm III-b	6	45 × 110	10	0^o, $\pm 30^o$
Arm IV-a	6	90 × 260	10	0^o, $\pm 30^o$
Arm IV-b	6	90 × 360	10	0^o, $\pm 30^o$

Table II-2. Characteristics of the Spark Chambers

The very large arm V chambers (fig.II-1) were not essential for the part of the experiment described in this thesis. They were built for K^+K^- and $p\bar{p}$ final states. The K^+K^- and $p\bar{p}$ final states have to be separated using the signals of the second large Cerenkov counter hodoscope. The arm V chambers were used to determine if one of the secondary particles had an interaction or decay in the first Cerenkov counter.

Not counting the arm V chambers, a total of 40 chambers, i.e. 80 active planes was used. This is more than the minimum needed for track reconstruction; it provided the necessary redundancy in case of chamber inefficiency.

II-a-3 The Multiwire Proportional Chambers

In front of the target four small multiwire proportional chambers were used, these chambers had a sensitive area of 64 × 64 mm^2 and 1 mm wire pitch. The chambers were used to extend the lever arm of the second arm of the beam spectrometer towards the target, thus improving the accuracy of the measured beam momentum and the trajectory of the beam particle near the target. Two chambers had horizontal, the other two had vertical wires. The multiwire proportional chambers are labelled MWPC in fig.II-1.

Behind the target, inside the field of the target magnet, a proportional chamber was placed, consisting of two planes of vertical wires. The purpose of this chamber was to get a measurement of the trajectories of the outgoing particles as close to the vertex as possible. This is

important in this experiment where, since the vertex is in a magnetic field, the accuracy of the vertex enters into the determination of the angles at the vertex.

Proportional chambers were used instead of spark chambers because of the magnetic field of the target magnet. Because of the small memory time of proportional chambers, these chambers were also useful eliminating extra beam tracks in the off-line analysis.

During part of the experiment two large (1.02×0.4 m^2) proportional chambers were used as trigger chambers. The chambers were placed between the target and the spark chambers of arm III. From the two chambers a multiplicity signal was derived which was used to veto any event with only one track in arm III. Triggers with only one track were mainly caused by beam tracks with an interaction behind the target. This rate was about 30% of the total trigger rate; it was reduced to practically zero after the introduction of the multiplicity veto. The loss of good events under this scheme was less than 0.1%[8].

All multiwire proportional chambers including the readout electronics, were designed and built by the Max Planck Institut für Physik und Astrophysik in Munich[7].

II-a-4 The Veto Counters

The missing mass resolution of the spectrometer at 17.2 GeV beam momentum ($\sigma MM^2 = 0.180$ GeV^2) is insufficient to select a clean sample of the reaction I-1. In order to reduce the background below the neutron peak, events with additional particles in the final state had to be efficiently vetoed.

For this purpose, the target was completely surrounded by veto counters, except for two openings for the beam and secondary particles emerging from the target. A sketch of the layout of the veto counters around the target is given in fig.II-2.

The counter system around the target consisted of two sets. The inner counters F1-6, were single 1 mm scintillation counters, sensitive to charged particles. The outer counters F7-12 consisted of 5 layers of 1 mm scintillation material interleaved with 5 layers of 3.3 mm tungsten;

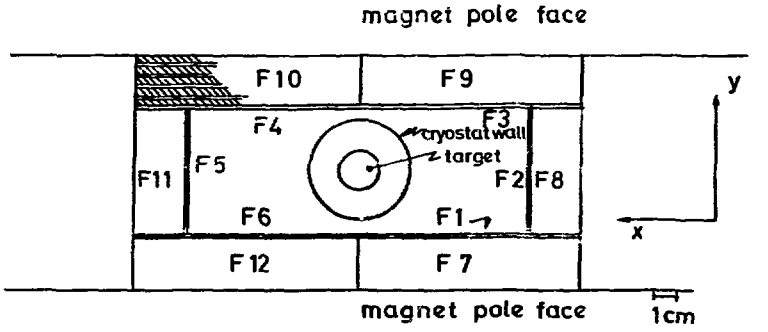

fig.II-2a Anticounter arrangement (looking downstream)

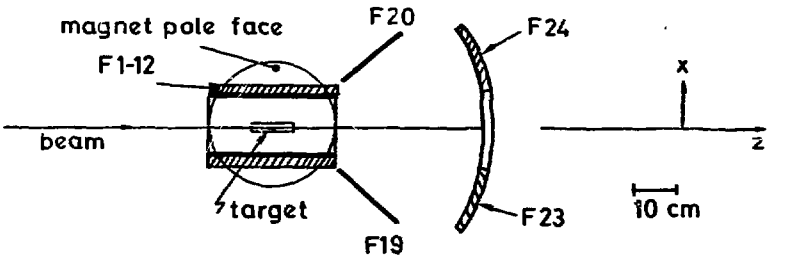

fig.II-2b Top view of anticounter system

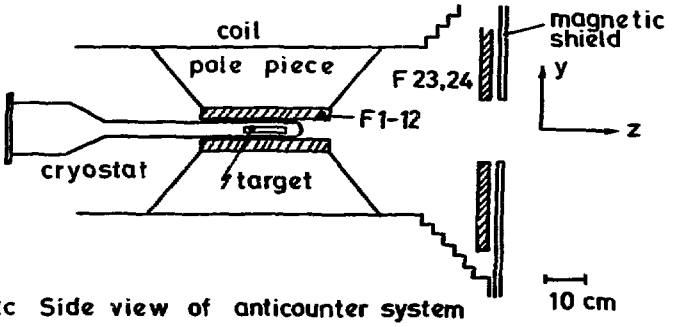

fig.II-2c Side view of anticounter system

the counters were sensitive to gamma rays mainly coming from neutral pions. Behind the target, inside the field of the target magnet, two counters (F19 and F20) were placed to detect low energy charged particles, swept out by the magnetic field.

Further downstream, two counter windows, F23-24 (fig. II-2) and F14-17 (fig.II-1) were placed to veto particles outside the geometrical acceptance of the spectrometer. Both windows consisted of lead scintillator sandwiches: the first was mounted on the target magnet, the second was placed between the arm III spark chambers.

II-a-5 The Spectrometer Magnet

The analysing magnet for the secondary particles (AEG) had a gap of 110 × 150 × 50 cm^3 (length × width × height). The dimensions of the magnet gap, together with the target position essentially determine the angular acceptance of the spectrometer. The main vertical component of the magnetic field strength was 15.01 kGauss in the centre of the magnet, the field integral $\int B\, d\ell$ 20 kG.m. The three components of the magnetic field strength have been measured at 30,000 points in the magnet gap with an accuracy of 0.3% of the main component[9]).

The magnetostrictive readout wires of the spark chambers (arms III and IV) were shielded from the stray field of the magnet. This also resulted in a better homogeneity of the magnetic field.

The gap of the magnet was lined with veto counters (H-counters, see fig.II-1), which vetoed neutral and charged particles going into the magnet yoke and pole faces.

II-a-6 The Cerenkov Hodoscopes

For indentification of the secondary particles, two large atmospheric pressure Cerenkov hodoscopes were used (fig.II-3). Both counters were placed at the downstream end of the spectrometer, as shown in fig. II-1. The first counter, used to separate $\pi^+\pi^-$ events from K^+K^- and $p\bar{p}$ final states, consisted of 14 separate cells[10]). The counter was filled with CO_2 at atmospheric pressure, giving a theoretical threshold for pions of 4.7 GeV, (kaons 16.7 GeV and protons 30 GeV). The second Cerenkov, used to separate K^+K^- from $p\bar{p}$ final states, consisted of 8 separate cells and was filled with neopentane at atmospheric pressure.

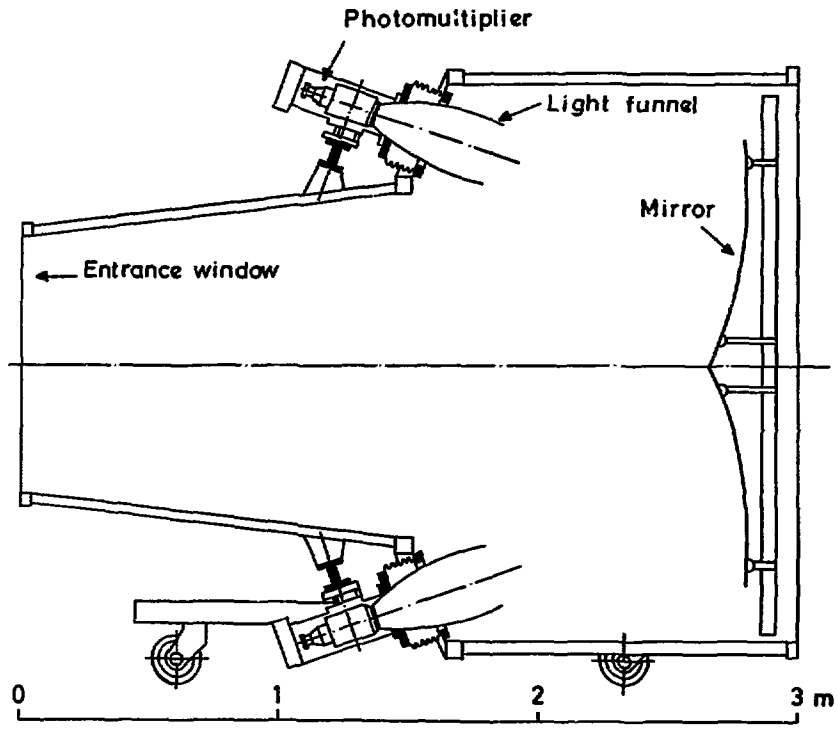

Fig. II-3 Vertical Section through the Large Gas Cerenkov Hodoscope.

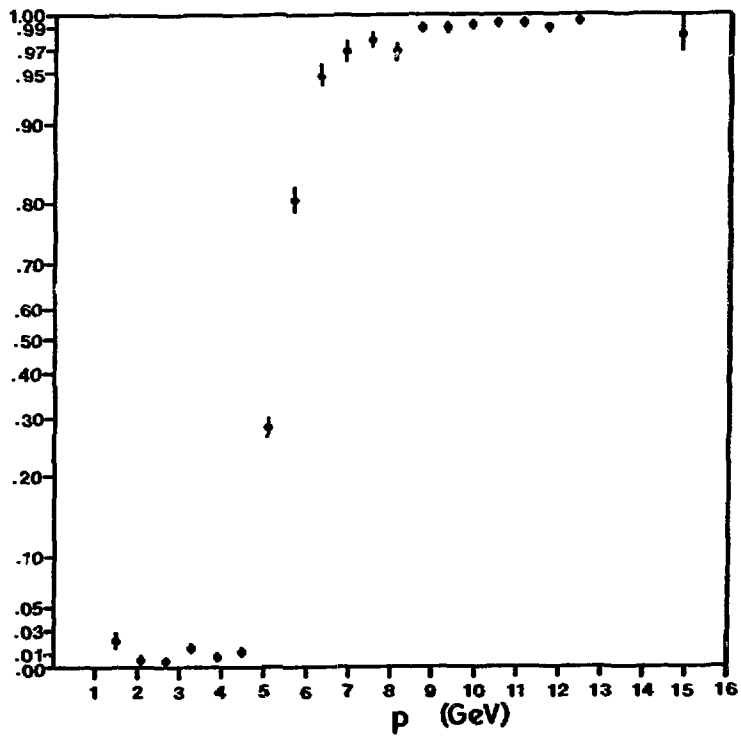

Fig II-4 Cerenkov Efficiency for Pions.

The criterion to distinguish $\pi^+\pi^-$ events from K^+K^- and $p\bar{p}$ final states was the requirement that at least one of the secondary particles fire the first Cerenkov. The signals from the two large Cerenkovs were not used in the trigger condition. The separation of the $\pi^+\pi^-$, K^+K^- and $p\bar{p}$ final states was, therefore done during the off-line analysis.

Fig.II-4 shows the efficiency of the first large Cerenkov hodoscope for pions. As can be deduced from this graph, the probability that at least one of the two secondary pions is seen by the Cerenkov is over 99%. The efficiency of the counter has been determined as described in ref.[10].

II-a-7 The Trigger Condition

Many processes can simulate a two prong event, in particular beam tracks plus delta rays, and 3π final states. An efficient trigger scheme had to be designed to suppress such background processes. In order to satisfy the trigger condition for two prong events, the following conditions had to be fulfilled: (see fig. II-5 for a simplified diagram of the trigger logic)

1. Negative pion into the target.
   Signals were required from the beam Cerenkov C_1, and the beam defining counters B_1, B_2 and B_3, with no signal from the counter B_4. The scintillation counter B_4 defined the useful dimensions of the beam at the target position.

2. Interaction.
   A signal was demanded from the I-counter, a scintillation counter placed between the arm III chambers. This counter had a hole at the beam position, thus a signal from it implied the passage of at least one non-beam particle.

3. No Veto.
   No signal was allowed from any of the veto counters surrounding the target, the counter windows or the counters lining the gap of the spectrometer magnet.

4. Two-prong Topology.
   Two hits were required in the EG array. The EG array consisted of a set of 32 10 cm wide scintillation counters; the EG array was placed between the arm IV chambers and the first Cerenkov counter, (fig.II-1).

5. No Beam Particle after the Target.

A large fraction of all "events" satisfying the conditions 1-4 consists of beam particles accompanied by one or more delta electrons produced along its path. The D-counter is a small scintillation counter, about the size of the beam, placed in the path of the beam just behind the EG array (fig.II-1). Any event having a hit in the D-counter was vetoed.

The trigger condition as described above, did not include the signals of the Cerenkov hodoscopes C_2 and C_3. Therefore, not only events of the reaction I-1 were obtained, but also K^+K^-n and $\bar{p}pn$ final states. During the experiment parallel triggers were used for the following reactions:

$$\pi^- p_\uparrow \rightarrow K^- K^0 p$$

$$\pi^- p_\uparrow \rightarrow \pi^- \pi^- \pi^+ p$$

An independent trigger channel was constructed to record elastic events.

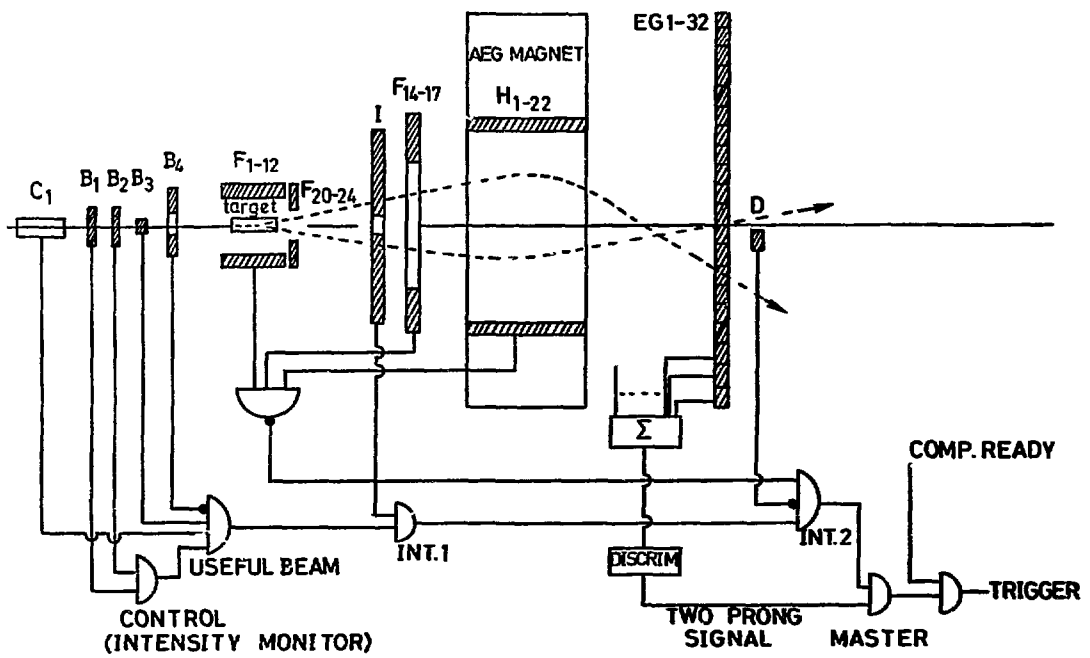

Fig.II-5 PRINCIPLE OF TRIGGER LOGIC

II-a-8 Computer Monitoring

The experiment was monitored by an on-line DEC PDP-9 computer. The data from the spark chambers were read via a SEN Spadac digitizer together with coincidence patterns and counter flags, while the pulse heights of some counters were read via CAMAC electronics. All relevant information was written onto magnetic tape for off-line analysis. While not busy with data acquisition or transmission, the on-line computer was able to do a geometrical reconstruction of a small fraction of the recorded triggers. The result of this reconstruction was displayed on an on-line storage oscilloscope. This proved to be a powerful tool in monitoring the performance of the spectrometer.

II-b The Polarized Target

In this chapter the polarized target is described. The target, together with all electronics and cryogenics has been designed and built by the CERN Polarized Target Group. In the first section, some aspects of the theory of dynamical nuclear orientation are discussed. This will lead to the conclusion that the sign of the target polarization is uniquely determined by the frequency of the microwaves going into the target. The second section briefly describes the NMR technique used to measure the target polarization. The third section describes some details of the polarized target setup. In the last section, the complications arising from the presence of the complex nuclei in the target is mentioned.

II-b-1 Some aspects of the Theory of Dynamical Nuclear Orientation

It is not intended to give here an extensive description of all phenomena contributing to Dynamic Nuclear Orientation. We want rather to point out the principle and refer the reader to refs.[11] and [12] for a thorough treatment.

Consider a system of spins I. When subject to an external magnetic field H, the energy levels split up into 2I+1 magnetic sublevels.
We will restrict ourselves to the case $I = \frac{1}{2}$.
We define the fraction in the state $\langle I_z \rangle = +\frac{1}{2}$ to be n+, the fraction in the state $\langle I_z \rangle = -\frac{1}{2}$ as n-.
Then one can define the polarization P to be

$$P = n+ - n-$$

The difference ΔE in energy between the two magnetic sublevels, is given by $\Delta E = \hbar\omega_L = 2\mu H$, where $\hbar$ is Planck's constant divided by 2π, ω_L the Larmor frequency and μ the magnetic moment of the spin ½ particle. From the Boltzmann distribution, n_+ and n_- satisfy:

$$\frac{n-}{n+} = \exp(-\Delta E/kT)$$

So it follows

$$P = \tanh(\mu H/kT)$$

This expression for the polarization P gives the polarization at thermal equilibrium, and so far no assumption has been made whether the spins I are electronic or nuclear spins.

For free protons, the polarization at thermal equilibrium is much smaller than the polarization for free electrons, since the magnetic moment of the electron is about three orders of magnitude greater than that of the proton. Typically, the value for P_e is 0.99 while P_p is 0.005 at $T = 0.5^oK$ and $H = 25$ kG.

The fact that, under these experimental conditions, the free electrons are almost fully polarized, is the basis of the technique of dynamic nuclear orientation.

Consider a diamagnetic material doped with some paramagnetic impurities, for example ions having an unpaired electron in one of the outer shells. The electrons of the impurities are almost fully polarized at $T = 0.5^oK$ and $H = 25$ kG, so one can attempt to transfer the orientation of the electrons to the free proton by microwave pumping.

To elaborate on this, consider fig.II-6. It shows a graph of the energy levels of interest for a proton-electron pair in a magnetic field. The four energy levels can be written as $|I_e,I_p>$: $|+,+>$, $|+,->$, $|-,+>$ and $|-,->$.
The corresponding energy differences are given as $\hbar\omega_e$ and $\hbar\omega_p$, ω_e and ω_p being the Larmor frequencies for electrons and protons respectively.

At thermal equilibrium, the two lowest levels $|-,->$ and $|-,+>$ will contain almost 100% of the total population since the electronic polarization is nearly 100%, almost equally distributed over the levels $|-,->$ and $|-,+>$ because the proton polarization is practically zero. In order to enhance positive proton polarization, an energy difference $\hbar(\omega_e - \omega_p)$ has to be supplied. The energy $\hbar(\omega_e \pm \omega_p)$ can be supplied by a suitable microwave source.

A steady state of enhanced nuclear polarization is reached due to the favourable ratio between the (long) proton relaxation time and the (short) electron relaxation time.

The effect, described above, has been called "solid effect" and was predicted by Overhauser[16]), and experimentally verified by Abragam and Proctor in 1958 in Li F [13]).

From this description , it follows that the sign of the induced polarization is determined solely by the frequency of the microwaves going into the target. Therefore, when using this technique for a polarized target, the experimental setup can be identical during periods with positive and negative target polarization.

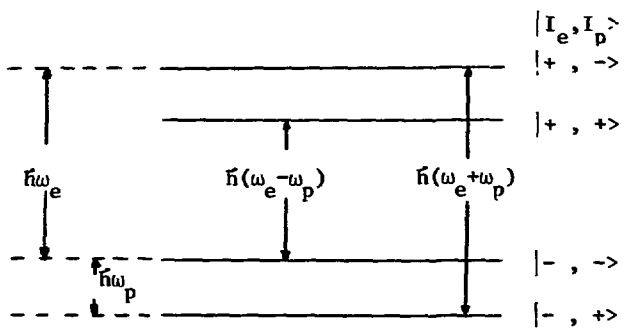

Fig. II-6 Energy levels of a proton-electron pair in a magnetic field.

II-b-2 Measurement of Polarization

The polarization of the target protons is measured by means of a Nuclear Magnetic Resonance (NMR) technique[15]). The relation between the nuclear Larmor frequency ω_L and the external magnetic field strength H_0 is given by $\omega_L = 4.256\ H_0$, where ω_L is in MHz and H_0 in kG.

For our case (H_0 = 25.02 kG) this means ω_L = 106.5 MHz. In order to measure the degree of polarization, a field H_1 is applied perpendicular to the main field H_0, the frequency sweeping between 106.3 and 106.7 MHz. The field H_1 is produced by a coil of a few turns, inside the target container. The degree of polarization of the target is proportional to the absorption of energy (or release) at the resonance frequency, for positive (negative) polarization the energy absorption (release) is measured. These quantities are measured as a change in the complex impedance of the coil as a function of the current I and the frequency ω. The signal is calibrated by the measured polarization at thermal equilibrium (i.e. no microwave power delivered to the target), the latter value can be calculated accurately and amounts to about 0.5% at 0.5°K and 25 kG. The absolute error in the polarization measurement $\left(\frac{\Delta P}{P}\right)$ is estimated to be 5%. During the experiment, the average degree of polarization of the target protons was measured to be 68%.

II-b-3 Experimental Details

As target material, a mixture of 95% 1-butanol and 5% water was used, saturated with the free radical porphyrexide which acted as the paramagnetic impurity. Water was added to increase the solubility of the butanol for porphyrexide. The butabol-water mixture was frozen into 1.5 mm diameter spheres by freezing drops of the mixture in liquid nitrogen using a hypdermic needle. This technique is chosen to secure a large surface to volume ratio which results in efficient cooling, and yields a good pentration of the microwaves.

The operating temperature of the target was 0.5°K. This temperature was obtained in a horizontal ^{3}He crystat with a ^{4}He precooling stage[14]).

The magnet was a conventional iron-core electromagnet with 11 cm gap width and 30 cm diameter pole faces. The field in the central region was 25.02 kG. For the operation of the target it is necessary that the homogeneity of the field is about $3 \cdot 10^{-4}$ over the target volume. To achieve this the magnet was "shimmed", i.e. a set of iron rings was screwed on the pole faces of the magnet, giving the desired field homogeneity.

The final alignment of the target was done by taking X-ray photographs. First the target is positioned on the ideal beam line using X-ray photographs. Then the B_4 counter (the counter defining the useful dimensions

of the beam), is positioned on this line using the same technique.

II-b-4 Consequences for the Experiment

A butanol molecule (C_4H_9OH) consists of 10 free protons, 32 bound protons and 32 bound neutrons. The free protons (the only protons which can be polarized) are on the average polarized to a degree of 68%. In the experiment the recoil neutron was not detected, therefore we have no kinematical constraint to separate events produced on bound protons and free protons. As a result of this, our sample of events contains a large fraction ($\simeq$ 67%) of events produced on bound protons.

The aim of the experiment, however, is to do a polarization measurement. In chapter IV (Acceptance Correction) it will be shown that the polarization dependent observables can be extracted from the data without contamination due to the large background from unpolarized protons. The fact however, that events off bound and free protons cannot be separated individually, does have severe consequences for the statistical errors on the polarization dependent observables. Our experiment, with about 1,200,000 recorded events is statistically equivalent to a hypothetical experiment measuring $\simeq$ 60,000 events on a 100% polarized pure proton target. This as compared with the previous hydrogen experiment where 300,000 events were recorded using a hydrogen target.

REFERENCES (Chapter II)

1) G. Grayer, B. Hyams, C. Jones, P. Schlein, P. Weilhammer, W. Blum, H. Dietl, W. Koch, E. Lorenz, G. Lütjens, W. Männer, J. Meissburger, W. Ochs and U. Stierlin, Nucl. Physics B75, (1974) 189.

2) J. Meissburger, Ph.D. thesis Univ. of Munich. MPI report MPI-PAE/Exp. El. 48 1974.

3) G. Hentschel, Ph.D. thesis Univ. of Munich. MPI report MPI-PAE/Exp.El. 56 1976.

4) G. Grayer, B. Hyams, C. Jones, W. Blum, H. Dietl, W. Koch, E. Lorenz, G. Lütjens, W. Männer, J. Meissburger, U. Stierlin and P. Weilhammer, Nucl. Instrum. Methods 99, (1972) 579.

5) L. Hubbeling, The design and construction of a spark gap assembly and associated electronics, CERN yellow report 72-6.

6) H. Utzat and P. Weissbach, "Verstärker und Zero Crosser für magnetostrictive Drahtfunkenkammer". MPI report MPI-PAE/Exp.El. 101.

7) Jahresbericht 1973 des Max Planck Institutes für Physik, MPI report MPI-PAE/Exp.El.35 (1973).

8) H. Becker, J. Gallivan, B. Gottschalk, E. Lorenz, R. Richter, M. Turala, MPI report MPI-PAE/Exp.El. 54 1976.

9) AEG measurement manual, CERN MSC Division April 1970.

10) G. Grayer, B. Hyams, C. Jones, P. Weilhammer, W. Blum, H. Dietl, J. Heisenberg, W. Koch, E. Lorenz, G. Lütjens, W. Männer, J. Meissburger and U. Stierlin, MPI report MPI-PAE/Exp.El.40.

11) W. de Boer, Dynamical Orientation of Nuclei at Low Temperatures, CERN yellow report 74-11.

12) M. Borghini, Mechanisms of Nuclear Dynamic Polarization by Electron-Nucleus Dipolar Coupling in Solids. Proc. of the IInd Int. Conf. on Polarized Targets, Berkeley, 1971.

13) A. Abragam and W.G. Proctor, CR Acad. Sci. B 246, (1958) 2253.

14) J. Vermeulen, ^{3}He Cooled Polarized Targets, Proc. of the Int. Conf. on Instrumentation for High Energy Physics, Dubna, 1970.

15) F. Udo, Some New Features in a Nuclear Magnetic Resonance Detection System for Measuring Poalrization of Highly Polarized Substances, IInd Int. Conf. on Polarized Targets, Berkeley, 1971.

16) A.V. [illegible]

CHAPTER III DATA PROCESSING

In this chapter some aspects of the off-line processing of the experimental data are described. In the first section the geometrical reconstruction is described. In the second section the selection according to Cerenkov information and the kinematic fit are briefly described. In the next section we describe in some detail a number of topology dependent corrections which were applied to the data. In section 4 the results of a Monte Carlo resolution study are presented. In the final section the efficiency of the event reconstruction is discussed.

III-1 Geometrical Reconstruction

During the experiment, some 1300 7 track 800 bpi magnetic tapes were written, comprising about 20 000 000 triggers. The first step in the analysis is the reconstruction of events with two charged particles of opposite charge in the final state. This task was performed by the geometrical reconstruction program TWOPOL, written in FORTRAN.

All spark chambers were in field-free regions, the program therefore searches for straight tracks in all arms of the spectrometer. The momentum of the beam particle is determined from the deflection angle between the two arms of the beam spectrometer. Next, the tracks of all charged secondary particles before the spectrometer magnet are matched with all tracks behind the magnet, and for each succesful combination the momentum is calculated. The algorithm[1]) which is used to compute the momenta makes use of a parametrization of the magnetic field. The field of the magnet is approximated by a "hard edge" homogeneous field with "thin lenses" at each end to account for the fringe field. The $\int B\,d\ell$ as function of the x and y coordinates is approximated by a simple polynomial in x and y. This model of the magnetic field was obtained by extensive comparison with Runge Kutta calculations of particle trajectories using the measured field map.

With the trajectories and momenta of all charged particles known at this stage, these tracks can be extrapolated towards the centre of the target magnet. The target itself is in the homogeneous region of the magnetic field, so the trajectories can be represented by helices near the target. The algorithm used to track the particles through the

non-homogeneous region of the field makes use of the measured field map of the target magnet. The extrapolation of the secondary particle trajectories towards the target is facilitated by the measurement close to the target of these trajectories by the proportional chambers.

Once the trajectories of the charged particles in the homogeneous region of the target magnet field are determined, the coordinates of the vertex are fitted. Only those events with two secondary particles of opposite charge, giving a satisfactory vertex fit, are accepted as being genuine two-prong events.

The reconstruction of the events was carried out using the IBM 360/91 computer of the Max Planck Institut für Plasmaphysik in Garching. This machine needed about 40 ms. CP time per trigger ($\simeq$ 20 ms. on the CDC 7600 computer), giving a total of more than 200 hours CP time on the IBM 360/91.

III-2 Selection, Kinematic Fit

The events which are accepted by the reconstruction program as being genuine two-prong events contain not only events of the type $\pi^- p \to \pi^-\pi^+ n$, but also $K^+K^- n$ and $p\bar{p}n$ final states.

The events are classified as belonging to one of the three groups using the information of the two large Cerenkov hodoscopes (C_2 and C_3 in fig.II-1). For the $\pi^-\pi^+ n$ final states the selection criterion was that at least one of the secondary particles should be detected by the first large Cerenkov hodoscope. As was already stated in Chapter II, the probability that at least one of the secondary pions is detected by the Cerenkov is at least 99% over the whole range of possible momenta.

At this point, the sample contains events where the beam particle and both charged secondary particles are identified as pions and their momenta are measured. Since the target proton is at rest, the four-vector of the recoil particle (or particles) can be calculated from energy and momentum conservation. In this experiment however, all events having a recoil system other than a neutron are suppressed by the veto counters. The mass of the recoil system is therefore known to be the neutron mass, which means that a one-constraint fit can be done to improve on the measured momenta.

After this kinematic fit the kinematic quantities $m_{\pi\pi}$, t, $\cos\theta$, ϕ and ψ are calculated. Before the events are written to an output tape, a number of corrections are applied to the data.

III-3 Geometry Dependent Corrections to the Data

Apart from the fact that only events with two charged secondary particles in a limited solid angle are accepted, the trigger condition has some more deficiencies. Some good two-prong events are lost for various reasons. Two classes of losses can be distinguished: topology dependent and topology independent losses. An example of a topology independent loss is inefficiency of the beam spark chambers. Obviously, this inefficiency is not correlated with $m_{\pi\pi}$, t or the angles θ, ϕ and ψ which are used to describe the events, therefore it only matters for cross section calculations. Losses however, which are correlated with these variables, result in a distortion of the intensity distribution, and need to be corrected for.

There is no outstanding reason why these corrections have not been included in the acceptance correction which is described in the next chapter. It is merely a matter of convenience since, in order to do the geometry dependent corrections, some calibration data had to be analysed. Including all geometry dependent losses in the acceptance correction would mean that the Monte Carlo calculations for the acceptance correction could only be done after the analysis of the calibration data. The following geometry dependent corrections have been applied to the data.

a) Neutron Loss

The recoil neutron in reaction I-1 has a certain probability of having an interaction in the veto counters surrounding the target. Obviously, this probability depends on the neutron momentum, and is therefore correlated with the four-momentum transfer squared t. An interaction of the neutron in one of of the counters (mainly elastic scattering in the t-range of interest) can cause the counter to fire, which vetoes the event. In order to determine the probability that the neutron fires the anticounter system, some special calibration data have been analysed: events were recorded with the condition that exactly one of the outer veto counters surrounding the target was required to fire. These events contain

genuine events of the type $\pi^- p \to \pi^- \pi^+ n$ plus events of the type $\pi^- p \to \pi^- \pi^+ n\pi^0$.. After selection of events with a missing neutron, the neutron lab momentum is calculated. From this the counter which was hit by the neutron is determined and compared with the counter that actually fired. Therefore it is possible to calculate the probability as a function of t of the neutron to fire the counter system. Let p(t) be the probability per mm of counter traversed that the neutron fires the counter. Then every accepted event is given a weight factor:

$$w_n = \frac{1}{1 - p \cdot d}$$

where d is the pathlength of the neutron in the counter.
The calibration data for the neutron loss had to be taken using the hydrogen target. Since most of the target protons in the butanol target are bound in complex nuclei, it would be impossible to calcualte the neutron direction accurately due to the Fermi motion of the bound protons if the butanol target were used. The average weight factor was 1.14.

b) Delta Ray Loss

Some good events are lost because a delta electron, produced in or near the target, triggers one of the inner veto counters. The number of delta electrons produced in the target depends on the pathlength of the beam particle and the secondary particles in the target, and therefore on the z coordinate of the vertex.

The production of delta rays has been studied using calibration data: beam tracks traversing the whole spectrometer while one of the inner veto counters was allowed to fire. From these data, the probability P_0 for beam tracks that no delta electron is detected can be determined. We assume a Poisson distribution:

$$P_n = \frac{\bar{n}^n e^{-\bar{n}}}{n!}$$

for the number of detected delta electrons. Using this formula the average number of detected delta rays per unit path length in the target $\bar{n}$ can be determined.

Let the pathlength of the beam and secondary particles in the target be L. Then the probability that no delta electron is detected is $e^{-\bar{n}\cdot L}$ which means a weight factor

$$w_d = e^{\bar{n}\cdot L}$$

is given to each accepted event. The average weight factor which was applied was 1.16.

c) Secondary Interactions

The probability that an outgoing particle has a secondary interaction in the target is proportional to the total cross section σ_{tot} in butanol, and the pathlength L of the particle in the target. Since the total cross section of pions in butanol is not known accurately, calculated values for the cross sections on carbon from ref.[2]) have been used.

The interaction probabilities P_{π^+} and P_{π^-} of the positive and negative pion respectively are proportional to the total cross section and the pathlength L in the target material:

$$P_{\pi^+} \propto \sigma^{tot}_{\pi^+} \cdot L_{\pi^+}$$
$$P_{\pi^-} \propto \sigma^{tot}_{\pi^-} \cdot L_{\pi^-}$$

Therefore a weight factor

$$w_s = \frac{1}{(1 - P_{\pi^+})(1 - P_{\pi^-})}$$

was applied to every accepted event; the average weight factor was 1.05.

d) Decay in Flight of Pions

Pions, decaying inside the spectrometer cause the loss of a small fraction of events. The loss occurs partly at the trigger level, but mainly at the level of the geometrical reconstruction, when the reconstruction program fails to accept the event as a good twoprong. Some Monte Carlo studies have been performed to determine the average path L of the secondary pions inside the spectrometer before which a pion decay causes a failure of the reconstruction program. The fractions n^+ and n^- of positive and negative pions respectively, not decaying before L are:

$$n^+ = e^{\frac{-L}{\gamma_+ c\, \tau_+}} \qquad n^- = e^{\frac{-L}{\gamma_- c\, \tau_-}}$$

where $\gamma_\pm$ is the Lorentz contraction factor and τ the pion lifetime. A weight factor

$$w_d = \frac{1}{n^+ \cdot n^-}$$

was therefore applied to each accepted event. The average weight factor

III-4 Resolution of the Spectrometer

The resolution of the spectrometer has been determined using the following procedure. At discrete values of the $\pi^+\pi^-$ invariant mass m and the four momentum transfer squared t, events are generated using the standard Monte Carlo program (for a description of this program see the next chapter). For those events which lie within the geometric acceptance of the spectrometer, a tape is written with spark chamber and proportional chamber coordinates. The format of this tape was identical to the format of the experimental tapes written by the on-line PDP-9 computer. In the calculation of the spark chamber coordinates the two sources of measurement uncertainties, i.e. the chamber resolution and multiple Coulomb scattering[3]) were taken into account. This tape was subsequently analysed using the standard reconstruction program and kinematic fitting procedure. Histograms of relevant variables (i.e. $m_{\pi\pi}$, t, missing mass) then served to determine the resolution of the spectrometer. The above procedure has been applied since analytical calculations of the resolution are complicated by the fact that the vertex is in a magnetic field.

Fig.III-1 shows the error in the invariant mass $m_{\pi\pi}$ as function of $m_{\pi\pi}$. The dots give the error in the measured values without application of the kinematic fit, the open circles give the error in the fitted mass. At low values of $m_{\pi\pi}$ the error in $m_{\pi\pi}$ is seen to be rising. The effect can be understood from the following consideration. The opening angle (at the vertex) between the two pions enters into the calculation of the invariant mass. Because of the magnetic field of the target magnet however, the uncertainty in the vertex z-coordinate and the opening angle are coupled. Clearly the uncertainty in the vertex z-coordinate is worst at low values of the $\pi^+\pi^-$ invariant mass. Some proof for the above explanation is given by the extra point at $m_{\pi\pi}$ = 0.5 GeV in fig.III-1. This point has been obtained by artificially switching off the effect of the target magnetic field in the software. No significant dependence on t of the mass resolution was observed.

Fig.III-2 shows the errors in t as function of $\sqrt{t}$. Again the dots denote unfitted values and the open circles fitted values. The error in the fitted values is seen to be slightly smaller than the calculated error in t for the hydrogen experiment[4]).

The width of the missing mass squared distribution at $m_{\pi\pi}$ = 0.75 GeV and t = 0.02 GeV^2, which was obtained using the above procedure amounts to $\sigma(MM^2)$ = 0.180 GeV^2.

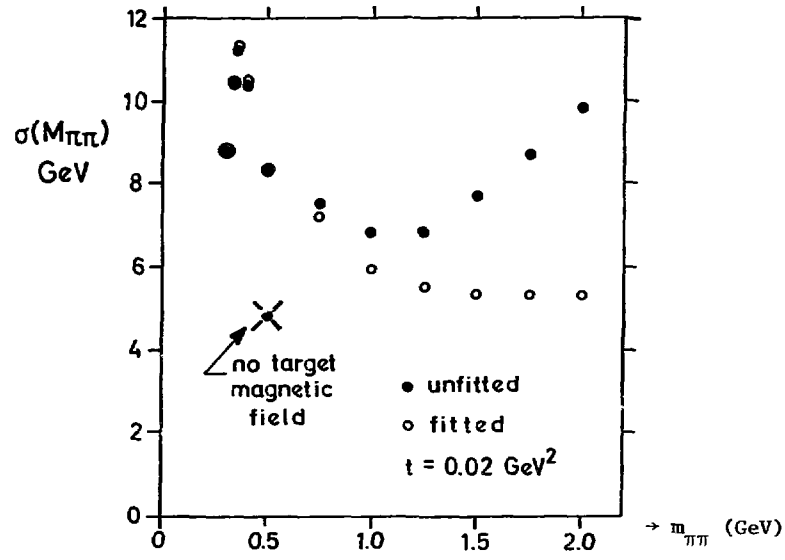

Fig. III-1 Error in the $\pi^+\pi^-$ Invariant Mass $m_{\pi\pi}$ as function of $m_{\pi\pi}$

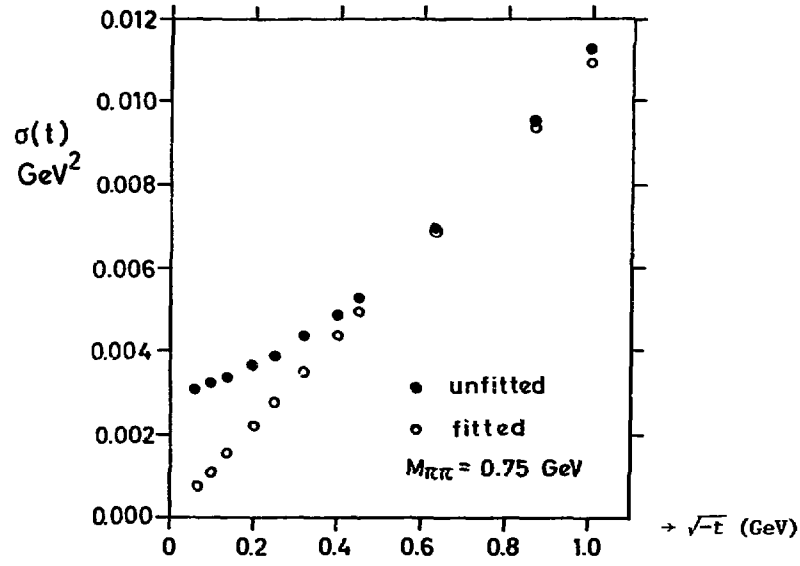

Fig. III-2 Error in the Four Momentum Transfer t as function of $\sqrt{-t}$

III-5 Reconstruction Efficiency

The procedure which is described above, i.e. Monte Carlo generation, reconstruction and kinematic fit, affords a good estimation for the combined efficiency of the reconstruction and kinematics programs. Genuine events of the reaction I-1 can fail reconstruction for several reasons; the main source of program failure being confusion of the two tracks in the chambers between the target and the spectrometer magnet. The fraction of failed events was determined to be independent of t, but was seen to be dependent on $m_{\pi\pi}$. Fig.III-3 shows the mass dependence of the combined efficiency of the geometrical reconstruction and kinematics programs. Below $m_{\pi\pi}$ = 0.5 GeV the efficiency is seen to be falling rapidly. This effect is caused by the small opening angle between the two secondary pions, which leads to superimposed tracks in arm III. Above $m_{\pi\pi}$ = 0.5 GeV a small but significant mass dependence is seen. For the analysis of the rho region which is presented in this thesis, a correction factor of 1.025 ± 0.003 was applied to account for reconstruction inefficiency.

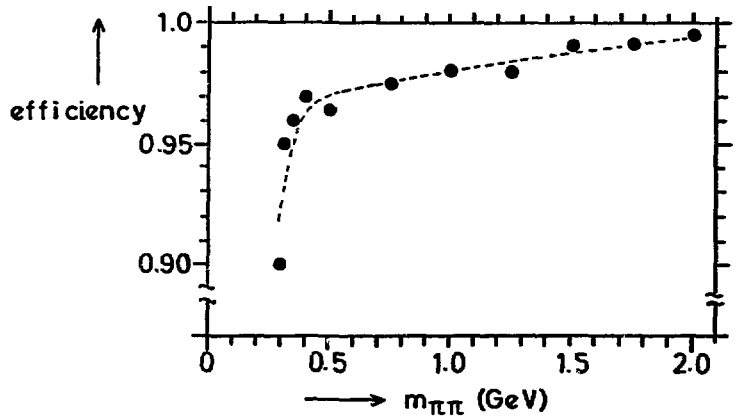

Fig. III-3 Mass Dependence of Reconstruction Efficiency

REFERENCES (Chapter III)

1) V.Chabaud, Pattern Recognition and Momentum Determination for Particles Analysed by a Rectangular Magnet having a 2 Dimensional Field, unpublished.
and:
K.Steffen: High Energy Beam Optics, Interscience Publishers, 1965.

2) V.Barasenkov "Interactions of High Energy Particles and Nuclei with Nuclei".

3) Particle Data Group, "Review of Particle Properties" 1976.

CHAPTER IV ACCEPTANCE CORRECTION

This chapter describes a method to obtain the spherical harmonic moments of the produced angular distribution from the experimental distribution measured with incomplete acceptance. The method which has been used for this experiment is a generalization of the "Method of Moments" which was developed for a previous experiment by the CERN-Munich (MPI) Group[1].

The first section of this chapter describes the Method of Moments i.e. the acceptance correction for the corresponding experiment using a hydrogen target. The second section describes the generalization of the "Method of Moments" for the case of an experiment using a polarized target. Numerical values of the acceptance of the spectrometer are presented in the final section.

IV-1 The Method of Moments

When an (unpolarized) hydrogen target is used for the measurement of the reaction I-1, the number of kinematical variables which are needed to describe the events reduces to four (see chapter I for definitions). Because the produced angular distribution is symmetric around the direction of the incident pion, the angle ψ, defining the orientation of the production plane with respect to the polarization vector, drops out.

As will be shown in the next chapter, the produced angular distribution I_{pr} can be expanded in a series of spherical harmonic functions $Y_\ell^m(\cos\theta,\phi)$:

$$I_{pr}(m_{\pi\pi},t,\cos\theta,\phi) = \sum_{\ell,m} t_\ell^m(m_{\pi\pi},t)\ \mathrm{Re}\ Y_\ell^m(\cos\theta,\phi) \qquad \text{IV-1-1}$$

The $t_\ell^m = \eta^m \langle \mathrm{Re}\ Y_\ell^m(\cos\theta,\phi)\rangle$ are the spherical harmonic moments of the produced angular distribution ("production moments"), $\eta^m = 1$ for $m = 0$, $\eta^m = 2$ for $m \neq 0$. The notation $\langle \mathrm{Re}\ Y_\ell^m(\cos\theta,\phi)\rangle$ stands for

$$\iint_{\theta\phi} I_{pr}(m_{\pi\pi},t,\cos\theta,\phi)\ \mathrm{Re}\ Y_\ell^m(\cos\theta,\phi)\, d\cos\theta d\phi$$

Because of parity conservation ($I_{pr}(\theta,\phi) = I_{pr}(\theta,-\phi)$), only the real parts of the spherical harmonic functions are present in the expansion. Assuming that at low values of the $\pi^+\pi^-$ invariant mass only states with low angular momentum are produced, a limited number of real parts is needed for the expansion.

Of the produced distribution $I_{pr}(m_{\pi\pi},t,\cos\theta,\phi)$, only the fraction $I_a(m_{\pi\pi},t,\cos\theta,\phi)$ is accepted by the geometry of the spectrometer. The acceptance A is then defined by ($\Omega = \theta,\phi$):

$$I_a(m_{\pi\pi},t,\Omega) = A(m_{\pi\pi},t,\Omega)\ I_{pr}(m_{\pi\pi},t,\Omega) \qquad \text{---IV-1-2}$$

The moments $b_{\ell}^{m'}$ of the accepted distribution ("experimental moments") can be defined as follows:

$$b_{\ell}^{m'}(m_{\pi\pi},t) = \int_{4\pi} I_a(m_{\pi\pi},t,\Omega)\ \mathrm{Re}\ Y_{\ell}^{m'}(\Omega)d\Omega$$

Using the definition IV-1-2 of the acceptance and the expansion IV-1-1 of the produced angular distribution this can be written as:

$$b_{\ell}^{m'}(m_{\pi\pi},t) = \int_{4\pi} A(m_{\pi\pi},t,\Omega)\ t_{\ell}^{m}(m_{\pi\pi},t)\ \mathrm{Re}\ Y_{\ell}^{m}(\Omega)\ \mathrm{Re}\ Y_{\ell}^{m'}(\Omega)d\Omega$$

or as:

$$b_{\ell}^{m'}(m_{\pi\pi},t) = \sum_{\ell,m} A_{\ell,\ell'}^{m,m'}(m_{\pi\pi},t,\Omega)\ t_{\ell}^{m}(m_{\pi\pi},t) \qquad \text{---IV-1-3}$$

with

$$A_{\ell,\ell'}^{m,m'}(m_{\pi\pi},t,\Omega) = \int_{4\pi} A(m_{\pi\pi},t,\Omega)\ \mathrm{Re}\ Y_{\ell}^{m}(\Omega)\ \mathrm{Re}\ Y_{\ell}^{m'}(\Omega)d\Omega \qquad \text{---IV-1-4}$$

The acceptance A of the spectrometer as a function of the variables $m_{\pi\pi}$, t, cos θ and ϕ can be calculated with a Monte Carlo technique. The $A_{\ell,\ell'}^{m,m'}$ ("acceptance correlations") can therefore be determined. The experimental moments $b_{\ell}^{m'}$ can be calculated directly from the measured (= accepted) intensity distribution. The production moments t_{ℓ}^{m} can then be determined by solving the linear equations IV-1-3.

In general the acceptance of the spectrometer introduces higher order terms in the experimental moments $b_{\ell}^{m'}$ than are present in the production moments t_{ℓ}^{m}. Still, the t_{ℓ}^{m} can be determined by inverting the square matrix $A_{\ell,\ell'}^{m,m'}$, thus ignoring these higher order terms. Alternatively these higher order terms can be used as constraints, in which case the production moments t_{ℓ}^{m} are fitted.

IV-2 Acceptance Correction in the Case of a Polarized Target

When the reaction I-1 is measured using a polarized target, five independent kinematical quantities $m_{\pi\pi}$,t,cosθ,ϕ and ψ are needed to describe an event (see chapter I for definitions). Therefore, equation IV-1-2, defining the acceptance in the case of an unpolarized target becomes:

$$I_a(m_{\pi\pi},t,\cos\theta,\phi,\psi) = A(m_{\pi\pi},t,\cos\theta,\phi,\psi)I_{pr}(m_{\pi\pi},t,\cos\theta,\phi,\psi) \quad \text{---IV-2-1}$$

Where again I_a and I_{pr} are the measured and produced intensity distributions respectively.

For any small $m_{\pi\pi}$,t bin, where the intensity distributions are constant as a function of $m_{\pi\pi}$,t equation IV-2-1 can be written ($\Omega = \theta,\phi$):

$$I_a(\Omega,\psi) = A(\Omega,\psi)\ I_{pr}(\Omega,\psi) \quad \text{---IV-2-2}$$

In the following, all equations are valid only for a small $m_{\pi\pi}$,t bin, so the indices $m_{\pi\pi}$ and t are dropped.

As will be shown in the next chapter, the produced intensity distribution $I_p(\Omega,\psi)$ can be written as:

$$I_{pr}(\Omega,\psi) = I_u(\Omega) + I_v(\Omega)\cos\psi + I_p(\Omega)\sin\psi \quad \text{---IV-2-3}$$

The produced angular distributions can be expanded in a series of spherical harmonic functions $Y_\ell^m(\Omega)$:

$$\begin{aligned} I_u(\Omega) &= \sum_{\ell,m}^{n_r} u_{t_\ell^m}\ \mathrm{Re}\ Y_\ell^m(\Omega) \\ I_v(\Omega) &= \sum_{\ell,m}^{n_r} v_{t_\ell^m}\ \mathrm{Re}\ Y_\ell^m(\Omega) \\ I_p(\Omega) &= \sum_{\ell,m}^{n_i} p_{t_\ell^m}\ \mathrm{Im}\ Y_\ell^m(\Omega) \end{aligned} \quad \text{----IV-2-4}$$

Because of parity conservation, real parts are used for the expansion of the I_u and I_v, and imaginary parts for the expansion of I_p. Assuming again that only states with low angular momentum are produced, limited numbers n_r and n_i of real and imaginary parts of the spherical harmonic functions are present in the expansions.

The t_ℓ^m are the spherical harmonic moments of the produced angular distribution ("production moments").

$$
\begin{aligned}
{}^{u}t_\ell^m &= \eta^m \langle \mathrm{Re}\ Y_\ell^m(\Omega) \rangle \\
{}^{v}t_\ell^m &= 2\eta^m \langle \mathrm{Re}\ Y_\ell^m(\Omega)\cos\psi \rangle \quad \eta^m = 1 \text{ for } m = 0, \\
{}^{p}t_\ell^m &= 4 \langle \mathrm{Im}\ Y_\ell^m(\Omega)\sin\psi \rangle \quad \eta^m = 2 \text{ for } m \neq 0
\end{aligned}
$$

The spherical harmonic moments of the accepted (= measured) distribution ("experimental moments") can be defined as follows:

$$
\begin{aligned}
{}^{u}b_{\ell'}^{m'} &= \frac{1}{2\pi} \iint_{\Omega\psi} I_a(\Omega,\psi)\ \mathrm{Re}\ Y_{\ell'}^{m'}(\Omega)\ d\Omega d\psi \\
{}^{v}b_{\ell'}^{m'} &= \frac{1}{2\pi} \iint_{\Omega\psi} I_a(\Omega,\psi)\ \mathrm{Re}\ Y_{\ell'}^{m'}(\Omega)\cos\psi\, d\Omega d\psi \qquad \text{----IV-2-5} \\
{}^{p}b_{\ell'}^{m'} &= \frac{1}{2\pi} \iint_{\Omega\psi} I_a(\Omega,\psi)\ \mathrm{Im}\ Y_{\ell'}^{m'}(\Omega)\sin\psi\, d\Omega d\psi
\end{aligned}
$$

With the help of equations IV-2-2 and IV-2-3 this can be written as:

$$
\begin{aligned}
{}^{u}b_{\ell'}^{m'} &= \frac{1}{2\pi} \iint_{\Omega\psi} A(\Omega,\psi)\ (I_u(\Omega) + I_v(\Omega)\cos\psi + I_p(\Omega)\sin\psi)\ \mathrm{Re}\ Y_{\ell'}^{m'}(\Omega) d\Omega d\psi \\
{}^{v}b_{\ell'}^{m'} &= \frac{1}{2\pi} \iint_{\Omega\psi} A(\Omega,\psi)\ (I_u(\Omega) + I_v(\Omega)\cos\psi + I_p(\Omega)\sin\psi)\ \mathrm{Re}\ Y_{\ell'}^{m'}(\Omega)\cos\psi\, d\Omega d\psi \\
{}^{p}b_{\ell'}^{m'} &= \frac{1}{2\pi} \iint_{\Omega\psi} A(\Omega,\psi)\ (I_u(\Omega) + I_v(\Omega)\cos\psi + I_p(\Omega)\sin\psi)\ \mathrm{Im}\ Y_{\ell'}^{m'}(\Omega)\sin\psi\, d\Omega d\psi
\end{aligned}
\qquad \text{---IV-2-6}
$$

When the expansions IV-2-4 in spherical harmonic functions are substituted for the I_u, I_v and I_p, this can be written as:

$$
\begin{aligned}
{}^{u}b_{\ell'}^{m'} &= \sum_{\ell,m} {}^{u}t_\ell^m\ {}^{uu}A_{\ell\ell'}^{mm'} + \sum_{\ell,m} {}^{u}t_\ell^m\ {}^{uv}A_{\ell\ell'}^{mm'} + \sum_{\ell,m} {}^{p}t_\ell^m\ {}^{up}A_{\ell\ell'}^{mm'} \\
{}^{v}b_{\ell'}^{m'} &= \sum_{\ell,m} {}^{u}t_\ell^m\ {}^{vu}A_{\ell\ell'}^{mm'} + \sum_{\ell,m} {}^{v}t_\ell^m\ {}^{vv}A_{\ell\ell'}^{mm'} + \sum_{\ell,m} {}^{p}t_\ell^m\ {}^{vp}A_{\ell\ell'}^{mm'} \\
{}^{p}b_{\ell'}^{m'} &= \sum_{\ell,m} {}^{u}t_\ell^m\ {}^{pu}A_{\ell\ell'}^{mm'} + \sum_{\ell,m} {}^{v}t_\ell^m\ {}^{pv}A_{\ell\ell'}^{mm'} + \sum_{\ell,m} {}^{p}t_\ell^m\ {}^{pp}A_{\ell\ell'}^{mm'}
\end{aligned}
\qquad \text{---IV-2-7}
$$

The ${}^{mm'}A_{\ell\ell'}$ can be written explicitly using equations IV-2-6 and the expansions IV-2-4 of the produced angular distribution. As an example, one of the matrices $A_{\ell\ell'}^{mm'}$ is given here explicitly:

$$ {}^{vp}A^{mm'}_{\ell\ell'} = \frac{1}{2\pi} \iint_{\Omega\psi} A(\Omega,\psi)\ \mathrm{Im}\ Y^{m}_{\ell}(\Omega)\ \mathrm{Re}\ Y^{m'}_{\ell'}(\Omega)\ \sin\psi\ \cos\psi\ d\Omega d\psi $$

A closer inspection of equations IV-2-7 shows that the equations constitute a matrix equation of the following form:

$$ \begin{pmatrix} {}^{u}b^{m'}_{\ell'} \\ \hline {}^{v}b^{m'}_{\ell'} \\ \hline {}^{p}b^{m'}_{\ell'} \end{pmatrix} = \left(\begin{array}{c|c|c} {}^{uu}A^{mm'}_{\ell\ell'} & {}^{uv}A^{mm'}_{\ell\ell'} & {}^{up}A^{mm'}_{\ell\ell'} \\ \hline {}^{vu}A^{mm'}_{\ell\ell'} & {}^{vv}A^{mm'}_{\ell\ell'} & {}^{vp}A^{mm'}_{\ell\ell'} \\ \hline {}^{pu}A^{mm'}_{\ell\ell'} & {}^{pv}A^{mm'}_{\ell\ell'} & {}^{pp}A^{mm'}_{\ell\ell'} \end{array}\right) \times \begin{pmatrix} {}^{u}t^{m}_{\ell} \\ \hline {}^{v}t^{m}_{\ell} \\ \hline {}^{p}t^{m}_{\ell} \end{pmatrix} \qquad \text{----- IV-2-7} $$

The vectors ${}^{u}b^{m'}_{\ell'}$, ${}^{v}b^{m'}_{\ell'}$ and ${}^{p}b^{m'}_{\ell'}$ can therefore be joined into one series $b^{m'}_{\ell'}$. When similar simplifications are made to t^{m}_{ℓ} and $A^{mm'}_{\ell\ell'}$, the equations IV-2-7 read:

$$ b^{m'}_{\ell'} = \sum_{\ell,m} A^{mm'}_{\ell\ell'}\ t^{m}_{\ell} \qquad \text{---IV-2-8} $$

Again, the vector $b^{m'}_{\ell'}$ contains the moments of the accepted distribution, the elements of the matrix $A^{mm'}_{\ell\ell'}$ are the acceptance correlations. The acceptance correlations are calculated using a Monte Carlo technique which determines the acceptance of the spectrometer. The experimental moments $b^{m'}_{\ell'}$ are calculated directly from the measured intensity distribution. The spherical harmonic moments t^{m}_{ℓ} of the produced distribution can therefore be determined by solving the matrix equation IV-2-8.

The set of experimental moments $b^{m'}_{\ell'}$ will again generally contain higher order terms than the set of production moments t^{m}_{ℓ}, due to the acceptance of the spectrometer. Therefore a fit can be done to determine the production moments t^{m}_{ℓ}. For this experiment this option has not been chosen; the t^{m}_{ℓ} were determined by inverting the square matrix $A^{m,m'}_{\ell,\ell'}$, thus ignoring the higher order terms in the $b^{m'}_{\ell'}$. This option was chosen for reasons of computing time.

The moments which are obtained by the above method consist of two groups: the polarization independent moments of the type $\langle \mathrm{Re}\ Y^{m}_{\ell}(\Omega)\rangle$ and the polarization dependent moments $\langle \mathrm{Re}\ Y^{m}_{\ell}(\Omega)\cos\psi\rangle$ and $\langle \mathrm{Im}\ Y^{m}_{\ell}(\Omega)\sin\psi\rangle$.

The latter two can be expressed as integrals over Ω and ψ of the produced intensity distribution I_p, the spherical harmonic functions and $\sin\psi$ or $\cos\psi$:

$$\langle \mathrm{Re}\ Y_\ell^m(\Omega)\cos\psi \rangle = \frac{1}{2\pi}\int_\Omega\int_\psi I_{pr}(\Omega,\psi)\ \mathrm{Re}\ Y_\ell^m(\Omega)\cos\psi d\Omega d\psi \qquad \text{---IV-2-9}$$

$$\langle \mathrm{Im}\ Y_\ell^m(\Omega)\sin\psi \rangle = \frac{1}{2\pi}\int_\Omega\int_\psi I_{pr}(\Omega,\psi)\ \mathrm{Im}\ Y_\ell^m(\Omega)\sin\psi d\Omega d\psi$$

Since the production distribution $I_{pr}(\Omega,\Psi)$ for unpolarized protons is independent of ψ ($=I_{pr}(\Omega)$), from these equations it follows that the polarization dependent moments contain no contribution from the unpolarized target protons.

If however the acceptance correction is not done correctly (e.g. an asymmetry in the experimental apparatus is not properly accounted for), this could introduce a spurious effect in the polarization dependent moments. In order to be sure that an observed polarization effect can not be introduced by the acceptance correction, the experiment was carried out in two parts, one half with positive, the other with negative target polarization. For both directions of the target polarization the moments are calculated independently. Let $I_p^+(\Omega,\psi)$ be the intensity distribution produced with positive target polarization:

$$I_{pr}^+(\Omega,\psi) = I_u(\Omega) + I_v(\Omega)\sin\psi + I_p(\Omega)\cos\psi$$

Changing the direction of the target polarization changes ψ to $\psi+\pi$. the produced distribution $I_{pr}^-(\Omega,\psi)$ with negative target polarization is therefore given by:

$$I_{pr}^-(\Omega,\psi) = I_u(\Omega) + I_v(\Omega)\cos(\psi+\pi) + I_p(\Omega)\sin(\psi+\pi)$$

or

$$I_{pr}^-(\Omega,\psi) = I_u(\Omega) - I_v(\Omega)\cos\psi - I_p(\Omega)\sin\psi$$

which means that the polarization dependent moments change sign when changing the sign of the target polarization. If we assume, that the absolute values of the degree of target polarization are the same for positive and negative target polarization, then we can obtain the final polarization dependent moments by taking half the difference of the moments measured with positive and negative target polarization. The degree of target polarization was measured to be the same for positive and negative polarization.

The acceptance correction cannot introduce a spurious polarization effect when this procedure is applied. A polarization effect is observed as the difference between two distributions, one with positive and the other with negative target polarization. The only difference between the two distributions is a small change in the microwave frequency which determines the sign of the target polarization. Any significant difference between the two distributions must therefore be attributed to a polarization effect.

As was described in ref.[1]) several methods of acceptance correction are possible in principle. For the present experiment some tests have been carried out to determine which method is best suited for this experiment. One of the results of the investigation is that the method of moments, which has been described above, is applicable only if the number of accepted events per $m_{\pi\pi}$,t bin is not too low and if the acceptance does not vary too wildly as a function of θ, ϕ and ψ. It has been established that this procedure does not lead to meaningful results at high values of $m_{\pi\pi}$. The χ^2 method[1]) does produce good results at all values of $m_{\pi\pi}$. It was verified however that both methods produce the same results below $m_{\pi\pi}$ = 1 GeV.

IV-3 The Acceptance of the Spectrometer

The acceptance of the spectrometer for events of the reaction I-1 at 17.2 GeV incident momentum has been calculated using a Monte Carlo program. The observable interval of the $\pi^+\pi^-$ invariant mass (threshold to $\sim$2 GeV) was divided into 35 bins of 50 MeV width. The t-interval (t_{min} to $\sim$1 GeV^2) was divided into 11 bins. For each $m_{\pi\pi}$,t bin 50,000 events were generated in the $\pi^+\pi^-$ rest frame, isotropically in the angles θ and ϕ. The pair is transformed into the laboratory system after isotropic generation of the angle ψ. With the production momenta of the two charged secondaries known, these particles are tracked through the spectrometer, to determine whether both particles are everywhere within the acceptance of the spectrometer.

Fig.IV-1 shows the acceptance of the spectrometer for reaction I-1 at 17.2 GeV, as a function of the four momentum transfer $\sqrt{t}$, for different values of $m_{\pi\pi}$, integrated over θ, ϕ and ψ. A rather smooth behaviour of the acceptance is observed.

Fig.IV-2 shows the acceptance as a function of the $\pi^+\pi^-$ invariant mass $m_{\pi\pi}$ for 3 different t-values, again integrated over θ, ϕ and ψ. The acceptance is seen to decrease rapidly towards higher values of $m_{\pi\pi}$. This is due to the increase in the opening angle between the π^+ and π^- in the laboratory system. In fig.IV-3 the acceptance is shown as a function of the polar angles θ and ϕ in the t-channel helicity system. The invariant mass $m_{\pi\pi}$ is chosen in the regions of the ρ, f and g mesons respectively. Finally, in fig.IV-4 the ψ-dependence of the acceptance is shown for $m_{\pi\pi}$ = 0.75, 1.25 and 1.70 GeV for t = 0.01 and 1.0 GeV^2, integrated over θ and ϕ.

REFERENCES (Chapter IV)

1) G.Grayer, B.Hyams, C.Jones, P.Schlein, P.Weilhammer, W.Blum, H.Dietl, W.Koch, E.Lorenz, G.Lütjens, W.Männer, J.Meissburger, W.Ochs and U.Stierlin, Nucl. Physics B75 (1974) 189.

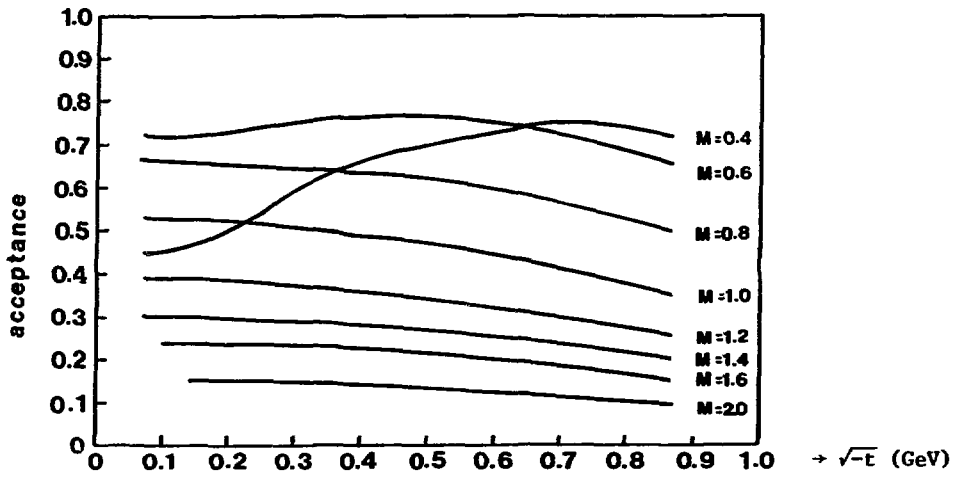

Fig. IV-1 t-Dependence of acceptance

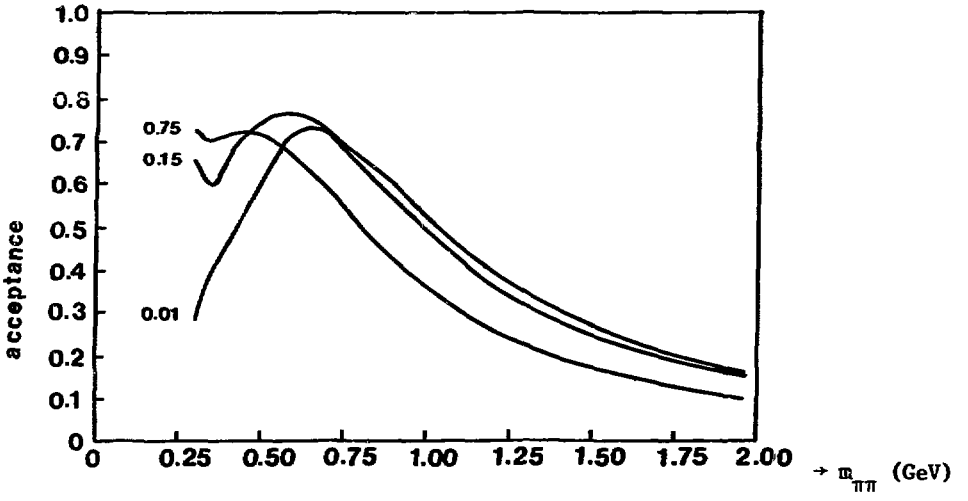

Fig. IV-2 Mass dependence of acceptance

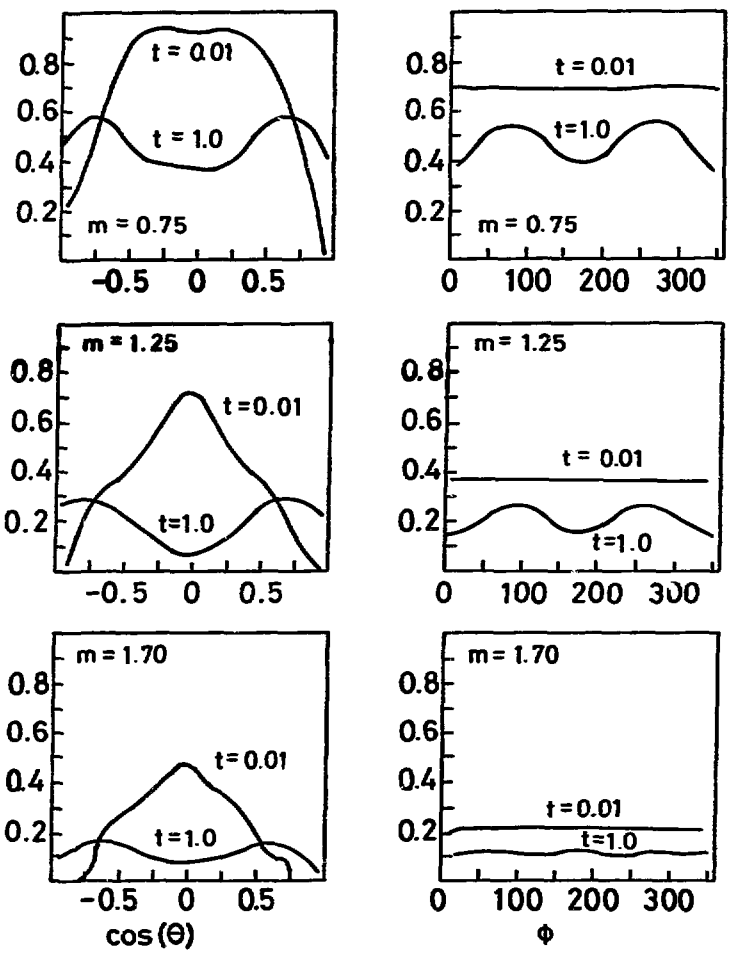

Fig. IV-3 Acceptance as a function of cos(θ) and ϕ (Gottfried Jackson frame) for $m_{\pi\pi}$ = 0.75 , 1.25 and 1.75 GeV.

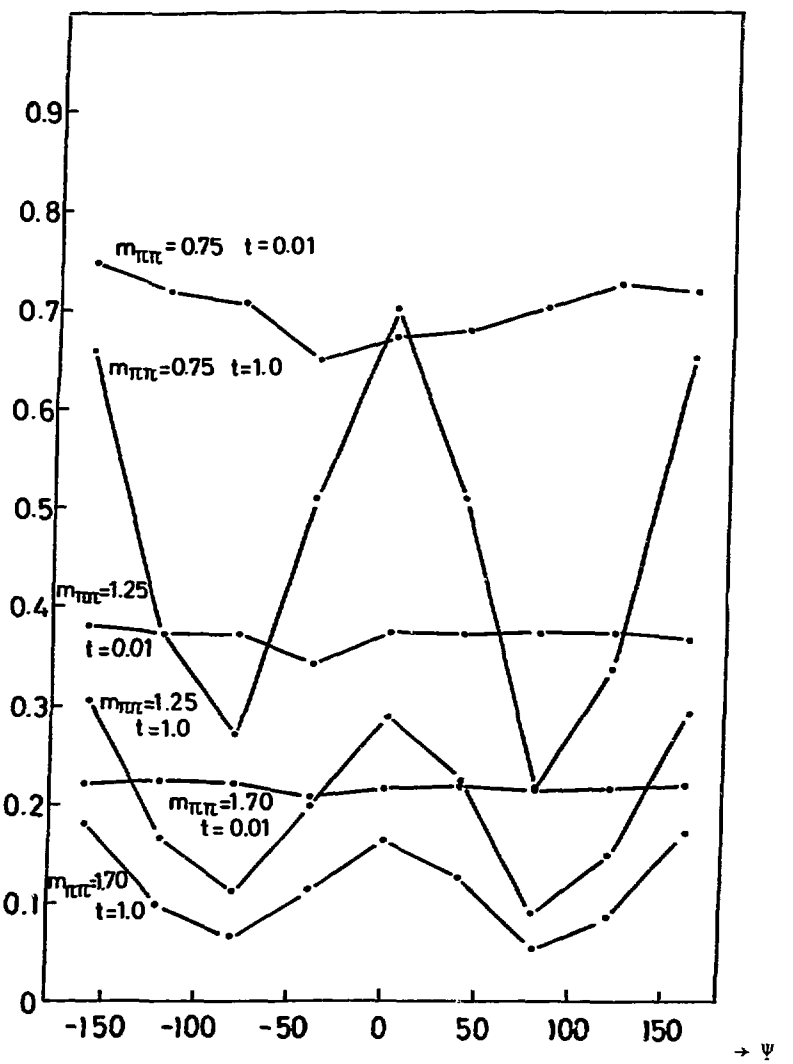

Fig. IV-4 Ψ-Dependence of acceptance for $m_{\pi\pi}$ = 0.75 , 1.25 and 1.70 GeV

CHAPTER V AMPLITUDE ANALYSIS

In this chapter it will be shown that a model independent amplitude analysis of the reaction $\pi^- p \to \pi^-\pi^+ n$ is possible, when the reaction is measured using a transversely polarized target.

The different amplitudes which can be used to describe the process are defined in the first section. In the second section, the final state $\pi^+\pi^-$ density matrix is derived. In the next section, the observed $\pi^+\pi^-$ decay angular distribution is written in terms of the final state density matrix, leading to a number of relations between the amplitudes and the production moments. The relation between amplitudes and moments are given for the case that only S and P waves contribute to the $\pi^+\pi^-$ system. The last section describes the analytical solution of this set of equations. The inherent ambiguities are discussed.

V-1 Definition of Amplitudes

The reaction $\pi^- p \to \pi^-\pi^+ n$ can, either in the s-channel or t-channel helicity frame, be described by a set of helicity amplitudes[1]).

$$\langle j,m,n|T|\lambda\rangle$$

where: j = spin of the final state $\pi^+\pi^-$ system
m = helicity of the dipion, $m = -j, -j+1 \ldots\ldots j$
n = helicity of the recoil neutron, $n = \pm\frac{1}{2}$
λ = helicity of the target proton, $\lambda = \pm\frac{1}{2}$

The number of independent amplitudes is limited by parity conservation:

$$\langle j,m,n|T|\lambda\rangle = (-1)^{m+n+\lambda} \langle j,-m,-n|T|-\lambda\rangle$$

For convenience, the following notation will be used:

$$N_j^m = \langle j,m,+|T|+\rangle = (-1)^{m+1} \langle j,-m,-|T|-\rangle \qquad \text{nucleon spin nonflip}$$

$$F_j^m = \langle j,m,+|T|-\rangle = (-1)^m \langle j,-m,-|T|+\rangle \qquad \text{nucleon spin flip}$$

It is sometimes convenient (see following sections) to work with a different set of amplitudes:

a) Transversity amplitudes

For these amplitudes, the spin components of the recoil neutron is specified along the normal on the production plane, i.e. the y-axis (fig.I-1). Transversity amplitudes were introduced by Kotanski[2]) in 1966. As will be shown in the next section the relations between the measured moments and the unknown amplitudes are simplest when tranversity amplitudes are used. This is known to be true more generally[3]). The transversity amplitudes are obtained from the helicity amplitudes by rotating the spin quantization axis 90° around the x axis[4]).

The following transversity amplitudes are defined:

$$G_j^m = \frac{1}{\sqrt{2}}\left(N_j^m + i(-1)^m F_j^{-m}\right)$$

$$H_j^m = \frac{1}{\sqrt{2}}\left(N_j^m - i(-1)^m F_j^{-m}\right)$$

The G and H amplitudes correspond to opposite directions of the neutron spin component along the y-axis ("transversity"). The term transversity amplitudes is somewhat misleading. Only the neutron spin component is taken along the y-axis. The dipion spin component is taken along the z-axis, so the amplitudes are really mixed helicity-transversity amplitudes.

b) Transversity Amplitudes corresponding to Natural and Unnatural Parity Exchange

From the helicity amplitudes, combinations can be formed which correspond asymptotically (for infinite centre of mass energy) to the exchange in the t-channel of natural or unnatural parity[5]). This is done by adding and subtracting amplitudes with the helicities in one vertex reversed. The same can be done for the transversity amplitudes defined above, as the helicity of the π-pair is still defined:

$$U_{g_j}^m = a_m\left(G_j^m + (-1)^m G_j^{-m}\right) \qquad U_{g_j}^{-m} = (-1)^m U_{g_j}^m$$

$$N_{g_j}^m = a_m\left(G_j^m - (-1)^m G_j^{-m}\right) \qquad N_{g_j}^{-m} = (-1)^{m+1} N_{g_j}^m$$

$$U_{h_j}^m = a_m\left(H_j^m + (-1)^m H_j^{-m}\right) \qquad U_{h_j}^{-m} = (-1)^m U_{h_j}^m$$

$$N_{h_j}^m = a_m\left(H_j^m - (-1)^m H_j^{-m}\right) \qquad N_{h_j}^{-m} = (-1)^{m+1} N_{h_j}^m$$

where $a_m = \frac{1}{2}$ for $m = 0$ and $a_m = \frac{1}{\sqrt{2}}$ for $m \neq 0$.

The U and N label unnatural and natural parity exchange respectively; the g and h amplitudes again correspond to opposite directions of the neutron spin component transverse to the reaction plane.

For the special case where the $\pi^+\pi^-$ system is in an S or P wave state, the amplitudes which describe the reaction $\pi^- p \to \pi^-\pi^+ n$ are:

a) Helicity Amplitudes

$$N_S = \langle 0,0,+|T|+\rangle \qquad F_S = \langle 0,0,+|T|-\rangle$$

$$N_0 = \langle 1,0,+|T|+\rangle \qquad F_0 = \langle 1,0,+|T|-\rangle$$

$$N_1 = \langle 1,1,+|T|+\rangle \qquad F_1 = \langle 1,1,+|T|-\rangle$$

$$N_{-1} = \langle 1,-1,+|T|+\rangle \qquad F_{-1} = \langle 1,-1,+|T|-\rangle$$

b) Transversity Amplitudes

$$G_S = \frac{1}{\sqrt{2}}(N_S + iF_S) \qquad H_S = \frac{1}{\sqrt{2}}(N_S - iF_S)$$

$$G_0 = \frac{1}{\sqrt{2}}(N_0 + iF_0) \qquad H_0 = \frac{1}{\sqrt{2}}(N_0 - iF_0)$$

$$G_1 = \frac{1}{\sqrt{2}}(N_1 - iF_{-1}) \qquad H_1 = \frac{1}{\sqrt{2}}(N_1 + iF_{-1})$$

$$G_{-1} = \frac{1}{\sqrt{2}}(N_{-1} - iF_1) \qquad H_{-1} = \frac{1}{\sqrt{2}}(N_{-1} + iF_1)$$

c) Transversity Amplitudes corresponding to Natural and Unnatural Parity Exchange

$$g_S = G_S \qquad h_S = H_S$$

$$g_0 = G_0 \qquad h_0 = H_0$$

$$g_u = \frac{1}{\sqrt{2}}(G_1 - G_{-1}) \qquad h_u = \frac{1}{\sqrt{2}}(H_1 - H_{-1})$$

$$g_N = \frac{1}{\sqrt{2}}(G_1 + G_{-1}) \qquad h_N = \frac{1}{\sqrt{2}}(H_1 + H_{-1})$$

Here the amplitudes g_N, h_N describe natural parity exchange, the other amplitudes describe unnatural parity exchange.

For the case where only S and P waves contribute, we therefore have 8 (complex) amplitudes to determine. This means that, in order to do a complete and model independent amplitude analysis, 15 real quantities have to be determined, 8 moduli of amplitudes and 7 relative phases. One overall phase does not correspond to a measurable quantity.

V-2 The Final State Density Matrix

The orientation of a system of spins j is described by a $(2j+1)\cdot(2j+1)$ density matrix.

The density matrix $\overline{\rho}_{\lambda\lambda'}$, describing the orientation of the spins of the target protons therefore, is a 2×2 matrix. It can be written as[6]):

$$\overline{\rho}_{\lambda\lambda'} = \tfrac{1}{2}(I + \vec{P}\cdot\vec{\sigma})$$

where I is the 2×2 unit matrix

$\vec{P}$ is the polarization vector

$\vec{\sigma}$ are the Pauli spin matrices.

When the s-channel helicity frame is used for the proton helicity, the polarization vector has the following components (fig.I-2):

$$P_x = P_t \sin\psi$$

$$P_y = P_t \cos\psi$$

$$P_z = P_L$$

where P_t and P_L are the transverse and longitudinal components of the polarization vector with respect to the beam direction. In the experiment, a transversely polarized target was used, therefore there was no longitudinal polarization component. We will first consider the more general case however, where the polarization vector makes an arbitrary angle with the beam. The initial state density matrix $\overline{\rho}_{\lambda\lambda'}$, can then be written as:

$$\overline{\rho}_{\lambda\lambda} = \frac{1}{2}\begin{pmatrix} 1 + P_L & P_t\sin\psi - i\,P_t\cos\psi \\ P_t\sin\psi + i\,P_t\cos\psi & 1 - P_L \end{pmatrix} \qquad \text{V-2-1}$$

The final state density matrix $\hat{\rho}$ describing the orientations of both the dipion system and the recoil neutron is then given by:

$$\frac{d^2\sigma}{dm_{\pi\pi}dt}\,\hat{\rho}^{j'm'n'}_{jmn} = \sum_{\lambda\lambda'} \langle j,m,n|T|\lambda\rangle \bar{\rho}_{\lambda\lambda'} \langle j',m',n'|T|\lambda'\rangle^*$$

The final state density matrix describes both the orientation of the spins of the dipion and the neutron polarization. For this experiment however, only the $\pi^+\pi^-$ decay angular distribution is measured and not the neutron polarization. The final state density matrix which describes the spin alignment of the $\pi^+\pi^-$ system is therefore obtained by taking the trace with respect to the neutron polarization.

$$\frac{d^2\sigma}{dm_{\pi\pi}dt}\,\hat{\rho}^{j'm'}_{jm} = \sum_{n}\sum_{\lambda\lambda'} \langle j,m,n|T|\lambda\rangle \bar{\rho}_{\lambda\lambda'} \langle j',m',n|T|\lambda'\rangle^*$$

---V-2-2

Using the explicit form V-2-1 of the initial state density matrix $\bar{\rho}_{\lambda\lambda'}$ this can be written as:

$$\frac{d^2\sigma}{dm_{\pi\pi}dt}\,\hat{\rho}^{j'm'}_{jm} = {}_U R^{j'm'}_{jm} + P_t\cos\psi\ {}_C R^{j'm'}_{jm} + P_t\sin\psi\ {}_S R^{j'm'}_{jm} + P_L\ {}_L R^{j'm'}_{jm}$$

---V-2-3

Using the definitions of the last section, the $R^{j'm'}_{jm}$ can be expressed in terms of amplitudes:

$${}_U R^{j'm'}_{jm} = \tfrac{1}{2}\left({}^U g^m_j\, {}^U g^{m'*}_{j'} + {}^N g^m_j\, {}^N g^{m'*}_{j'} + {}^U h^m_j\, {}^U h^{m'*}_{j'} + {}^N h^m_j\, {}^N h^{m'*}_{j'}\right)$$

$${}_C R^{j'm'}_{jm} = \tfrac{1}{2}\left({}^U g^m_j\, {}^U g^{m'*}_{j'} - {}^N g^m_j\, {}^N g^{m'*}_{j'} - {}^U h^m_j\, {}^U h^{m'*}_{j'} + {}^N h^m_j\, {}^N h^{m'*}_{j'}\right)$$

$${}_S R^{j'm'}_{jm} = \tfrac{1}{2}\left(-{}^U g^m_j\, {}^N g^{m'*}_{j'} + {}^N g^m_j\, {}^U g^{m'*}_{j'} + {}^U h^m_j\, {}^N h^{m'*}_{j'} - {}^N h^m_j\, {}^U h^{m'*}_{j'}\right)$$

$${}_L R^{j'm'}_{jm} = \tfrac{1}{2}\left({}^U g^m_j\, {}^N g^{m'*}_{j'} + {}^N g^m_j\, {}^U g^{m'*}_{j'} + {}^U h^m_j\, {}^N h^{m'*}_{j'} + {}^N h^m_j\, {}^U h^{m'*}_{j'}\right)$$

---V-2-4

The elements of the final state density matrix can of course be written in terms of each set of amplitudes defined in the first section of this chapter. Only the relations V-2-4 are given here however, because this form of the density matrix is of particular interest for the experiment.

Since the $\pi^+\pi^-$ final density matrix completely determines the $\pi^+\pi^-$ final state, an important conclusion can be drawn at this stage already. The explicit expressions V-2-4 for the elements of the final state density matrix do not contain a product between "g" and "h" amplitudes. Therefore, the relative phase between the "g" and "h" amplitudes cannot be determined by this experiment. In order to determine all amplitudes and phases (i.e. a complete experiment), a measurement of the neutron polarization would be needed along with the $\pi^+\pi^-$ decay angular distribution.

It is observed in particular, that a measurement with longitudinal target polarization, would not result in a determination of the phase between the amplitudes with different transversities.

V-3 Relations between Moments and Amplitudes

Having established the explicit form V-2-3/4 of the final state density matrix, we now turn our attention to the $\pi^+\pi^-$ decay angular distributions. The measurable $\pi^+\pi^-$ decay angular distributions $I(\cos\theta,\phi,\psi) = I(\Omega,\psi)$ can be written in terms of the final state density matrix $\hat{\rho}$ and the spherical harmonic functions $Y_j^m(\Omega)$:

$$I(\Omega,\psi) = \frac{d^2\sigma}{dm_{\pi\pi}dt} \sum_{j,m,j',m'} \hat{\rho}_{jm}^{j'm'} \; Y_j^m(\Omega) \; Y_{j'}^{m'*}(\Omega) \qquad \text{---V-3-1}$$

Using the expressions for the matrix elements $\hat{\rho}_{jm}^{j'm'}$ obtained in the previous section, this leads to the form of the produced decay angular distribution which was used in chapter IV:

$$I(\Omega,\Psi) = I_U(\Omega) + I_C(\Omega).\cos(\Psi) + I_S(\Omega).\sin(\Psi) + I_L(\Omega)$$

At this stage, we will drop the term $I_L(\Omega)$ describing longitudinal polarization. Because the target protons were polarized transverse to the beam direction there was no longitudinal polarization component.

The I_U, I_C and I_S are given by:

$$\begin{aligned} I_U(\Omega) &= \sum_{jmj'm'} \mathrm{Re}({}_U R_{jm}^{j'm'}) \; \mathrm{Re}(Y_j^m Y_{j'}^{m'*}) \\ I_C(\Omega) &= \sum_{jmj'm'} \mathrm{Re}({}_C R_{jm}^{j'm'}) \; \mathrm{Re}(Y_j^m Y_{j'}^{m'*}) \\ I_S(\Omega) &= \sum_{jmj'm'} \mathrm{Im}({}_S R_{jm}^{j'm'}) \; \mathrm{Im}(Y_j^m Y_{j'}^{m'*}) \end{aligned} \qquad \text{---V-3-2}$$

Using the orthonormality relations for the spherical harmonic functions $Y_\ell^m(\Omega)$, and the Clebsch-Gordan coefficients this can be written in the following form:

$$I_U(\Omega) = \sum_{L,M} U t_L^M \quad \text{Re } Y_L^M(\Omega)$$

$$I_C(\Omega) = \sum_{L,M} C t_L^M \quad \text{Re } Y_L^M(\Omega) \qquad \text{---V-3-3}$$

$$I_S(\Omega) = \sum_{L,M} S t_L^M \quad \text{Im } Y_L^M(\Omega)$$

The coefficients t_L^M are, except for a normalization factor, equal to the observable spherical harmonic moments of the produced decay angular distribution.

Inserting the explicit expressions V-2-4 of the final state density matrix into equations V-3-2, the spherical harmonic moments can therefore be expressed in terms of the amplitudes defined in section 1. In the case where only S and P waves contribute to the $\pi^+\pi^-$ angular distribution one obtains a set of 15 equations. The relations between the production moments and the helicity amplitudes are given in table V-1, the relations between the moments and the transversity amplitudes corresponding to natural and unnatural parity exchange in table V-2.

V-4 Solutions and Ambiguities

Inspecting table V-2, which gives the relations between the transversity amplitudes and the moments, the right hand side is seen not to contain a product between amplitudes of different transversity ("g" and "h" amplitudes). As a consequence the phase between these two sets of amplitudes cannot be determined by solving equations in table V-2. But then it follows that on the right hand side there are only 14 unknown parameters, so in order to obtain the amplitudes from the moments a 1 constraint fit can be done. It is in principle possible to solve the amplitudes from these equations by using a χ^2 minimization method alone. But we will first see if analytical solutions can be found, and if so, how many ambiguities there are to be expected.

From the original equations in table V-2 the following set of equations is formed by addition and subtraction:

$$t_1 = \langle \mathrm{Re}\, Y_0^0 \rangle = \frac{1}{\sqrt{4\pi}} \{|N_S|^2+|F_S|^2+|N_0|^2+|F_0|^2+|N_1|^2+|F_1|^2+|N_{-1}|^2+|F_{-1}|^2\}$$

$$t_2 = \langle \mathrm{Re}\, Y_1^0 \rangle = \frac{1}{\sqrt{\pi}} \mathrm{Re}\{N_0 N_S^* + F_0 F_S^*\}$$

$$t_3 = 2\langle \mathrm{Re}\, Y_1^1 \rangle = \frac{1}{\sqrt{\pi}} \mathrm{Re}\{(N_1-N_{-1})N_S^* + (F_1-F_{-1})F_S^*\}$$

$$t_4 = \langle \mathrm{Re}\, Y_2^0 \rangle = \frac{1}{\sqrt{5\pi}} \{|N_0|^2+|F_0|^2 - \tfrac{1}{2}(|N_1|^2+|F_1|^2+|N_{-1}|^2+|F_{-1}|^2)\}$$

$$t_5 = 2\langle \mathrm{Re}\, Y_2^1 \rangle = \sqrt{\frac{3}{5\pi}} \mathrm{Re}\{(N_1-N_{-1})N_0^* + (F_1-F_{-1})F_0^*\}$$

$$t_6 = 2\langle \mathrm{Re}\, Y_2^2 \rangle = \sqrt{\frac{6}{5\pi}} \mathrm{Re}\{N_1 N_{-1}^* + F_1 F_{-1}^*\}$$

$$t_7 = 2\langle \mathrm{Re}\, Y_0^0 \cos\psi \rangle = \frac{1}{\sqrt{\pi}} \mathrm{Im}\{N_S F_S^* + N_0 F_0^* + N_1 F_1^* + N_{-1} F_{-1}^*\}$$

$$t_8 = 2\langle \mathrm{Re}\, Y_1^0 \cos\psi \rangle = \frac{1}{\sqrt{\pi}} \mathrm{Im}\{N_0 F_S^* - F_0 N_S^*\}$$

$$t_9 = 4\langle \mathrm{Re}\, Y_1^1 \cos\psi \rangle = \frac{1}{\sqrt{\pi}} \mathrm{Im}\{(N_1-N_{-1})F_S^* - (F_1-F_{-1})N_S^*\}$$

$$t_{10} = 2\langle \mathrm{Re}\, Y_2^0 \cos\psi \rangle = \frac{1}{\sqrt{5\pi}} \mathrm{Im}\{2N_0 F_0^* - N_1 F_1^* - N_{-1} F_{-1}^*\}$$

$$t_{11} = 4\langle \mathrm{Re}\, Y_2^1 \cos\psi \rangle = \sqrt{\frac{3}{5\pi}} \mathrm{Im}\{(N_1-N_{-1})F_0^* - (F_1-F_{-1})N_0^*\}$$

$$t_{12} = 4\langle \mathrm{Re}\, Y_2^2 \cos\psi \rangle = \sqrt{\frac{6}{5\pi}} \mathrm{Im}\{N_{-1} F_1^* - N_1 F_{-1}^*\}$$

$$t_{13} = 4\langle \mathrm{Im}\, Y_1^1 \sin\psi \rangle = -\frac{1}{\sqrt{\pi}} \mathrm{Im}\{(N_1+N_{-1})F_S^* + (F_1+F_{-1})N_0^*\}$$

$$t_{14} = 4\langle \mathrm{Im}\, Y_2^1 \sin\psi \rangle = -\sqrt{\frac{3}{5\pi}} \mathrm{Im}\{(N_1+N_{-1})F_0^* + (F_1+F_{-1})N_0^*\}$$

$$t_{15} = 4\langle \mathrm{Im}\, Y_2^2 \sin\psi \rangle = -\sqrt{\frac{6}{5\pi}} \mathrm{Im}\{N_1 F_{-1}^* - N_{-1} F_1^*\}$$

Table V-1 Relations between production moments and helicity amplitudes for S and P waves

$$t_1 = \langle \mathrm{Re}\, Y_0^0 \rangle = \frac{1}{\sqrt{4\pi}} \{|g_S|^2+|h_S|^2+|g_0||+|h_0|^2+|g_U|^2+|h_U|^2+|g_N|^2+|h_N|^2\}$$

$$t_2 = \langle \mathrm{Re}\, Y_1^0 \rangle = \frac{1}{\sqrt{\pi}} \mathrm{Re}\{g_0 g_S^* + h_0 h_S^*\}$$

$$t_3 = 2\langle \mathrm{Re}\, Y_1^1 \rangle = \sqrt{\frac{2}{\pi}} \mathrm{Re}\{g_U g_S^* + h_U h_S^*\}$$

$$t_4 = \langle \mathrm{Re}\, Y_2^0 \rangle = \frac{1}{\sqrt{20\pi}} \{2|g_0|^2+ 2|h_0|^2-|g_U|^2-|h_U|^2-|g_N|^2-|h_N|^2\}$$

$$t_5 = 2\langle \mathrm{Re}\, Y_2^1 \rangle = \sqrt{\frac{6}{5\pi}} \mathrm{Re}\{g_U g_0^* + h_U h_0^*\}$$

$$t_6 = 2\langle \mathrm{Re}\, Y_2^2 \rangle = \sqrt{\frac{3}{10\pi}} \{|g_U|^2+|h_U|^2-|g_N|^2-|h_N|^2\}$$

$$t_7 = 2\langle \mathrm{Re}\, Y_0^0 \cos\psi \rangle = \frac{1}{\sqrt{4\pi}} \{|g_S|^2-|h_S|^2+|g_0|^2-|h_0|^2+|g_U|^2-|h_U|^2-|g_N|^2+|h_N|^2\}$$

$$t_8 = 2\langle \mathrm{Re}\, Y_1^0 \cos\psi \rangle = \frac{1}{\sqrt{\pi}} \mathrm{Re}\{g_0 g_S^* - h_0 h_S^*\}$$

$$t_9 = 4\langle \mathrm{Re}\, Y_1^1 \cos\psi \rangle = \sqrt{\frac{2}{\pi}} \mathrm{Re}\{g_U g_S^* - h_U h_S^*\}$$

$$t_{10} = 2\langle \mathrm{Re}\, Y_2^0 \cos\psi \rangle = \frac{1}{\sqrt{20\pi}} \{2|g_0|^2-2|h_0|^2-|g_U|^2+|h_U|^2+|g_N|^2-|h_N|^2\}$$

$$t_{11} = 4\langle \mathrm{Re}\, Y_2^1 \cos\psi \rangle = \sqrt{\frac{6}{5\pi}} \mathrm{Re}\{g_U g_0^* + h_U h_0^*\}$$

$$t_{12} = 4\langle \mathrm{Re}\, Y_2^2 \cos\psi \rangle = \sqrt{\frac{3}{10\pi}} \{|g_U|^2-|h_U|^2+|g_N|^2-|h_N|^2\}$$

$$t_{13} = 4\langle \mathrm{Im}\, Y_1^1 \sin\psi \rangle = -\sqrt{\frac{2}{\pi}} \mathrm{Re}\{g_N g_S^* - h_N h_S^*\}$$

$$t_{14} = 4\langle \mathrm{Im}\, Y_2^1 \sin\psi \rangle = -\sqrt{\frac{6}{5\pi}} \mathrm{Re}\{g_N g_0^* - h_N h_0^*\}$$

$$t_{15} = 4\langle \mathrm{Im}\, Y_2^2 \sin\psi \rangle = -\sqrt{\frac{6}{5\pi}} \mathrm{Re}\{g_N g_U^* - h_N h_U^*\}$$

Table V-2 Relations between production moments and transversity amplitudes corresponding to natural and unnatural parity exchange for S and P waves.

$$
\begin{aligned}
g_S^2 + 3g_0^2 &= \sqrt{\pi}\,(t_1 + t_7) + \sqrt{5\pi}\,(t_4 + t_{10}) = C_1 \\
g_0^2 - 2g_U^2 &= \sqrt{\frac{5\pi}{4}}\,(t_4 + t_{10}) - \sqrt{\frac{5\pi}{24}}\,(t_6 + t_{12}) = C_2 \\
g_0 g_S \cos\gamma_{S0} &= \sqrt{\frac{\pi}{4}}\,(t_2 + t_8) = C_3 \qquad \text{---V-4-1} \\
g_U g_S \cos\gamma_{US} &= \sqrt{\frac{\pi}{8}}\,(t_3 + t_9) = C_4 \\
g_U g_0 \cos\gamma_{U0} &= \sqrt{\frac{5\pi}{24}}\,(t_5 + t_{11}) = C_5
\end{aligned}
$$

where the g_U, g_0 and g_S denote the magnitudes of the transversity amplitudes and γ_{S0}, γ_{U0} and γ_{US} their relative phases. The set of equations V-4-1 can, by substituting $\gamma_{US} = \gamma_{U0} - \gamma_{S0}$, be transformed into a cubic equation in $z = g_0^2$:

$$
3z^3 - (C_1+3C_2)z^2 + (C_1C_2+2C_4^2+C_3^2-6C_5^2)z + (2C_1C_5^2-4C_3C_4C_5-C_2C_3^2) = 0
\qquad \text{---V-4-2}
$$

In their amplitude analysis in the region of the ρ meson, Estabrooks and Martin[7] arrive at a cubic equation of the same form. Their analysis made use of the data of an earlier experiment[8] measuring the reaction I-1 on a hydrogen target, and was based on the supposed absence of A_1 exchange contributions. It is easily verified that, when only the polarization independent moments are measured, and the g and h amplitudes are equal (which would be the case for vanishing A_1 exchange amplitudes) one arrives at a cubic equation of the same form as eq. V-4-2.

In general we would obtain 3 solutions from the cubic equation V-4-2, but one of these solutions is unphysical. The set of equations V-4-1 leads therefore to two ambiguous solutions for the magnitudes g_S, g_0 and g_U and their relative phases. For the h amplitudes a similar set of equations can be found, which leads to two solutions for h_S, h_0 and h_U and their relative phases. Without the natural parity exchange amplitudes g_N and h_N determined, we have therefore at most 4 ambiguous solutions.

From the relations in table V-2, two further equations can be formed:

$$
\begin{aligned}
g_U^2 - h_N^2 &= \sqrt{\frac{5\pi}{6}}\,(t_6 + t_{12}) = C_7 \\
h_U^2 - g_N^2 &= \sqrt{\frac{5\pi}{6}}\,(t_6 - t_{12}) = C_8
\end{aligned}
\qquad \text{---V-4-3}
$$

For every one of the existing solutions, this gives only one solution for h_N and g_N. The only two quantities which are left undetermined therefore are γ_{N0} and χ_{N0}, the phase between g_N and g_0 and the phase between h_N and

h_0 respectively. From the relations in table V-2 we form the following set of equations:

$$g_N g_S \cos\gamma_{NS} - h_N h_S \cos\chi_{NS} = -\sqrt{\frac{\pi}{2}}\, t_{13} = C_9$$

$$g_N g_0 \cos\gamma_{NO} - h_N h_0 \cos\chi_{NO} = -\sqrt{\frac{5\pi}{6}}\, t_{14} = C_{10} \qquad \text{---V-4-4}$$

$$g_U g_N \cos\gamma_{UN} - h_U h_N \cos\chi_{UN} = -\sqrt{\frac{5\pi}{6}}\, t_{15} = C_{11}$$

where $\gamma_{NS} = \gamma_{NO} - \gamma_{SO}$ $\qquad \chi_{NS} = \chi_{NO} - \chi_{SO}$

$\gamma_{UN} = \gamma_{UO} - \gamma_{NO}$ $\qquad \chi_{UN} = \chi_{UO} - \chi_{NO}$

The equations V-4-4 contain only two unknowns, γ_{NO} and γ_{NO}. When solving these equations, two solutions result, for γ_{NO} and two for γ_{NO}. The set of equations V-4-3 however, is overdetermined, so one sign ambiguity vanishes by taking the solutions with the best χ^2.

Solving the equations of table V-2 analytically therefore leads to at most eight ambiguous solutions. Experimentally, some of these ambiguous solutions might vanish because they are indistinguishable within the experimental errors. To select physical solutions, there is furthermore the powerful tool of requiring the amplitudes and phases to be continuous as a function of the dipion mass $m_{\pi\pi}$ and the four momentum transfer t.

REFERENCES (Chapter V)

1) M.Jakob and G.C.Wick, Ann. of Phys. 7 (1959) 404.

2) A. Kotanski, Acta Physica Polonica 29 (1966) 699.

3) R.J.N.Phillips and R.P.Worden, "Polarization in Strong Interactions at High Energy", Rutherford High Energy Laboratory report RL-73-088 (1973).

4) B.R.Martin, D.Morgan and G.Shaw: "Pion-Pion Interactions in Particle Physics", Academic Press, New York 1976.

5) J.P.Ader, M.Capdeville, G. Cohen Tannoudji and Ph.Salin, Nuovo Cimento 56A (1968) 952.

6) A.D.Martin and T.D.Spearman: "Elementary Particle Theory", North Holland, Amsterdam 1970.

7) P.Estabrooks and A.D.Martin, Phys. Lett. 41B (1972) 350
and:
P.Estabrooks, A.D.Martin, G.Grayer, B.Hyams, C.Jones, P.Weilhammer, W.Blum, H.Dietl, W.Koch, E.Lorenz, G.Lütjens, W.Männer, J.Meissburger and U.Stierlin, Int. Conf. on $\pi\pi$ Scattering and Associated Topics, Tallahassee, 1973 (eds. P.K.Williams and V.Hagopian) AIP Conf. Proc. 13 New York (1973) p.37.

8) G.Grayer, B.Hyams, C.Jones, P.Schlein, P.Weilhammer, W.Blum, H.Dietl, W.Koch, E.Lorenz, G.Lütjens, W.Männer, J.Meissburger, W.Ochs and U.Stierlin, Nucl. Physics B75 (1974) 189.

CHAPTER VI RESULTS

In this chapter some of the results of the experiment are presented. The emphasis will be on the $\pi^+\pi^-$ invariant mass region of the rho meson. For this data sample it is assumed that the dipion system can be fully described in terms of s and p waves only.

In the first section some striking features of the raw data will be discussed. It is shown that, even before acceptance correction, a sizable nucleon polarization effect is indicated by the data. In section 2 the normalization procedure of the polarization dependent moments $\langle \mathrm{Re}\ Y_\ell^m \cos\psi \rangle$ and $\langle \mathrm{Im}\ Y_\ell^m \sin\psi \rangle$ is discussed. In section 3 the acceptance corrected moments of the $\pi^+\pi^-$ decay angular distribution are presented and discussed. Moments are given for data obtained both with the hydrogen calibration target and the butanol polarized target. The polarization dependent moments show large non-zero effects. In order to explain these effects, we need amplitudes corresponding to the exchange of an object with the quantum numbers of the A_1, in addition to the well known π and A_2 exchange contributions. In section 4 results are presented of a model independent amplitude analysis. From this, more quantitative statements can be derived about the importance of the A_1 exchange contributions. In section 5 we compare our results regarding the rank of the $\pi^+\pi^-$ final state density matrix with an earlier model independent analysis of previous hydrogen data. In section 6 we discuss the result of a Regge model fit to the data. It is shown that a conventional Regge model which includes π, A_2 and A_1 exchange amplitudes plus absorption effects, describes the data very well. Finally, in section 7, the consequences of our findings for the published $\pi^+\pi^-$ phase shifts will be discussed.

VI-1 Raw Data Spectra

In this section some of the features of the raw experimental data are discussed. It is shown that even before any corrections, in particular acceptance corrections, have been applied, important conclusions can be drawn.

In fig.VI-1 the distribution of the missing mass squared (MM^2) is given for the 39,459 events measured with the hydrogen calibration target.

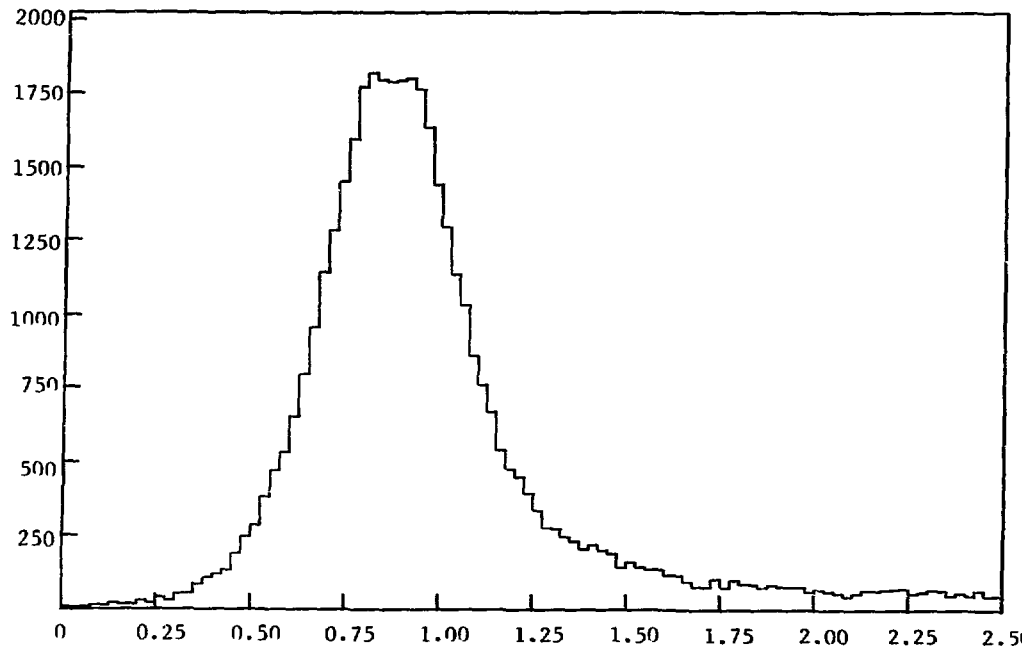

Fig.VI-1 Missing Mass Squared Distribution for Hydrogen events

→ $MM^2(GeV^2)$

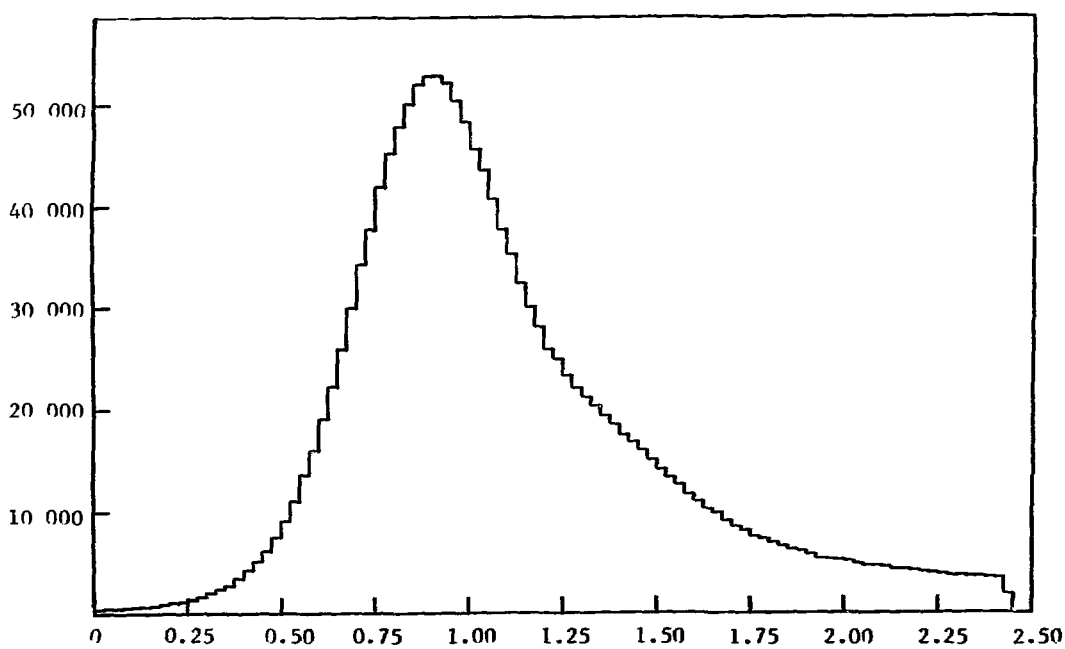

Fig.VI-2 Missing Mass Squared Distribution for Butanol events

→ $MM^2(GeV^2)$

The distribution appears to be nearly symmetric around the square of the neutron mass, but a slight tail is seen towards higher values of the MM^2. The latter is attributed to a small inefficiency of the target veto counter system. Neglecting all events with a MM^2 greater than 1.3 GeV^2, the distribution can be fitted by a gaussean with a width $\sigma(MM^2)$ = 0.197 GeV^2. This is in reasonable agreement with the predicted width of 0.180 GeV^2 as determined in a Monte Carlo resolution study (see Chapter III).

Fig.IV-2 shows the MM^2 distribution for the 1,527,569 events measured with the butanol polarized target. This distribution is strongly asymmetric, with a large excess of events at high values of the MM^2. The asymmetry of the distribution is independent of the $\pi^+\pi^-$ invariant mass, but is strongly t-dependent, as is shown in figs.VI-3 and VI-4, showing the MM^2 distribution for $-t < 0.001$ and $-t > 0.2$ GeV^2 respectively.

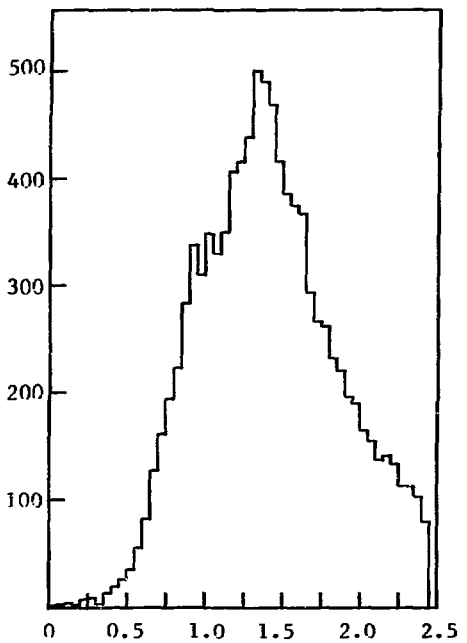

Fig.VI-3 MM^2 distribution for $t<0.001$ GeV^2

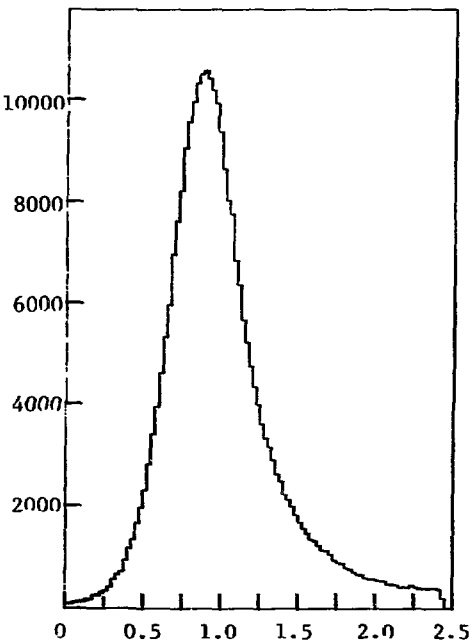

Fig.VI-4 MM^2 distribution for $t>0.2$ GeV^2

Since this effect is not observed for the hydrogen events, veto counter inefficiency can be excluded as a possible source. Both the hydrogen and the butanol target were operated in the same cryostat under identical experimental conditions. The asymmetry therefore must be due to the use of a different target material. The interaction probability in the butanol target is larger (approximately a factor 5) than in the hydrogen target. This difference, however, is too small to explain the asymmetry of the MM^2 by multiple interactions in the target. We therefore have to look for alternative explanations. Two obvious hypotheses to explain the shape of the MM^2 distribution for butanol events have to be rejected.

(a) The process

$$\pi^- \, {}^{12}C \rightarrow \pi^-\pi^+ \, {}^{12}B$$

causes a shift in the expectation value for the MM^2, the mass difference between ^{12}C and ^{12}B being not the same as that of the proton and the neutron. This shift is much smaller however than the effect we observe in the MM^2 distribution for butanol events.

(b) For the process:

$$\pi^- \, {}^{12}C \rightarrow \pi^-\pi^+ n \, {}^{11}B$$

the MM^2 distribution is expected to be different from the same distribution for hydrogen events because of the Fermi motion of the bound protons in the carbon nucleus. Monte Carlo studies[1]) were carried out to get an estimate of the size of this difference. Although the expectation value for the MM^2 is slightly shifted (0.903 GeV^2 as compared to m_n^2 = 0.883 GeV^2 for hydrogen events), the width of the distribution is hardly affected.

The only other explanation we may think of is that excited nuclei are formed in the target which decay in a mode not detected by our veto counters. We stress, however, that the exact nature and magnitude of this background remain unclear, but, as we will show in the following, it has no influence on our measurement of the polarization dependent observables. let us assume that the effect is due to interactions on the complex nuclei in the target. Then, since the protons (and neutrons) bound in carbon and oxygen are not polarized, no interference with the measurement of the polarization dependent observables should occur. It is therefore interesting to verify if in the background events nucleon polarization effects are indeed absent.

A nuclear polarization effect should manifest itself as a non-flat distribution of the polarization angle ψ. However, since we are dealing with raw data spectra at this stage, structure in the ψ-distribution for one target polarization direction alone does not necessarily prove a nuclear polarization effect. The acceptance of the spectrometer is not uniform in ψ, so that the structure could be due to the acceptance losses. A nucleon polarization effect is present however, if a clear difference is observed between the two distributions measured with opposite target polarization directions. Here we recall that, in order to reverse the target polarization direction, only the frequency was changed of the microwaves going into the target. Figs.VI-5 and VI-6 show the distributions of ψ for events with positive and negative target polarization respectively. A missing mass cut ($MM^2 < 1.4$ GeV^2) has been imposed. A large difference between the two distributions is obvious. The nuclear polarization effect is appreciably larger than suggested by the difference between the two figures. A large ($\sim$60%) unpolarized background is present due to events off unpolarized protons bound in complex nuclei. Figs.VI-7 and IV-8 show the same distributions, but for events with $MM^2 > 1.4$ GeV^2. No significant difference is seen between these two distributions. This confirms our assumption that the background at high values of the MM^2 is due to events off unpolarized protons. This is demonstrated even more clearly using the asymmetry parameter

$$A = \frac{n_l - n_r}{n_l + n_r}$$

where n_l and n_r are defined as the numbers of $\pi^+\pi^-$ pairs to the left (right) of a plane defined by the beam direction and the positive target polarization direction. Thanks to the large statistics of the experiment, we are able to calculate this asymmetry for different bins in MM^2. If it is true that the nucleon polarization effect is solely due to genuine events of the reaction I-1 off polarized protons, then the MM^2 distribution, multiplied bin-by-bin by the asymmetry parameter A should give a clean symmetric peak around the square of the neutron mass. In fig.VI-9 the MM^2 distribution is given again for all butanol events, this time in 25 bins. Fig.VI-10 shows the same distribution multiplied with the left-right asymmetry, the units on the vertical scale are arbitrary. In the latter figure a clean symmetric neutron signal is seen with no appreciable background. This conclusively shows that, whatever the nature of the background, it does not interfere with the measurement of the polarization dependent observables.

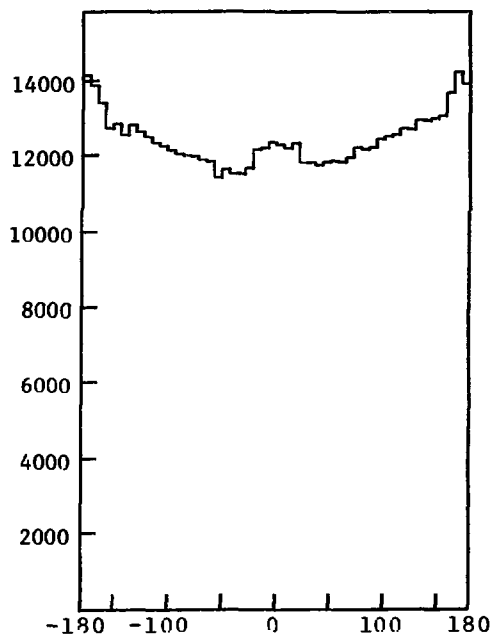

Fig.VI-5 ψ distribution for Positive Polarization $MM^2<1.4$ GeV^2

$\rightarrow$ ψ (degrees)

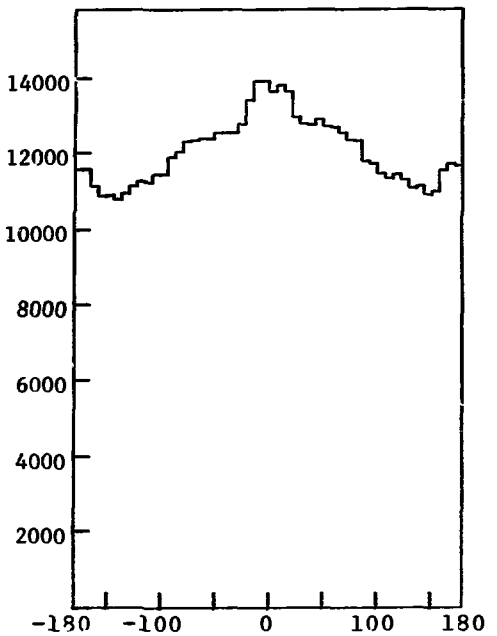

Fig.VI-6 ψ distribution for Negative Polarization $MM^2<1.4$ GeV^2

$\rightarrow$ ψ (degrees)

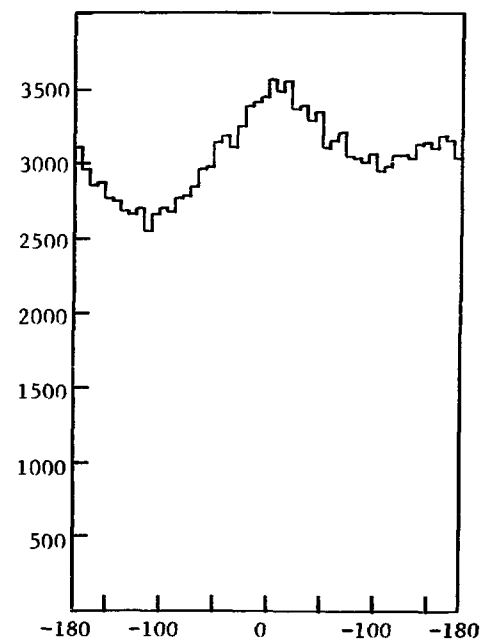

Fig.VI-7 ψ distribution for Positive Polarization $MM^2>1.4$ GeV^2

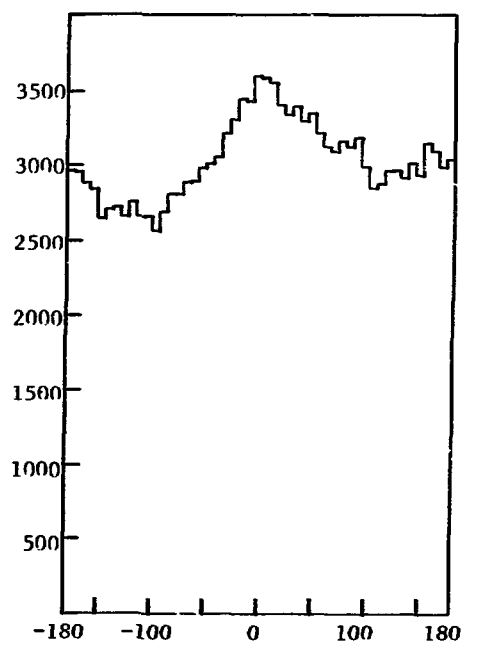

Fig.VI-8 ψ distribution for Negative Polarization $MM^2>1.4$ GeV^2

The fit of a Gaussian curve to the distribution in fig.VI-10, neglecting all events with $MM^2 > 1.4\ GeV^2$ results in $\sigma(MM^2) = 0.191\ GeV^2$, which is again in good agreement with the width of the MM^2 distribution obtained from the resolution study. For all further analysis, unless stated otherwise, a cut in MM^2 at $1.4\ GeV^2$ has been applied.

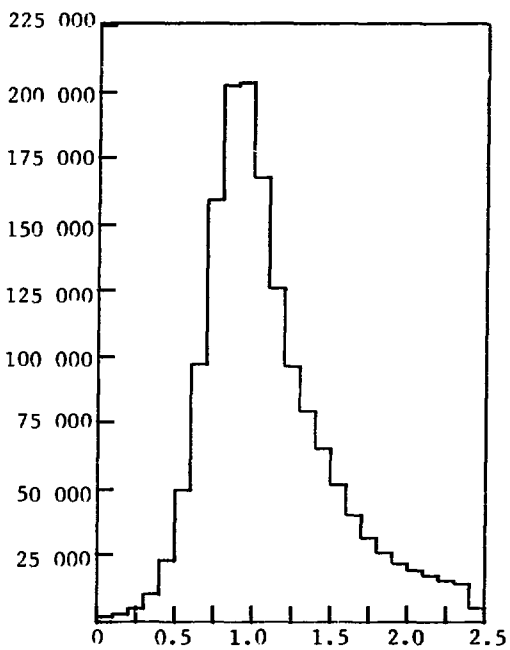

Fig.VI-9 MM^2 distribution for Butanol events

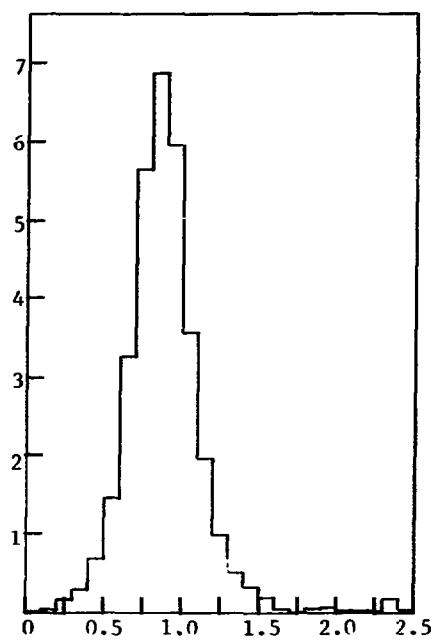

Fig.VI-10 MM^2 distribution for Butan events, multiplied with left-right asymmetry.

Fig.VI-11 shows the $\pi^+\pi^-$ invariant mass distribution for events measured using the hydrogen calibration target. The ρ, f and g resonances are clearly visible. The same distribution for events produced in the butanol polarized target is shown in fig.VI-12. Taking into account the difference in statistical significance, the two distributions appear to be indistinguishable. This is remarkable in view of the fact that in butanol about 60% of all events are produced off protons bound in oxygen and carbon nuclei.

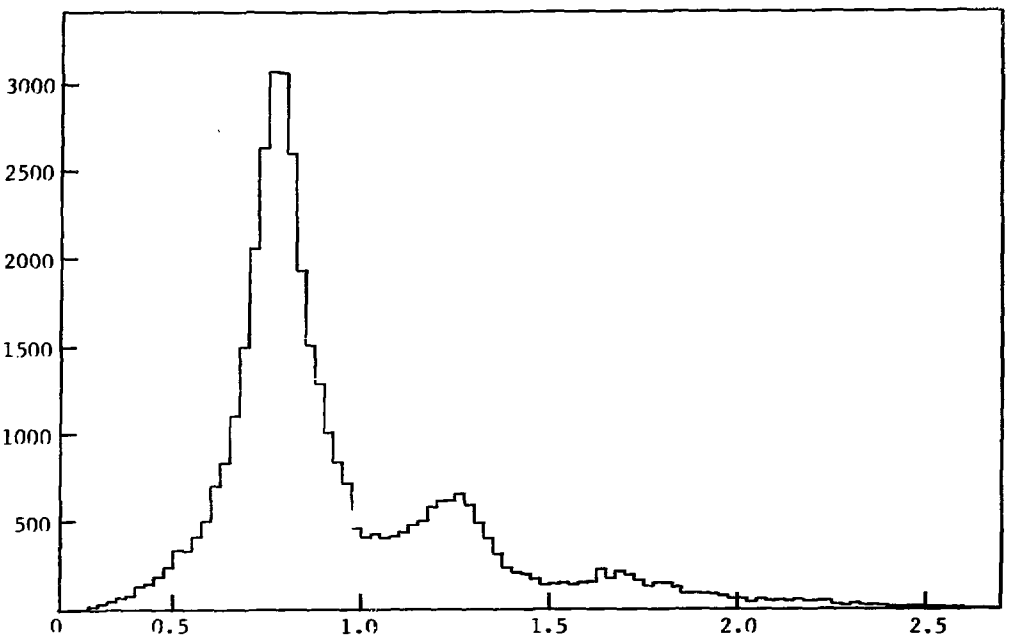

Fig.VI-11 $\pi^+\pi^-$ Invariant Mass Distribution for Hydrogen events

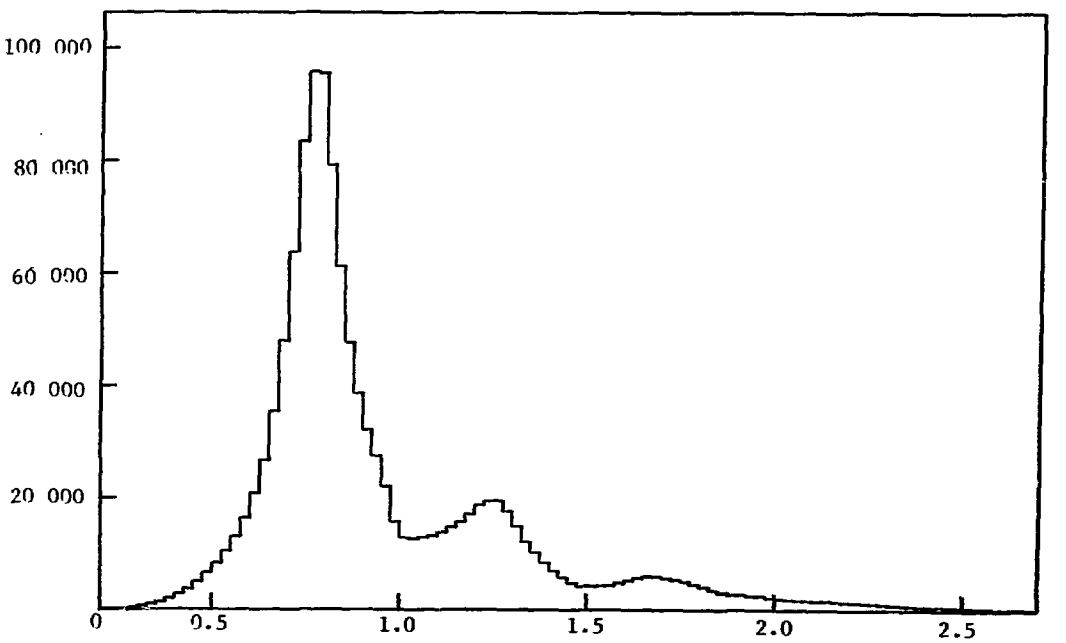

Fig.VI-12 $\pi^+\pi^-$ Invariant Mass Distribution for Butanol events

VI-2 Normalization of the Polarization Dependent Moments

In order to do the amplitude analysis which was proposed in Chapter V, the data of two different experiments had to be combined. The polarization dependent moments $\langle \mathrm{Re}\ Y_\ell^m \cos\psi \rangle$ and $\langle \mathrm{Im}\ Y_\ell^m \sin\psi \rangle$ were taken from the present experiment, while the polarization independent moments $\langle \mathrm{Re}\ Y_\ell^m \rangle$ were taken from a previous experiment on hydrogen[2]). The reason for this is that, unlike the polarization dependent moments, the polarization independent moments cannot be extracted from the present experiment without contamination due to the carbon and oxygen nuclei in the target. When combining two different experiments the problem is to get the proper relative normalization. This means that one has to rely on the correct determination of the cross section in both experiments. The cross section is given by the expression:

$$\sigma = w \frac{N_e}{N_t \cdot N_b} = w \cdot \sigma_1 \cdot N_e \quad (\mathrm{cm}^2)$$

where

N_e is the number of events produced on (polarized) protons
N_t " " " " (polarized) target protons per cm^2
N_b " " " " beam particles entering the target
σ_1 " " cross section for one produced event
w " a weight factor which corrects for all known losses and inefficiencies which were independent of event topology. Corrections for acceptance losses and other topology dependent corrections are included in N_e.

The correct determination of the cross section therefore depends on a proper determination of N_b, N_t and of all possible losses and inefficiencies contributing to w. For the hydrogen experiment, the normalization factor $w \cdot \sigma_1$ was determined to be 0.106 ± 0.005 nb [2]). We will discuss the determination of the corresponding normalization factor for the polarized target experiment here in some detail.

During the experiment summaries of counting rates were recorded on the data tapes. Using rates records which were taken during particularly stable running conditions the total number of incident π^- was determined to be:

$$N_b = (3.95 \pm 0.01) \cdot 10^{10} .$$

In order to determine the number of polarized target protons per cm^2 the target butanol was weighed at the end of the experiment. Using the

Table VI-1 Geometry Independent Corrections

Source	Loss (%)	Comments
1 Beam Contamination		
muons	2.5 ± 2.0	measured
electrons	0.4 ± 0.2	measured
2 Interaction loss in front of Target		
B_2,B_3 counters	0.5 ± 0.1	estimate
Cryostat wall	1.9	known material, thickness
3 Electronics, trigger Counters		
Array overefficiency	1.8 ± 0.1	from calibration data
Array inefficiency	3.8 ± 0.2	from calibration data
Anticounter deadtime	2.9 ± 0.5	rates summaries
4 Reconstruction, Trigger efficiency		
Reconstruction loss	2.5 ± 0.3	resolution study (see Ch.III)
Chamber inefficiency	2.8 ± 0.5	program diagnostics
Extra beam tracks	8.6 ± 1.5	program diagnostics
5 Secondary Interaction		
Interaction in chambers, counters etc.	5.6 ± 0.3	see table VI-2
6 Other		
K^+K^-, $p\bar{p}$ contamination	-0.7 ± 0.1	Cerenkov efficiency below threshold
MM^2 cut	0.6 ± 0.1	
Beam missing target	10.5 ± 0.5	beam distribution at target

Material	Length/Thickness(cm)	Interaction Length(cm)	Loss(%)
Copper	0.0384	9.3	0.41
Scintillator	0.5	55.2	0.9
Mylar	0.276	42.1	0.65
Aclar	0.12	30.0	0.4
Helium	241	230 000	0.1
Neon	154	80 000	0.19
Air	100	53 620	0.19
Paper/Polyetylene	0.024	55	0.04

Table VI-2 Material between Target and Counter Hodoscope

dimensions of the target, a butanol filling factor of 0.59 was determined, in agreement with the expected value of 0.6 [3]). Taking into account the average degree of target polarization (68%) the number of polarized protons per cm^2 was determined to be:

$$N_t = (2.79 \pm 0.28) \cdot 10^{23}\ cm^{-2}$$

The error quoted is mainly due to the uncertainties in the dimensions of the target. The weight factor w lumps together corrections for all known losses and inefficiencies which are not yet accounted for in N_e. Table VI-1 lists the individual contributions with a short description of how the corrections were determined. Table VI-2 gives a breakdown of the total amount of material between the target and the scintillator array EG (fig.II-1) and the corresponding losses due to secondary interaction (the correction for secondary interaction in the target was treated in Chapter III and accounted for in N_e). The data for the interaction lengths has been taken from ref.[4]); where no published values were available estimated values were used. From the values quoted in table VI-1, the overall weight factor w was determined to be

$$w = 1.53 \pm 0.06$$

The normalization factor $w \cdot \sigma_1$ for the polarization dependent moments therefore becomes:

$$w \cdot \sigma_1 = 0.139 \pm 0.015\ nb\ .$$

In order to obtain normalized polarization dependent moments, both sets of unnormalized moments (polarization independent moments from the hydrogen experiment and polarization dependent moments from the present experiment) are multiplied by their appropriate normalization factors $w \cdot \sigma_1$. The full set of moments is then normalized such that $\langle Y_0^0 \rangle = \frac{1}{\sqrt{4\pi}}$.

VI-3 The Moments of the Angular Distribution

During part of the experiment a 10 cm hydrogen target was installed in the cryostat which normally housed the butanol target. For the limited amount of calibration data obtained with this target, the moments of the $\pi^+\pi^-$ decay angular distribution have been determined. The comparison of these moments with the moments obtained during the previous experiment on hydrogen at the same beam momentum, reveals to what extent we were able to

reproduce these results. For the two experiments the spectrometer for the charged secondary particles was essentially the same, but for the present experiment the geometry of the target region changed significantly by the introduction of the polarized target (and target magnet). A new target veto counter system was installed.

Fig.VI-13 shows the t-dependence of the normalized moments of the $\pi^+\pi^-$ decay angular distribution for events obtained from the hydrogen target. As a reference frame the t-channel helicity frame (Gottfried Jackson frame) has been chosen; the $\pi^+\pi^-$ mass range was taken around the peak of the rho meson: $0.71 < m_{\pi\pi} < 0.83$ GeV. Fig.VI-14 shows the same moments but now from the large statistics hydrogen experiment[2]). In both cases the moments are normalized such that $\langle Y_0^0 \rangle = 1/\sqrt{4\pi}$. Clearly the statistical significance of the present experiment is inferior, but within statistics the agreement is good. We therefore conclude that no systematic effects are introduced by the change in the experimental setup and the corresponding different method of analysis.

Although it was never the intention to use the polarization independent moments $\langle \mathrm{Re}\ Y_\ell^m \rangle$ from the polarized target experiment for our analysis, it is neverthless interesting to compare these moments with the moments off hydrogen. In fig.VI-15 the t-channel helicity moments $\langle \mathrm{Re}\ Y_\ell^m \rangle$ are given as a function of t in the rho mass region $0.71 < m_{\pi\pi} < 0.83$ GeV for events produced in the butanol target. A systematic difference with the moments off hydrogen (fig.VI-14) is seen in the lowest three or four t-bins. At higher t-values there appears to be no difference between the two sets of moments. This indicates that the background process at low t-values, which also gives rise to the widening of the MM^2 distribution, seriously distorts the moments. The fact however that at higher values of t no difference is seen between the hydrogen and butanol data is a very interesting observation. It indicates the possibility to study spectroscopy using nuclear targets.

The formal definition of the acceptance corrected polarization dependent moments which are presented next, is given by the following expression:

$$\langle \mathrm{Re}\ Y_\ell^m \cos\psi \rangle \equiv \frac{1}{2\pi} \int_\Omega \int_\psi I_{pr}(\Omega,\psi)\ \mathrm{Re}\ Y_\ell^m(\Omega)\cos\psi\ d\Omega d\psi$$

$$\langle \mathrm{Im}\ Y_\ell^m \sin\psi \rangle \equiv \frac{1}{2\pi} \int_\Omega \int_\psi I_{pr}(\Omega,\psi)\ \mathrm{Im}\ Y_\ell^m(\Omega)\sin\psi\ d\Omega d\psi$$

where $I_{pr}(\Omega,\psi)$ is the produced $\pi^+\pi^-$ decay angular distribution for a given $m_{\pi\pi}$,t bin.

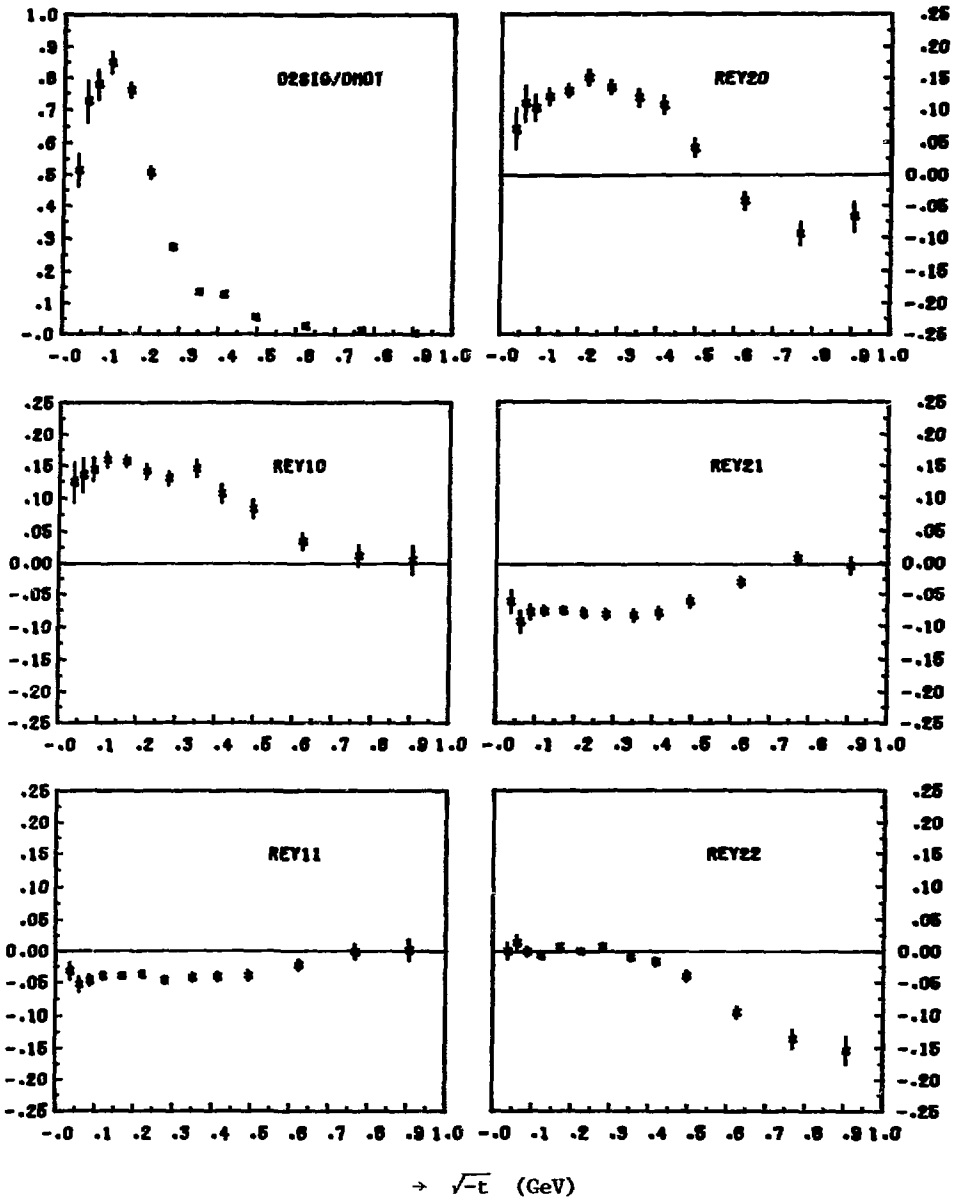

Fig.VI-13 t-dependence of the normalized t-channel moments measured with the hydrogen calibration target. ($0.71 < m_{\pi\pi} < 0.83$ GeV)

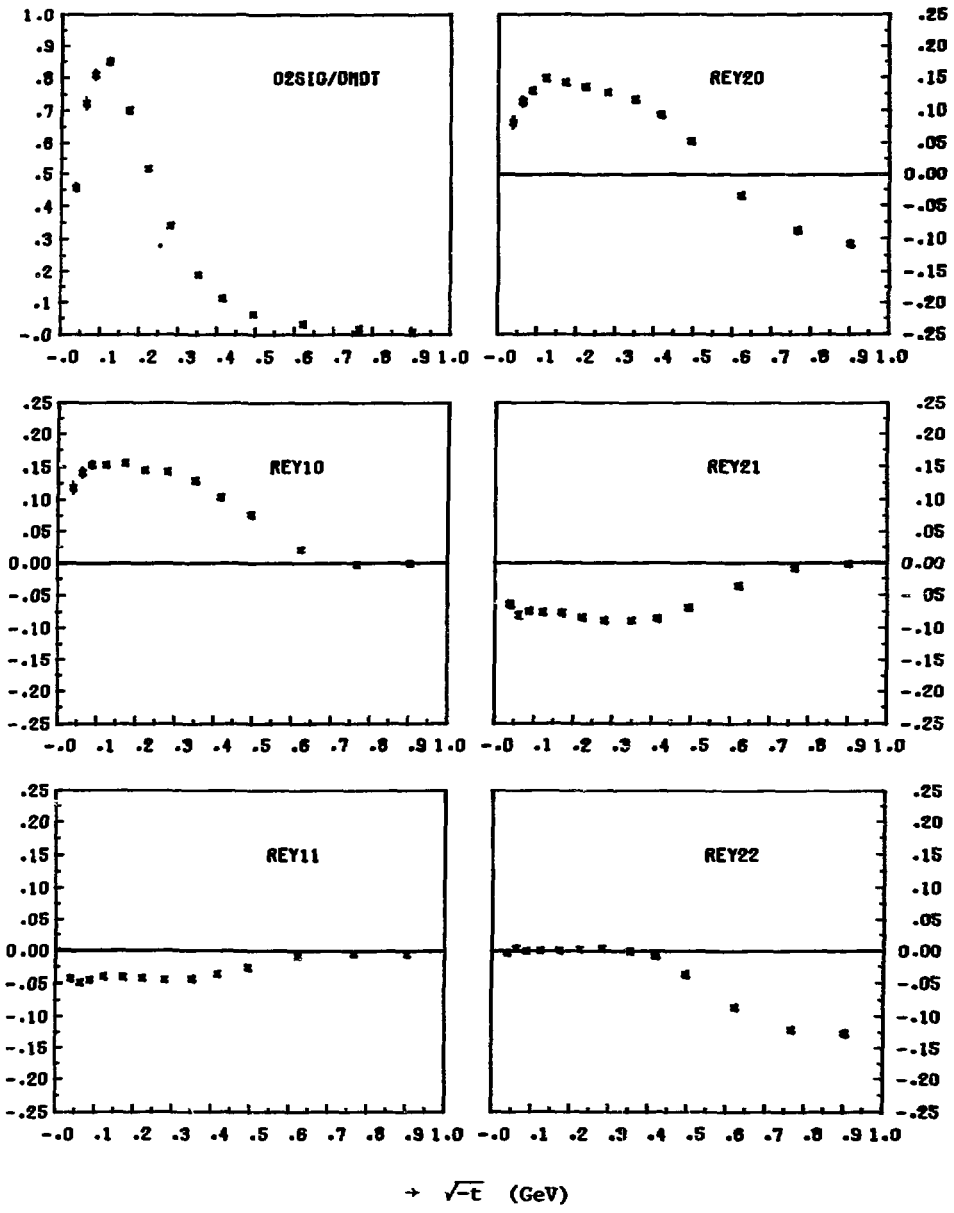

Fig. VI-14 t-dependence of the normalized t-channel moments as measured by a previous experiment using a hydrogen target. ($0.71 < m_{\pi\pi} < 0.83$ GeV)

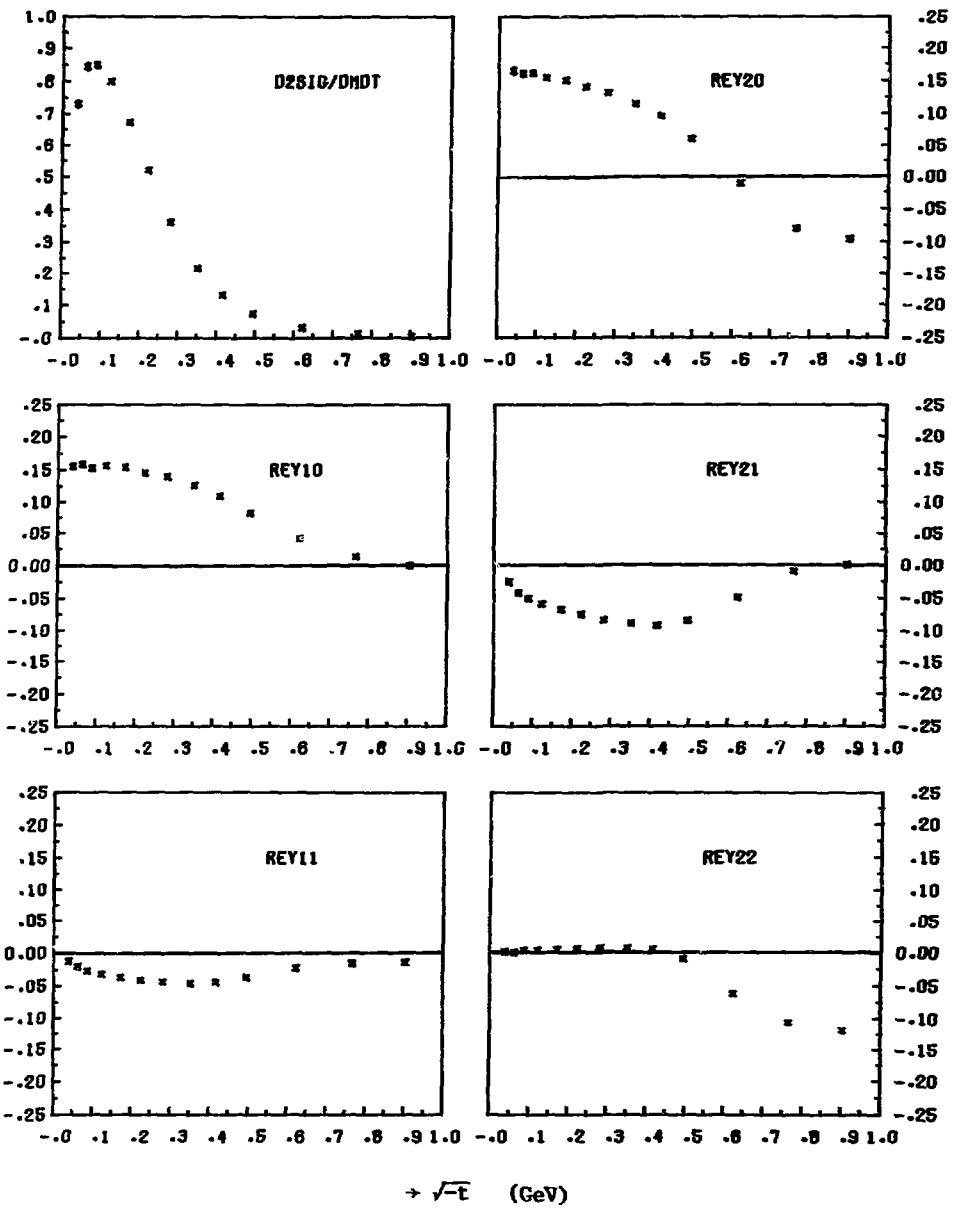

Fig. VI-15 t-dependence of the normalized t-channel polarization independent moments measured with the butanol target. ($0.71 < m_{\pi\pi} < 0.83$ GeV)

The normalization $\langle Y_0^0 \rangle = \frac{1}{\sqrt{4\pi}}$ is used throughout.

Fig. VI-16 shows the t-dependence of the polarization dependent moments $\langle \mathrm{Re}\, Y_\ell^m \cos\psi \rangle$ and $\langle \mathrm{Im} Y_\ell^m \sin\psi \rangle$ in the $\pi^+\pi^-$ invariant mass region of the rho meson: $0.71 < m_{\pi\pi} < 0.83$ GeV. The t-channel helicity frame (Gottfried Jackson frame) for the $\pi\pi$ rest system is chosen. In calculating these moments ℓ_{max} and m_{max} were set to two, i.e. any contributions other than s- and p waves are neglected. We thus ignore the small d-wave contribution which is known[2]) to be present under the ρ. We do so in order to keep down the number of amplitudes in our amplitude analysis (sectionVI-4); preferring the small systematic error introduced by neglecting d-wave to the large statistical errors which would be the result of including d-wave contribution. Strikingly large non-zero effects are seen in several of the moments, even down to the lowest values of t. In particular $\langle \mathrm{Re}\, Y_0^0 \cos\psi \rangle$ shows a nucleon polarization effect of many standard deviations over almost the whole t-range. This is in clear contradiction with earlier assumptions about the production mechanism of our reaction. The low t region was supposed to be dominated by one pion exchange and should therefore exhibit little or no polarization effects[5]). It can be shown that the left-right asymmetry A of the pion pair with respect to a plane defined by the beam direction and the polarization vector is related to $\langle \mathrm{Re}\, Y_0^0 \cos\psi \rangle$ by the following expression:

$$A \equiv \frac{n_L - n_r}{n_L + n_r} = \frac{8}{\sqrt{\pi}} \langle \mathrm{Re}\, Y_0^0 \cos\psi \rangle$$

with the normalization $\langle \mathrm{Re}\, Y_0^0 \rangle = \frac{1}{\sqrt{4\pi}}$. The data in fig. VI-16 indicate that asymmetries as large as 0.4 are observed on a scale where the maximum is 1.

In order to give a quantitative interpretation of the data in terms of one particle exchange amplitudes a full amplitude analysis is required (see section VI-4). However, some qualitative remarks can already be made at this stage. From table V-2, in which the relations are given between the moments and the transversity amplitudes, it is seen that $\langle \mathrm{Re}\, Y_0^0 \cos\psi \rangle$, $\langle \mathrm{Re}\, Y_2^0 \cos\psi \rangle$ and $\langle \mathrm{Re}\, Y_2^2 \cos\psi \rangle$ are expressed in both natural and unnatural parity exchange amplitudes. The moments $\langle \mathrm{Re}\, Y_1^0 \cos\psi \rangle$, $\langle \mathrm{Re}\, Y_1^1 \cos\psi \rangle$ and $\langle \mathrm{Re}\, Y_2^1 \cos\psi \rangle$ however, are expressed in unnatural parity exchange amplitudes only. On the other hand, table V-1, which gives the same relations for

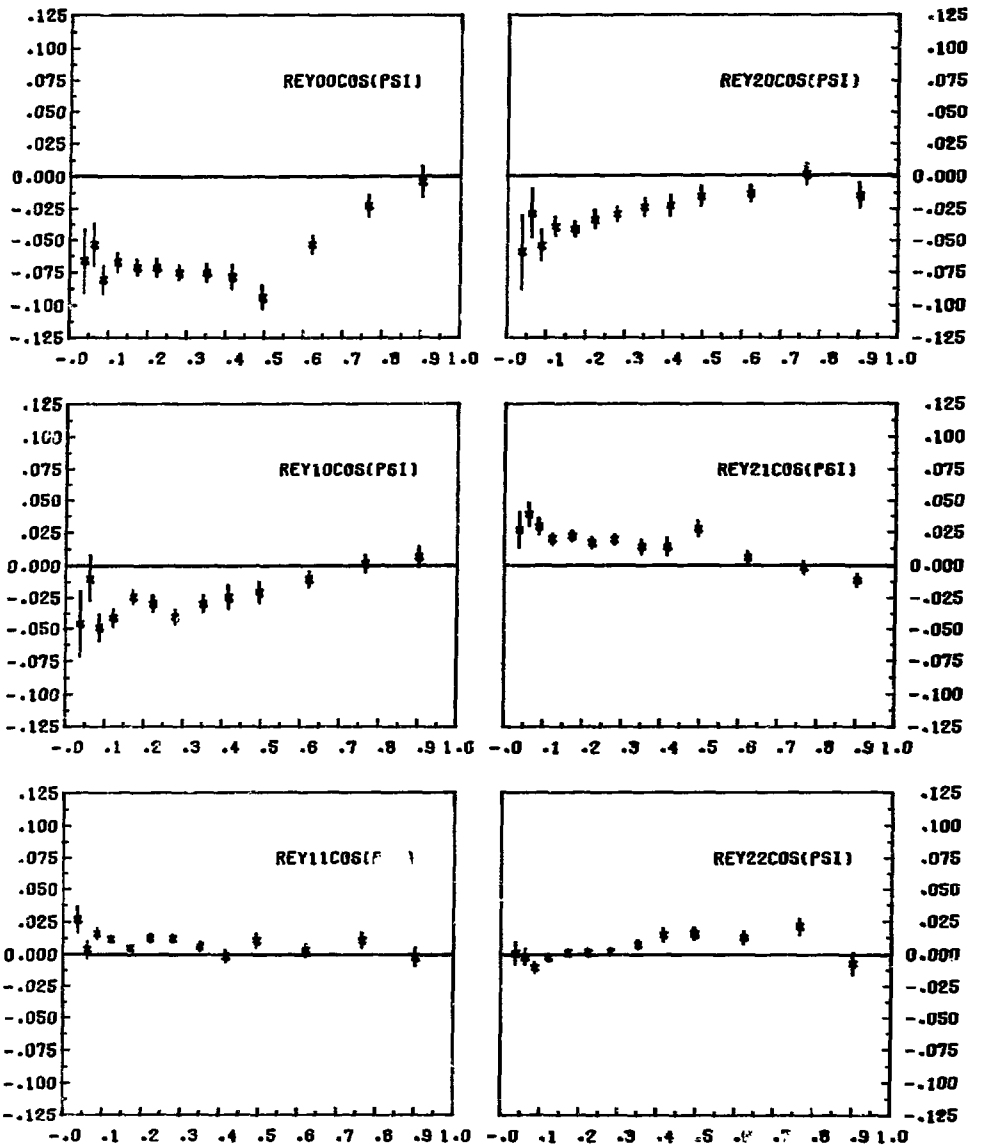

Fig.VI-16 t-dependence of the normalized t-channel polarization dependent moments. ($0.71 < m_{\pi\pi} < 0.83$ GeV)
a - "cosψ" moments

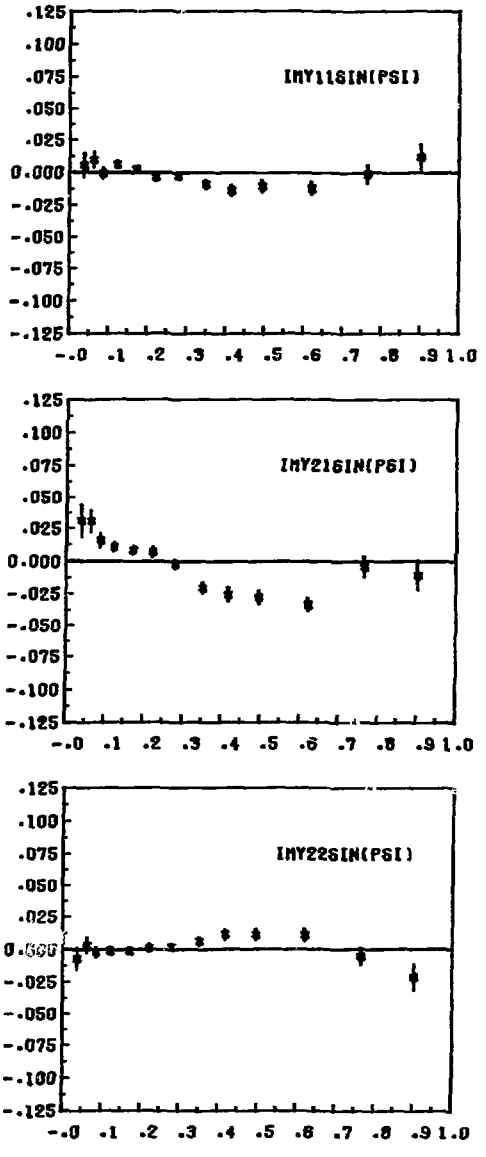

Fig.VI-16 t-dependence of the normalized t-channel polarization dependent moments ($0.71 < m_{\pi\pi} < 0.83$ GeV)

b - "sinψ" moments

the helicity amplitudes, shows that all polarization dependent moments are flip-noflip interference terms. This means that, in order to account for the nonzero effects in the moments $\langle \mathrm{Re}\ Y_1^0 \cos\psi \rangle$, $\langle \mathrm{Re}\ Y_1^1 \cos\psi \rangle$ and $\langle \mathrm{Re}\ Y_2^1 \cos\psi \rangle$ we need the simultaneous contribution of unnatural parity exchange flip and noflip amplitudes. We recall (ch. I-3) that π exchange leads to nucleon helicity flip while A_1 exchange would lead to nucleon helicity noflip (when the s-channel is used for the nucleon rest frames). Therefore, another way of stating this is that both pion exchange and the exchange of an object with the quantum numbers of the A_1 ("A_1 exchange") contribute. The three moments $\langle \mathrm{Im}\ Y_1^1 \sin\psi \rangle$, $\langle \mathrm{Im}\ Y_2^1 \sin\psi \rangle$ and $\langle \mathrm{Im}\ Y_2^2 \sin\psi \rangle$ are interference terms of natural and unnatural parity exchange amplitudes as can be seen from table V-2 The nonzero effects in these moments require the simultaneous presence of natural (i.e. A_2) and unnatural parity exchange amplitudes. From the above considerations we conclude therefore that a model for the production mechanism of the reaction I-1 should include amplitudes for both π and A_2 as well as A_1 exchange. Fig.VI-17 shows the mass dependence of the same set of polarization dependent moments for a t-interval between -0.005 and -0.2 GeV^2. A large polarization signal is present in several of these moments over the whole mass range ($0.6 < m_{\pi\pi} < 0.9$ GeV) considered. The non-zero effects in the moments $\langle \mathrm{Re}\ Y_1^0 \cos\psi \rangle$, $\langle \mathrm{Re}\ Y_1^1 \cos\psi \rangle$ and $\langle \mathrm{Re}\ Y_2^1 \cos\psi \rangle$ again require the presence of unnatural parity exchange spinflip and noflip amplitudes, i.e. both pion and A_1 exchange contributions. The three "$\sin\psi$" moments are compatible with zero over the whole mass range between 0.6 and 0.9 GeV^2. No conclusion about A_2 exchange contribution can be drawn for this t interval. Apparently the "$\sin\psi$" moments average out between $-t = 0.005$ and $-t = 0.2$ GeV^2 as suggested by their t-dependence in the ρ-region (fig.VI-16).

VI-4 Results of the Amplitude Analysis

In Chapter V we derived a set of relations between the observable moments and the transversity amplitudes. These relations are given explicitly in table V-2 for the case that only s- and p-waves contribute. It was pointed out that this set of equations can be solved analytically and that up to 8 ambiguous solutions could be expected. It is possible to solve the equations in table V-2 using a χ^2 minimization technique alone, since the relations V-2 contain 15 measured moments and 14 unknown quantities. However, where up to 8 ambiguous solutions are possible,

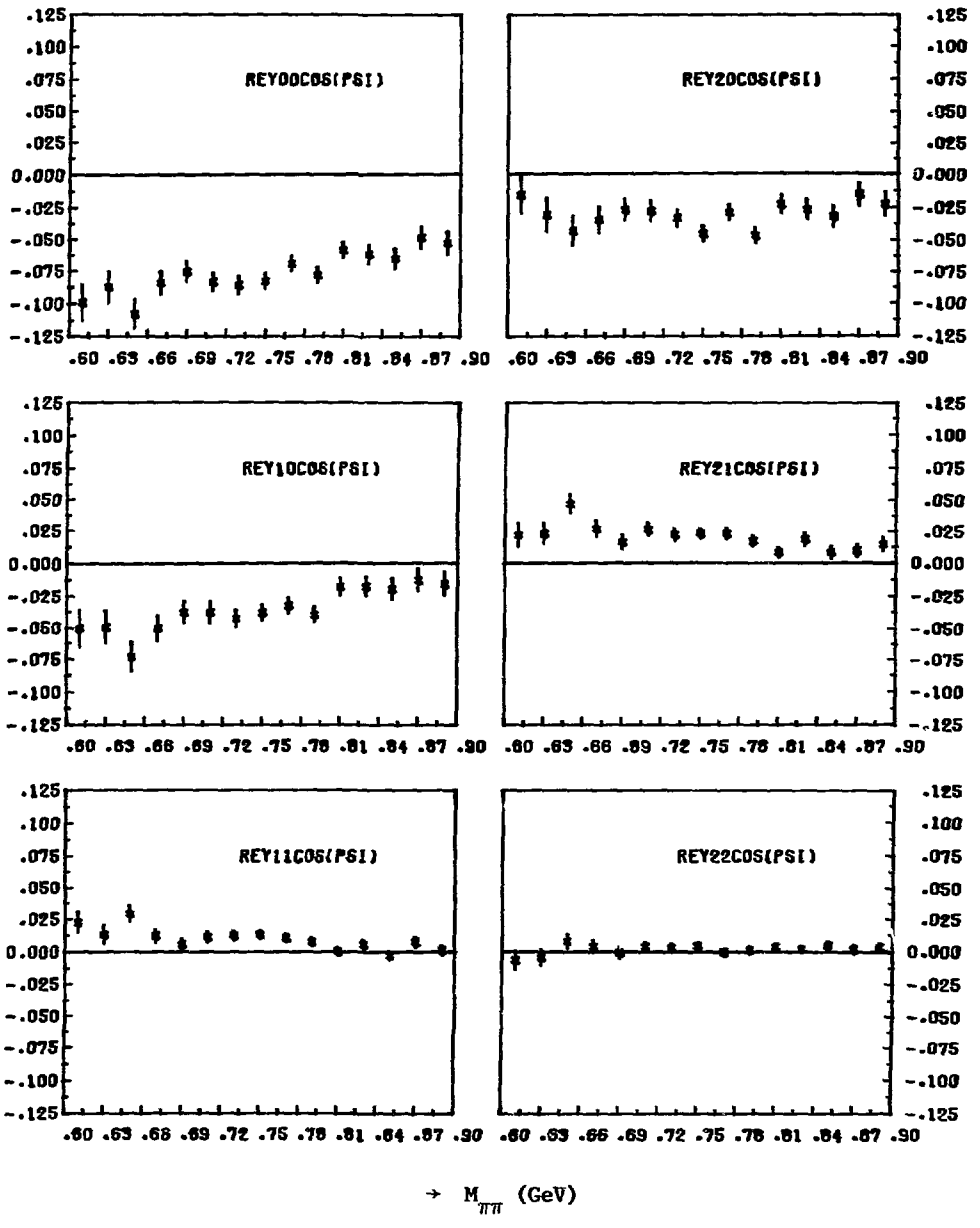

Fig. VI-17 Mass dependence of the normalized t-channel polarization dependent moments.
($0.005 < -t < 0.2$ GeV^2)

a - "cosψ" moments

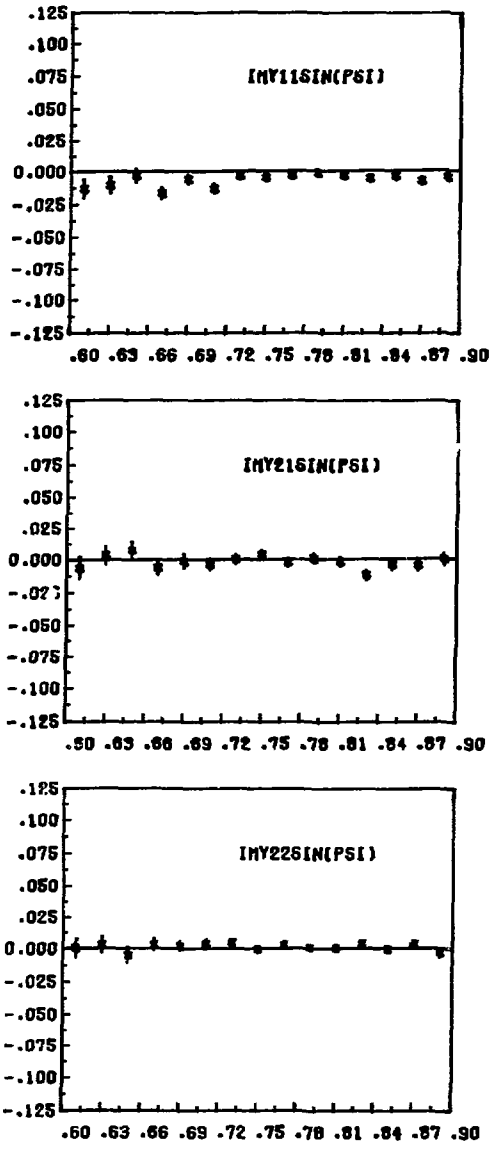

Fig.VI-17 Mass dependence of the normalized t-channel polarization dependent moments

$(0.005 < -t < 0.2\ \text{GeV}^2)$

b - "sinψ" moments

preference was given to a technique which exploits the analytical solutions as much as possible. In order to determine the amplitudes from the moments which were presented in the previous section, the FORTRAN program AMPFIT was written. The strategy of AMPFIT is as follows. The program looks first for a set of analytical solutions. When no analytical solutions are found (the moments are subject to measurement errors) the moments are varied within their respective errors and a new attempt is made. Each of the analytical solutions found in this way is input to the program MINUIT[6]) in the form of starting values for χ^2 minimalization. In this fitting process starting from a set of ambiguous solutions some of these ambiguities will vanish because they become mutually indistinguishable within the errors. In the actual analysis the phases γ_{NO} and χ_{NO} (the angles between g_0, g_N and h_0, h_N respectively, see Chapter V) appeared to be badly determined by the experiment. In contrast with all other phases, these two angles are constrained by only three moments: $\langle \text{Im } Y_1^1 \sin\psi \rangle$, $\langle \text{Im } Y_2^1 \sin\psi \rangle$ and $\langle \text{Im } Y_2^2 \sin\psi \rangle$ (see relations between moments and amplitudes; table V-2). As a consequence we obtained systematically solutions which were only different in these two phases, while the errors on those phases were very large. We therefore decided to consider two ambiguous solutions as identical when these solutions were only different in the magnitudes of the phases γ_{NO} and χ_{NO}. This effectively reduced to four the maximum number of ambiguous solutions to be expected.

The results presented in this section are obtained from the normalized moments discussed in the previous section. Contributions of higher spin states (i.e. d-wave in the mass- and t-range of interest) are thus neglected, assuming, as was mentioned in section VI-3, the resulting systematic error in our amplitudes and moments to be small.

The relations between moments and amplitudes (tables V-1 and V-2) are valid only if the s-channel reference frame for the proton is used (we made this choice explicitly in section V-2). Therefore, in what follows, flip and noflip amplitudes refers to the s-channel for the proton and the neutron. For the $\pi\pi$ helicity both the s- and t-channel helicity frame can be used, but we will use the $\pi^+\pi^-$ t-channel (Gottfried Jackson) frame throughout.

Fig.VI-18 shows the χ^2 distribution for the amplitude fits. For 1-constraint fits, the χ^2 distribution should ideally be peaked at 0, while the average χ^2 should be 1 [15]). Given the limited number of entries in the histogram (49) the peak value seems to be indeed close to 0; the average χ^2 is 0.73. We conclude that the χ^2 distribution is satisfactory. This means that the errors of the moments, which were used to fit the amplitudes, were neither over- nor underestimated. For the determination of the errors on the fitted amplitudes and phases we used the MINOS command of the function minimization program MINUIT[6]). The errors were defined as the variation in the fitted quantity which increases the χ^2 by 1. Given the fact that the χ^2 distribution for the fits is satisfactory this results in optimal errors for the fitted amplitudes and phases. The errors are generally non-linear and asymmetric however.

Fig.VI-19 shows he t-dependence of the magnitudes of the transversity amplitudes in the $\pi^+\pi^-$ invariant mass range between 0.71 and 0.83 GeV, i.e. in a mass interval symmetrically around the ρ. Fig.VI-20 shows the cosines of the relative phases between the unnatural parity exchange amplitudes; the notation is as defined in section V-4. The amplitudes are normalized such that the sum of squares of all amplitudes equals unity. The phases γ_{NO} and χ_{NO} are left out for reasons explained before.

Two well known features of reaction I-1 are confirmed by the magnitudes of the transversity amplitudes (fig.VI-19). The helicity 0 p-wave amplitudes g_0 and h_0 dominate the reaction at low -t values, as would be expected for the dominance of π-exchange. At high values of t the two natural parity exchange amplitudes g_N and h_N dominate the process which is in agreement with the known dominance of A_2 exchange amplitudes at high -t. However, the data from this experiment make clear that this picture is not complete. From the definitions of the transversity amplitudes (section V-1) it is easily verified that, if the magnitudes of two amplitudes with opposite transversity $|g_i|$ and $|h_i|$ are different, the simultaneous contribution of both the corresponding flip and noflip amplitudes is required. The large difference between $|g_0|$ and $|h_0|$ therefore requires the contribution of both unnatural parity exchange spin flip and noflip amplitudes, i.e. both π and A_1 exchange. The difference between the magnitudes $|g_S|$ and $|h_S|$ of the two s-wave amplitudes also signals the contribution of an A_1 exchange amplitude. For the two helicity 1 unnatural

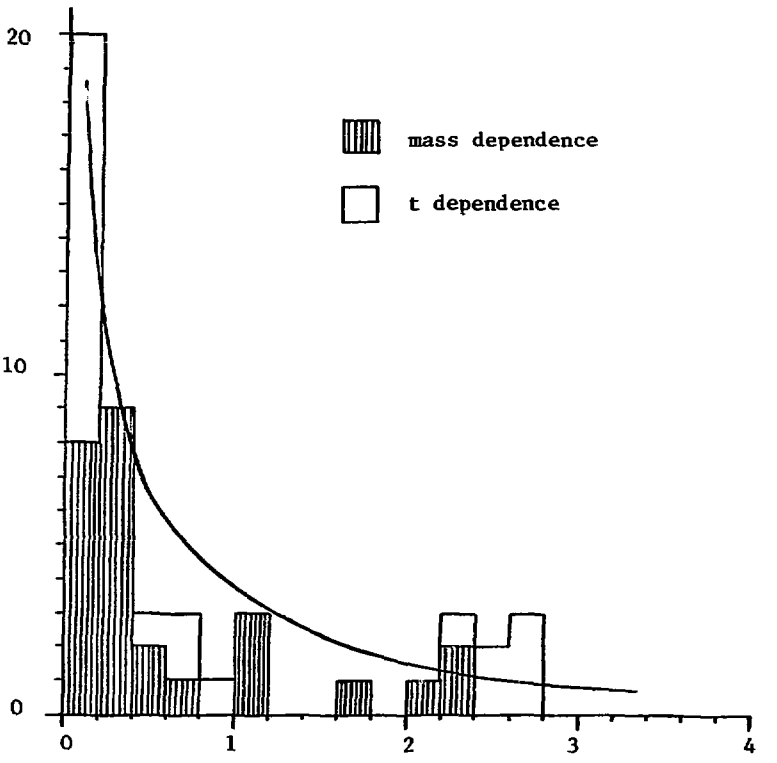

Fig. VI-18 χ^2 Distribution for the Amplitude Fits
Drawn: χ^2 distribution for 1C fits

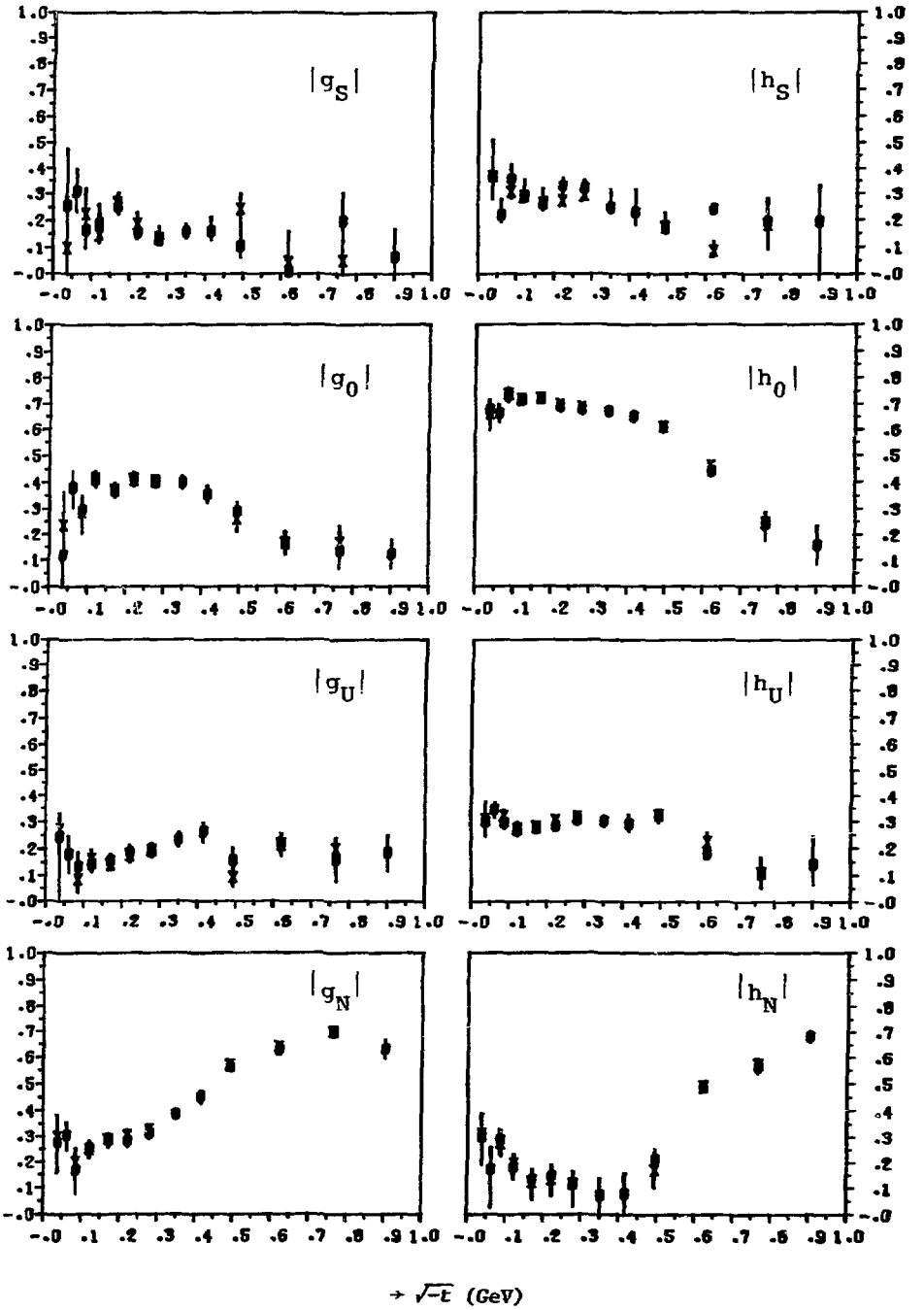

Fig.VI-19 t-dependence of the magnitudes of the transversity amplitudes.
($0.71 < m_{\pi\pi} < 0.83$ GeV)
The amplitudes are normalized such that $\sum_i g_i^2 + h_i^2 = 1$.

exchange amplitudes g_U and h_U the situation is more complicated. At low and medium t-values there is a systematic difference between the magnitudes of the two amplitudes, therefore both the corresponding flip and noflip amplitudes are required. The s-channel noflip amplitude corresponding to g_U and h_U can be accounted for by A_1 exchange. The corresponding flip amplitude however cannot be explained by π-exchange because an $m\neq 0$ state in the Gottfried Jackson frame cannot be produced by π-exchange (Treiman-Yang test). Here we clearly need an addition to the simple one particle exchange model, for example absorption effects. In earlier analyses of hydrogen data the m=1 unnatural parity exchange intensity (A_1 exchange amplitudes were assumed to vanish) was generally interpreted in terms of an absorption model[8]), particularly P.K. Williams' "Poor Man's Absorption Model"[9]). At medium t-values there is a large difference between the magnitudes of the two natural parity exchange amplitudes g_N and h_N. Consequently, both the natural parity exchange flip and noflip amplitudes contribute. A_2 exchange, contrary to π and A_1 exchange, can contribute to both flip and noflip amplitudes, but the s-channel noflip amplitude is expected to be small compared to the flip amplitude[10]). The difference between $|g_N|$ and $|h_N|$ requires the contribution of both flip and noflip amplitudes, but the flip and noflip amplitudes are also required to be out of phase. Therefore the polarization in the natural parity exchange amplitudes seems to implicate that an absorption effect contributes, since the A_2 exchange flip and noflip amplitudes are expected to be in phase[5]). Independent from this there is another indication that absorption effects play a role. The natural parity exchange amplitudes should vanish at t_{min}; the flip amplitude should vanish as $\sqrt{-t'}$, and the noflip amplitude as $-t'$ [11]) ($t' = t - t_{min}$). In earlier analyses of hydrogen data the non-vanishing of the natural parity exchange contribution at t_{min} was generally attributed to absorbed π-exchange[5]).

Fig.VI-20 shows the cosines of the relative phases between the unnatural parity exchange amplitudes. The cosines of the phases are plotted because the angles are subject to a sign ambiguity. It is interesting to see whether these phases agree with the "phase coherence" assumption[12]) which was used previously to reduce the number of independent variables in amplitude analyses. The phase coherence assumption entails that, for a given dipion spin, the unnatural parity exchange amplitudes are in phase,

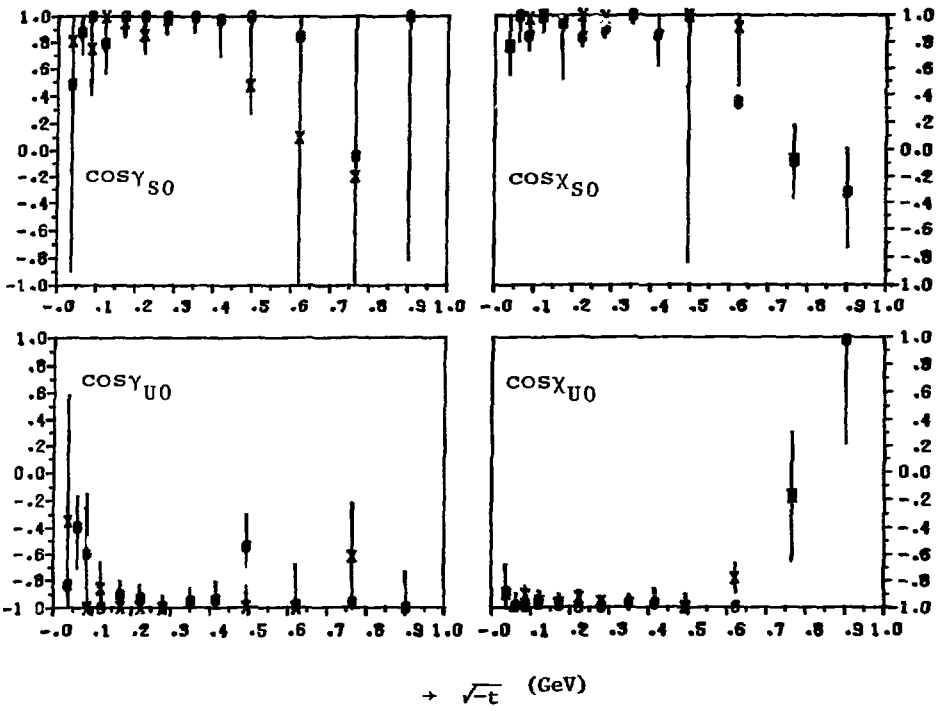

Fig.VI-20 Cosines of the relative phases between the unnatural parity exchange transversity amplitudes of fig. VI-19

i.e. their relative phase is either 0^o or 180^o. Let us assume phase coherence for the flip and noflip amplitudes separately, i.e. $\arg(n_0,n_U) = 0^o,180^o$ and $\arg(f_0,f_U) = 0^o,180^o$. Then we do not generally arrive at phase coherence for the transversity amplitudes; this is only the case if $\frac{|f_0|}{|n_0|} = \frac{|f_U|}{|n_U|}$.

The apparent phase coherence of the transversity amplitudes ($\cos\gamma_{U0} \simeq -1$, $\cos\chi_{U0} \simeq -1$) for low to medium t-values is in agreement with the assumption that the unnatural parity exchange flip and noflip amplitudes are in phase separately. This has to be taken with some caution however. If the noflip amplitudes are small compared to the flip amplitudes (or vice versa), the resulting transversity amplitudes are generally nearly phase coherent once the flip (or noflip) amplitudes are phase coherent.

In Chapter V it was shown that the amplitude analysis may lead to at most 8 discrete ambiguous solutions. Ignoring the ambiguities in the phases of the natural parity exchange amplitudes, we are left with at most 4 ambiguous solutions. In our analysis, however, we never obtained more than two ambiguous solutions in any mass- or t-bin. When ambiguous solutions were found, the ambiguity showed up mainly in the s-wave amplitudes g_S and h_S and in the corresponding phases. Earlier analyses of hydrogen data for $\pi^+\pi^-$ masses below 900 MeV led to the well known "up-down ambiguity" in the s-awave amplitude. Estabrooks and Martin[13], ignoring A_1 exchange in the absence of polarization data, found two distinct sets of solutions for the helicity amplitudes in the ρ region. In our analysis we have two sets of amplitudes with opposite transversities ("g" and "h" amplitudes). Within each set, our analysis is mathematically the same as the Estabrooks and Martin analysis. Moreover, we have one overall constraint between all ("g" and "h") amplitudes. Estabrooks and Martin were able to exclude a non-physical solution. The preferred solution gave a better agreement of the extrapolated $\pi^+\pi^-$ cross section with the observed $\pi^0\pi^0$ mass spectrum[13,14]). In our case the ambiguities do not allow to distinguish two distinct continuous solutions as a function of t. Therefore we cannot exclude solutions by imposing a physic l constraint. The ambiguities are displayed in figs. VI-19 and VI-20 by ϕ and $\nmid$. The occurrence of those ambiguities in some t-bins does not affect the conclusions which were drawn above.

The $\pi^+\pi^-$ invariant mass dependence of the magnitudes of the transversity amplitudes is shown in fig.VI-21 between 600 and 900 MeV, integrated over a t interval between -0.005 and -0.2 GeV^2. Fig.VI-22 shows the cosines of the phases between the unnatural parity exchange amplitudes. When two ambiguous solutions are found in a bin they are displayed by $\ddagger$ and ϕ in both figures. The amplitudes are normalized again such that, for each mass bin, the sum of squares of all amplitudes equals unity.

The dominant amplitudes in this mass- and t-region are the helicity 0 p-wave amplitudes g_0 and h_0 as would be expected for ρ production. Significant A_1 exchange contributions are present in all unnatural parity exchange amplitudes, as is demonstrated by the differences in magnitudes of the amplitudes with different transversities. Fig.VI-22 shows the relative phases between the amplitudes of fig.VI-21. Comparison of the two figures clearly sh ws two distinct sets of solutions indicated by ϕ and $\ddagger$ For the solution indicated with ϕ the cosine of χ_{U0} is everywhere compatible with -1, whereas $\cos\chi_{S0}$ is different from 1. We could call this the phase coherent solution. The other solution (indicated with $\ddagger$ in figs. VI-21 and VI-22) shows the opposite behaviour. For the latter the s-wave and the helicity 0 p-wave are in phase (χ_{S0} is either 0^o or 180^o). Given the fact that the amplitudes h_0 and h_S are larger than g_0 and g_S, this leads to an s-wave enhancement of approximately the same width as the ρ meson. This solution (indicated with $\ddagger$) can therefore be rejected as unphysical since no such narrow $\pi\pi$ s-wave structure appears in the measured $\pi^0\pi^0$ mass spectrum[14]).

From the magnitudes of the transversity amplitudes in figs. VI-19 and VI-21 we can calculate the relative intensities of the four different partial waves. It is easily verified (see the definitions of the amplitudes in section V-1) that $|g|^2 + |h|^2 = |f|^2 + |n|^2$, where f and n are the flip and noflip amplitudes corresponding to the transversity amplitudes g and h. Complications arise however for the determination of the errors on these intensities, as the errors given for the magnitudes of the transversity amplitudes are highly non-linear. Therefore the fitting of the amplitudes was repeated, this time fitting the quantities $|g|^2 + |h|^2$ instead of the amplitudes g and h. This procedure results in optimal errors for the fitted intensities. We stress that a model independent determination of the relative intensities of the contributing waves is only possible using polarized target data. From the previous hydrogen experiment as 17.2 GeV^2) only limits could be derived on the partial cross section for natural parity exchange[16]).

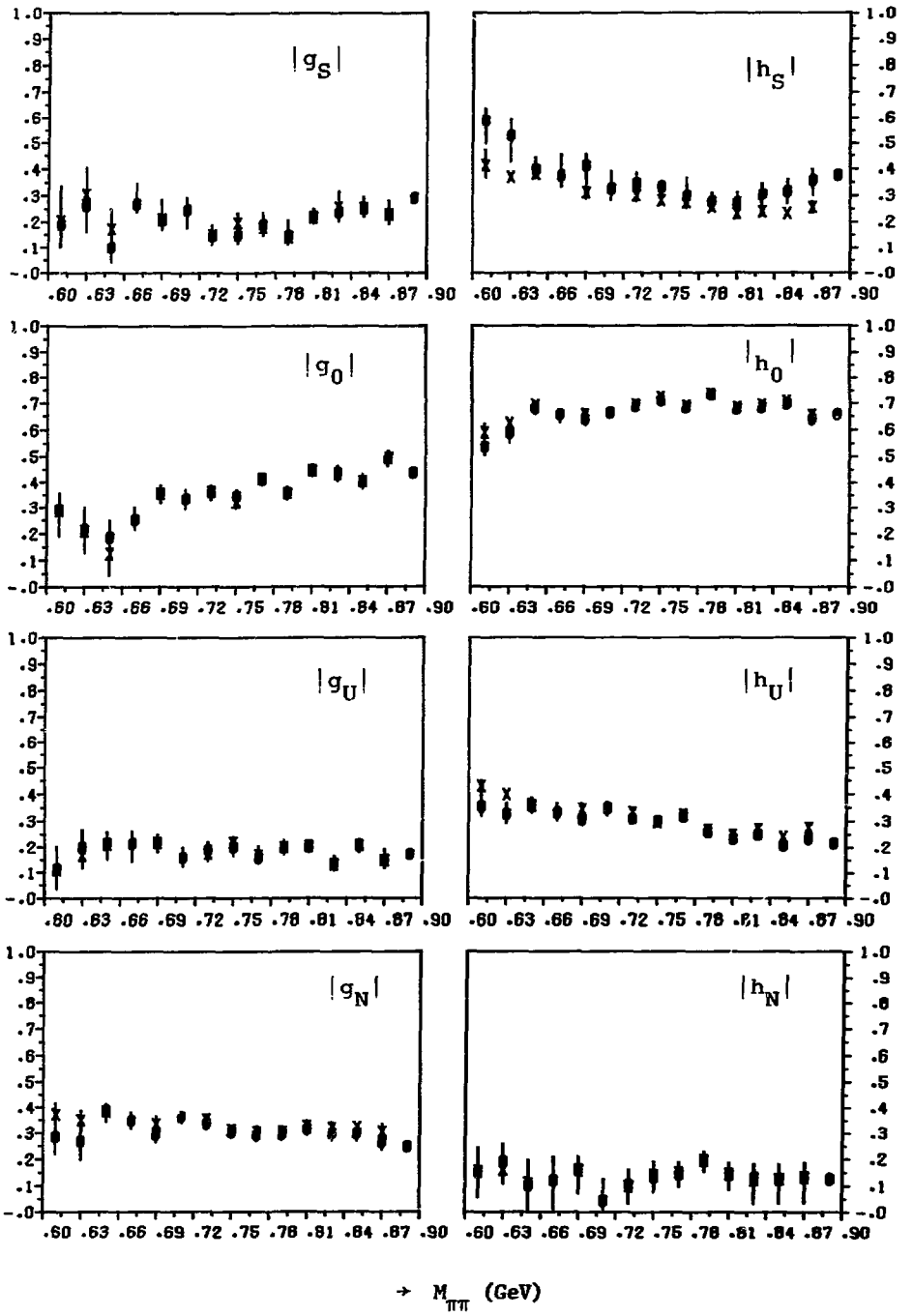

Fig. VI-21 Mass dependence of the magnitudes of the transversity amplitudes ($0.005 < -t < 0.2$ GeV^2). The amplitudes are normalized such that $\sum_i g_i^2 + h_i^2 = 1$.

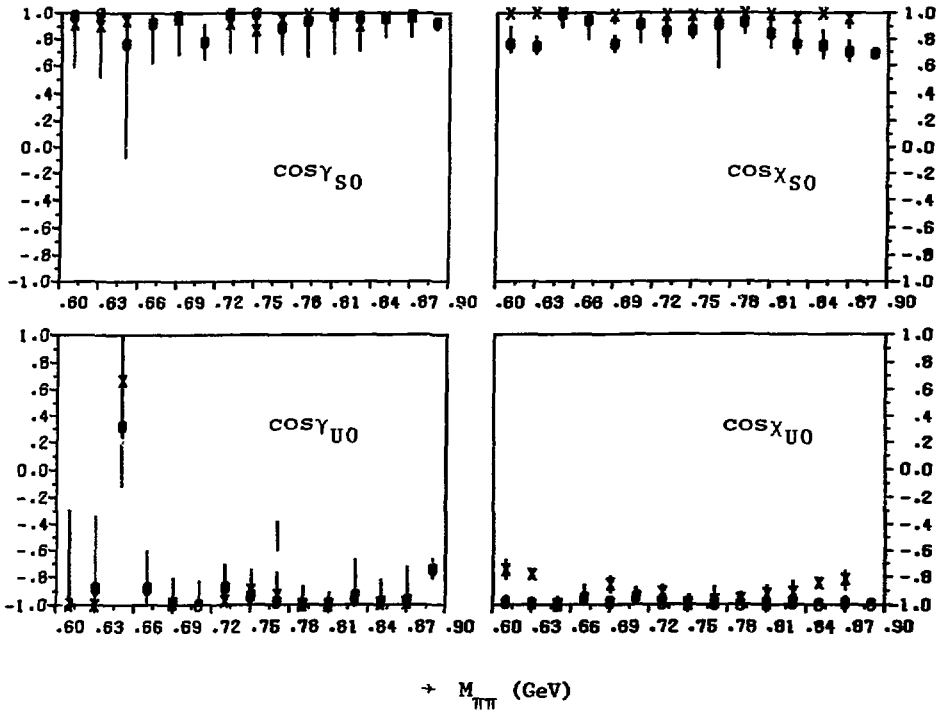

Fig.VI-22 Cosines of the relative phases between the unnatural parity exchange transversity amplitudes of fig. VI-21

Fig.VI-23 shows the mass and t-dependence of the relative intensities of the four $\pi^+\pi^-$ partial waves. The mass- and t-intervals are the same as for the amplitudes and moments which were presented before. As a function of t, the fraction of natural parity exchange rises from ∿15% at the lowest t-values to ∿85% at $t \approx -0.9$ GeV^2. The fraction of natural parity exchange decreases slowly with increasing $\pi^+\pi^-$ invariant mass. This is in excellent agreement with an earlier model independent analysis of the 17.2 GeV hydrogen data[16]). In the analysis, limits on the fractions of natural and unnatural parity exchange could be determined using the positivity constraint of the $\pi^+\pi^-$ final state density matrix.

In principle the knowledge of the helicity amplitudes would make it possible, in the absence of absorption effects, to determine what fraction of the total intensity is produced by π, A_1 and A_2 exchange. If absorption effects are to be taken into account (it was shown earlier that such effects play a role) we have to resort to a model fit. Unfortunately, the helicity amplitudes are not uniquely determined by the transversity amplitudes as obtained from our amplitude fits. The phase between the two sets of amplitudes with opposite transversity, which is needed to compute the helicity amplitudes, is not an observable in our experiment. In order to do a complete measurement, both the proton and the neutron polarization have to be measured. Apart from the technical difficulties of such a measurement, this is even impossible at t_{min} where the recoil neutron is at rest in the laboratory. Nevertheless, similar to the old hydrogen experiment, where limits on the fraction of natural parity exchange could be determined we are able to set lower limits on the unnatural parity exchange s-channel nucleon noflip (A_1) amplitudes. From the definitions of the amplitudes in section V-1, it is easily verified that the following relation holds:

$$|n_i| \geq \frac{||h_i| - |g_i||}{\sqrt{2}}$$

where n_i is the noflip amplitude corresponding to g_i and h_i (the same relation holds for the flip amplitude). We can therefore use the quantity

$$\frac{||h_i| - |g_i||}{\sqrt{2}}$$

evaluated for the three unnatural parity exchange $\pi^+\pi^-$ waves as lower limits for the A_1 exchange contributions to those waves.

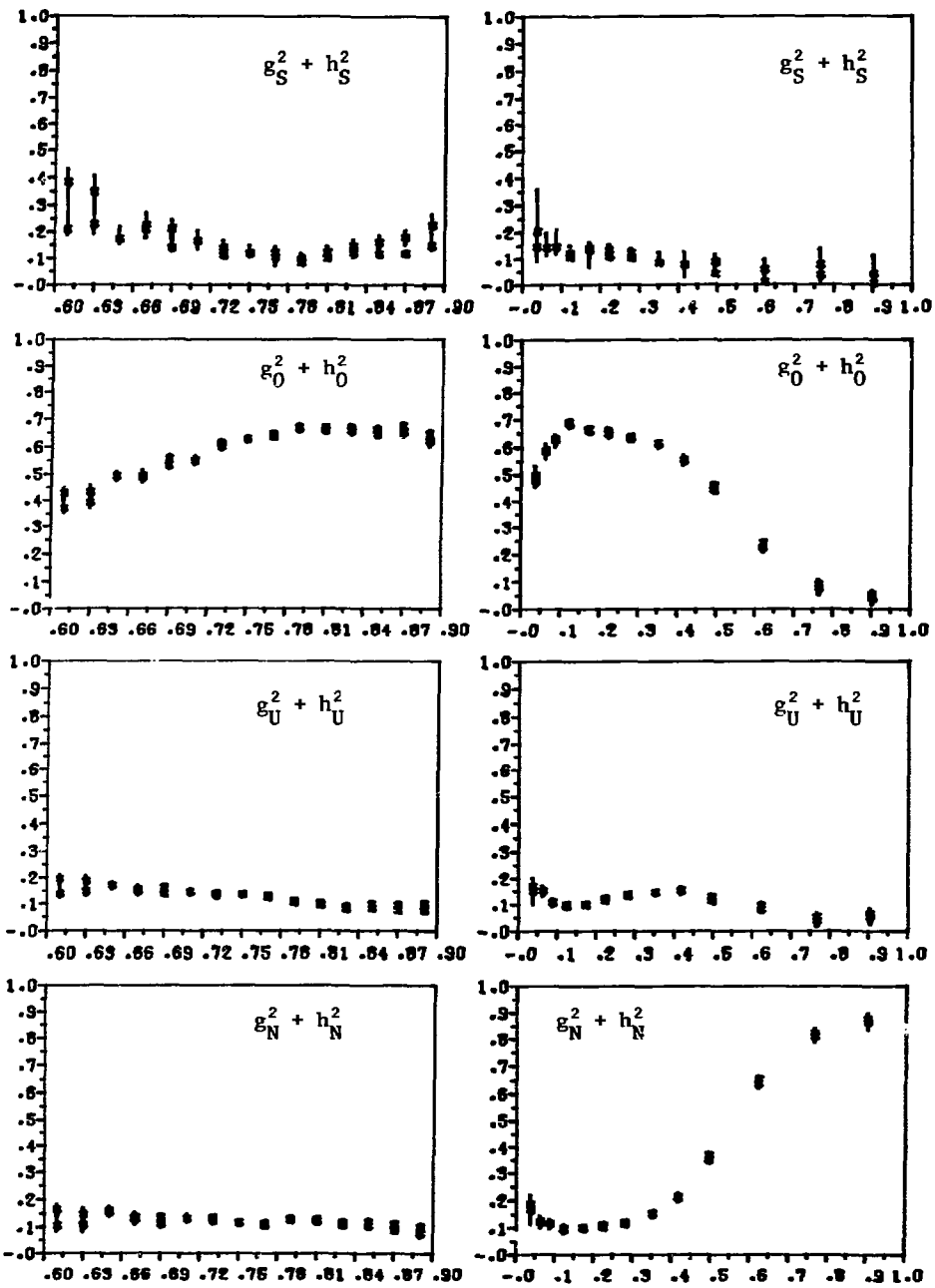

Fig. VI-23 Mass- and t-dependence of the relative intensities of the four $\pi^+\pi^-$ waves.

In fig.VI-24 we present the mass- and t-dependence of the lower limits for the three A_1 exchange amplitudes. Significant A_1 exchange contributions are present in all three waves over practically the whole mass- and t-interval. At high values of -t the lower limits for A_1 exchange are compatible with 0, which can be understood by recalling that at $-t = 0.9$ GeV^2 natural parity exchange accounts for about 85% of the cross section. There is an indication that the lower limit for the A_1 exchange amplitudes decreases with increasing $\pi^+\pi^-$ invariant mass. In terms of intensity, A_1 exchange accounts for about 5% of the cross section over the whole mass range. At $m_{\pi\pi} = 0.65$ GeV we seem to have some structure in the lower limits for the helicity 0 p-wave amplitude n_0. The statistical significance of this effect is marginal however. If the effect should not be a statistical fluctuation it would be due to the A_1 exchange amplitude. No particle or threshold effect is known, however, which could account for it.

VI-5 The Rank of the Density Matrix

In Chapter V we derived the expression V-2-4 relating the elements of the final state density matrix $\hat{\rho}$, which describes the spin alignment of the $\pi^+\pi^-$ system, to the transversity amplitudes. From these equations it can be seen that the final state density matrix ρ for the unpolarized target experiment can be written in the following form:

$$\rho = \begin{pmatrix} \rho_U & 0 \\ 0 & \rho_N \end{pmatrix}$$

where the submatrices ρ_U and ρ_N are expressed in amplitudes corresponding asymptotically (for large s) to unnatural resp. natural parity exchange. It can be shown[7,16] that neither of the two submatrices ρ_U and ρ_N has more than two eigenvalues, independent of the number of contributing amplitudes. For the particular case that only s- and p-waves contribute to the $\pi^+\pi^-$ system the elements of ρ, expressed in transversity amplitudes, are the following:

$$\rho = \begin{pmatrix} g_S^2 + h_S^2 & g_S g_0^* + h_S h_0^* & g_S g_U^* + h_S h_U^* & 0 \\ g_0 g_S^* + h_0 h_S^* & g_0^2 + h_0^2 & g_0 g_U^* + h_0 h_U^* & 0 \\ g_U g_S^* + h_U h_S^* & g_U g_0^* + h_U h_0^* & g_U^2 + h_u^2 & 0 \\ 0 & 0 & 0 & g_p^2 + h_N^2 \end{pmatrix}$$

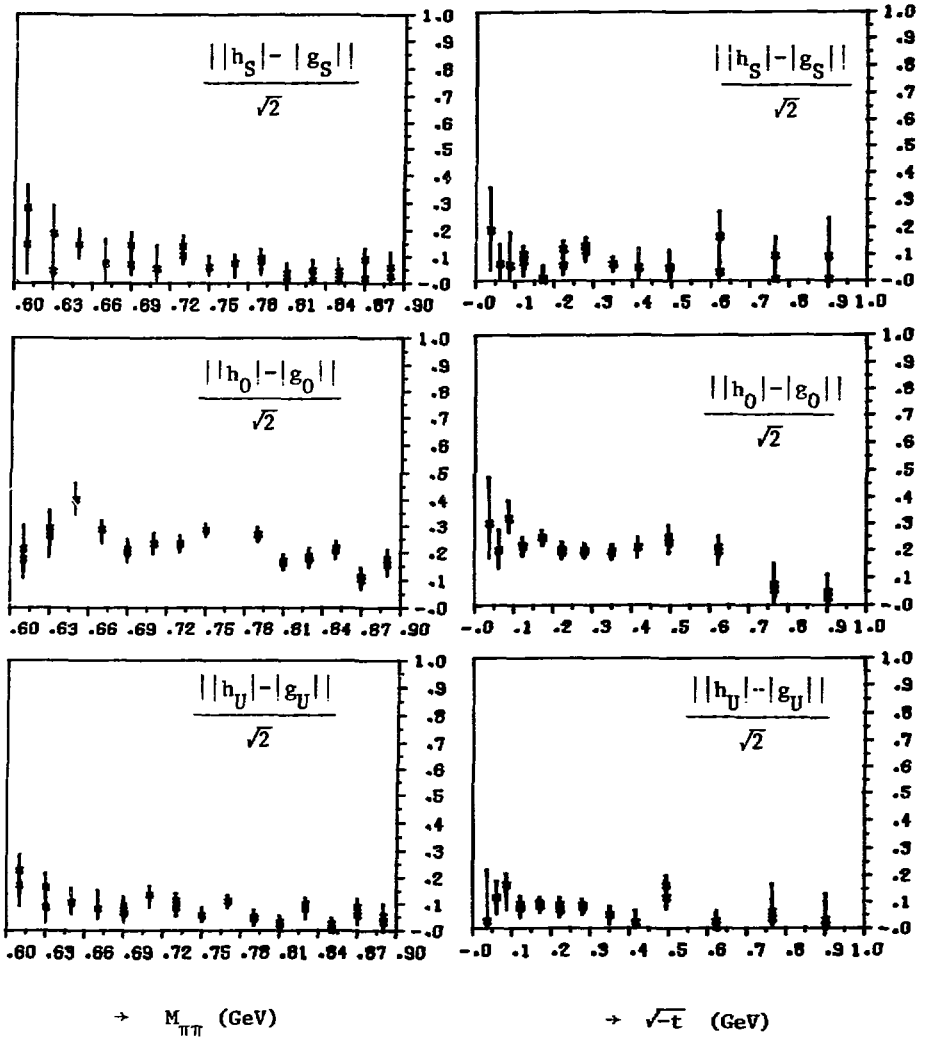

Fig.VI-24 Lower limits for A_1 exchange amplitudes as a function of $M_{\pi\pi}$ and t.

i.e. the submatrix ρ_N turns into a single element which equals the total intensity of natural parity exchange. As a consequence the submatrix ρ_N has only one eigenvalue, which means that the rank of ρ does not exceed 3 for $\pi^+\pi^-$ s- and p-waves.

In an analysis [16]) of the 17.2 GeV CERN-Munich(MPI) hydrogen data, limits could be derived for the eigenvalues of ρ using the positivity contraint for the density matrix. It was shown that the rank of the density matrix at the ρ mass is equal to two, while the rank is consistent with two for $m_{\pi\pi} < 900$ MeV. It can be shown[17]) that for one of the eigenvalues of ρ to vanish in this mass interval, a necessary and sufficient condition is that the following condition holds:

$$n_K = c\, f_K \qquad \text{--- VI-5-1}$$

with n_K and f_K the unnatural parity exchange noflip and flip amplitudes. In particular the case where either the flip or the noflip amplitudes vanish, leads to a rank two density matrix. The fact that, at least at the ρ mass, the rank was found to be two, has been used as an argument in favour of the assumed absence of A_1 exchange amplitudes. Using the definitions of the transversity amplitudes in section V-1, it is easily verified that the relation VI-5-1 leads to the following relation for the corresponding transversity amplitudes:

$$|g_K| = \frac{|c + i|}{|c - i|}\,|h_K| \qquad \text{--- VI-5-2}$$

Therefore, if the relations VI-5-1 hold for the unnatural parity exchange amplitudes, this should be manifest in the transversity amplitudes as equal ratios for:

$$\frac{|g_S|}{|h_S|}, \frac{|g_0|}{|h_0|} \text{ and } \frac{|g_U|}{|h_U|} \qquad \text{--- VI-5-3}$$

In particular the absence of A_1 exchange amplitudes predicts unity for these ratios. Inversely, however, the observation that, within the errors, the three ratios VI-5-3 are equal for any given mass- or t-bin does not necessarily imply relations VI-5-1; it is a necessary but not a sufficient condition. Our data therefore can only verify if at least to this extent there is agreement with a rank two for the unpolarized density matrix.

In fig.VI-25 we show the mass- and t-dependence of the three ratios VI-5-3. The mass- and t-binning are the same as for the amplitudes which were presented before. At low to medium t-values the three $|g|$ to $|h|$ ratios seem to be compatible with a value of about 0.6. At larger t-values the ratios are essentially undetermined due to the large experimental errors. As for the mass dependence, the ratios are compatible with a value of 0.6 with some indication for a slight increase with increasing $\pi^+\pi^-$ invariant mass. We conclude that our results agree with the earlier finding that the rank of the unpolarized density matrix below $m_{\pi\pi}$ = 900 MeV is consistent with two.

VI-6 Model Fit

So far we have established that for a satisfactory description of ρ production in the reaction I-1 at 17.2 GeV we need amplitudes corresponding to the exchange of an object with the quantum numbers of the A_1 in addition to the well known π- and A_2 exchange contributions and absorption effects. We were able to determine - model independently - the intensities of the four different $\pi^+\pi^-$ partial waves and we could derive lower limits for the unnatural parity exchange s-channel noflip (A_1 exchange) amplitudes. If we want to learn more about the production mechanism of reaction I-1 we have to resort again to more model dependent methods, i.e. do a model fit. Such an analysis could help particularly to answer the question whether the unnatural parity exchange s-channel noflip amplitudes can be represented by reasonably conceived expressions for A_1 exchange or, alternatively, can be accounted for by absorptive corrections to π- and A_2 exchange. Based on preliminary results from our experiment[18]), two model fits have been carried out. In both cases the t-dependence of the moments in the $\pi^+\pi^-$ invariant mass region of the ρ meson ($0.71 < m_{\pi\pi} < 0.83$ GeV) was used to fit a model which consisted of parametrization for π, A_1 and A_2 exchange with absorptive corrections.

The first model fit was reported in ref.[18]). The model which was used consisted of the well known amplitudes of the "Poor Man's Absorption Model"[9]) with amplitudes for A_2 and A_1 exchange added to describe the polarization measurement. Allowance was made for A_1 exchange contributions to the two helicity 0 unnatural parity exchange s-channel noflip amplitudes.

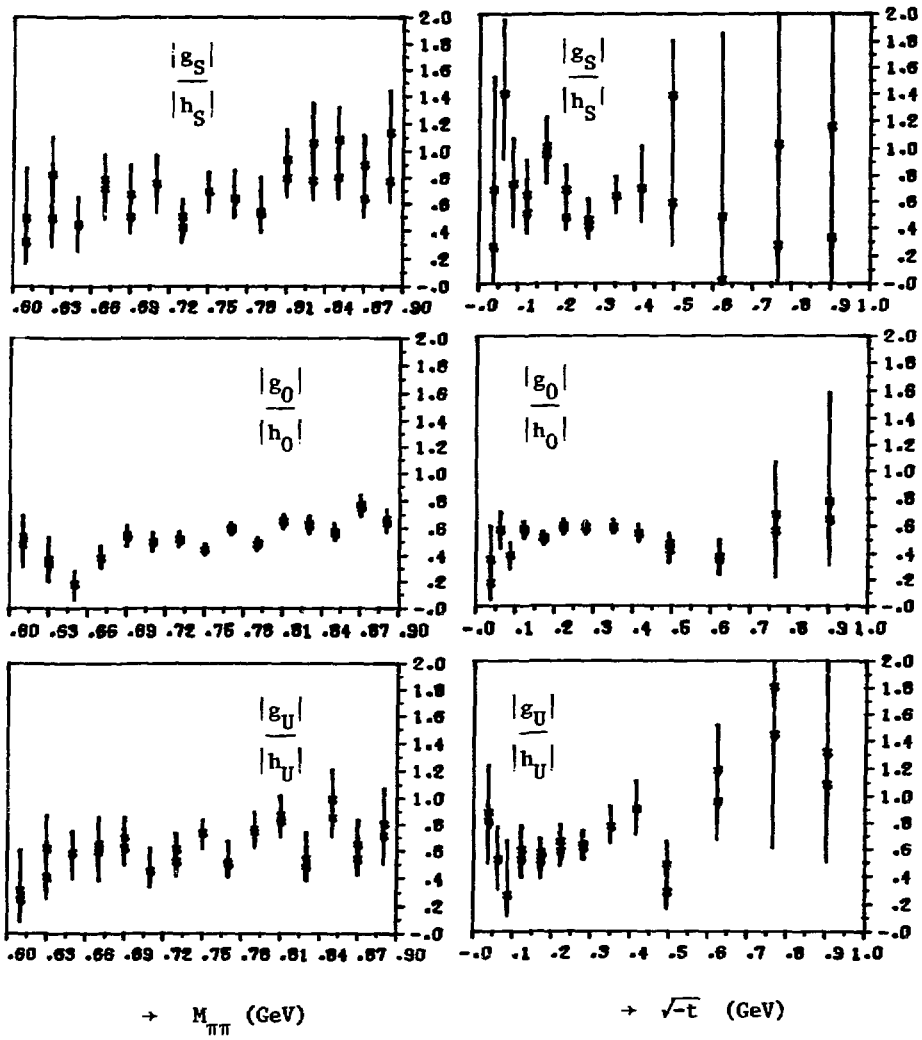

Fig.VI-25 Mass- and t-dependence of the ratios $|g|/|h|$ for the unnatural parity exchange amplitudes.

Considering the simplicity of this model, a rather good agreement with the data was found. In particular the model agreed well with the transversity amplitudes which were obtained in a preliminary model independent analysis. From this work the conclusion can be drawn that the addition to a conventional model of parametrization for A_1 exchange amplitudes results in a correct description of both the polarization dependent and - independent data.

A more elaborate model was used by Kimel and Owens[19]. The model is an extension of an earlier model which was developed for the analysis of a number of reactions:

$$\pi^- p \to \rho^0 n$$
$$\pi^+ p \to \rho^0 \Delta^{++}$$
$$\pi^+ p \to \omega \Delta^{++}$$
$$\pi^- p \to B^0 n$$

The model consists of Regge pole expressions for the relvant exchange contributions. In addition, so called "cut contributions" (absorptive corrections) are allowed in those amplitudes with s-channel net helicity flip n = 0. For the reaction I-1, the model comprised π and A_2 exchange amplitudes and π- cut contributions. Triggered by preliminary results from this experiment[18], Kimel and Owens added expressions for Regge-ized A_1 exchange and A_1-cut contributions to the model. As input for the fit, Kimel and Owens use previously published hydrogen data on the reaction I-1 at 17.2 GeV[2]) and preliminary data from this experiment[18]). The preliminary polarization data available at the time consisted of the t dependence (for $0.71 < m_{\pi\pi} < 0.83$ GeV) of the normalized m=0 polarization dependent moments and the magnitudes of the transversity amplitudes. In order to put additional constraints on some of the fitted parameters, 6 GeV hydrogen data on the reaction I.1[20]) was used. The model was fitted to the moments using a set of relations between moments and amplitudes as derived in Chpater V. The results of the fit was a good agreement with the data; Kimel and Owens drew the conclusion that: "A conventional Regge pole prescription gives a good description of the data". They argue explicitly against alternatives to A_1 exchange and reject, based on estimates of the magnitudes of these effects, Regge-Regge and Regge-Pomeron cuts as possible alternative explanations.

For the present analysis the fit of this model has been repeated, mainly because Kimel and Owens could only use an incomplete set of preliminary polarization data. We will not give a description of the Regge pole and -.cut expressions which were used for the amplitudes, as these expressions are given explicitly in Kimel and Owens' paper. We adopted the model without modification. In the model the 13 free parameters are the 6 pole parameters β and 7 coefficients α of exponential t-dependences; the Regge trajectories of π, A_1, A_2, π-cut and A_1-cut contributions were kept at fixed values. Fig.VI-26 shows the agreement of the model with the t-dependence of the transversity amplitudes and phases for $0.71 < m_{\pi\pi} < 0.83$ GeV. The agreement of the model with the amplitudes and phases is indeed impressive. We must conclude that the production mechanism of the reaction I-1 is described very well by the model. In table VI-3 we give the results for the fitted parameters together with the values published by Kimel and Owens[19]). For some of the fitted parameters there are large discrepancies between the two fits. Particularly the parameters of the A_1 and A_1 cut contributions show large differences. During the analysis it was noticed that the fit was not very sensitive to the parameters of the A_1 and A_1 cut contributions. When omitted, however, the model completely fails to describe the process.

Table VI-3 Fitted Parameters

	Kimel and Owens	This analysis	
β_π	51.73	48.62	GeV^{-2}
C_π^0	2.04	1.48	GeV^{-2}
C_π'	0.63	0.18	GeV^{-2}
$\beta_{A_1}^0$	411.5	260.3	
β_{A_1}'	67.6	146.6	GeV^{-1}
$C_{A_1}^0$	2.05	7.62	GeV^{-2}
C_{A_1}'	1.17	2.51	GeV^{-2}
β_{A_2}	6.08	6.35	GeV^{-1}
C_{A_2}	0.40	0.30	
$\beta_{\pi\text{-cut}}$	-67.2	-65.9	
$C_{\pi\text{-cut}}$	1.94	1.40	GeV^{-}
$\beta_{A_1\text{-cut}}$	-402.8	-29.74	
$C_{A_1\text{-cut}}$	1.53	0	GeV^{-2}

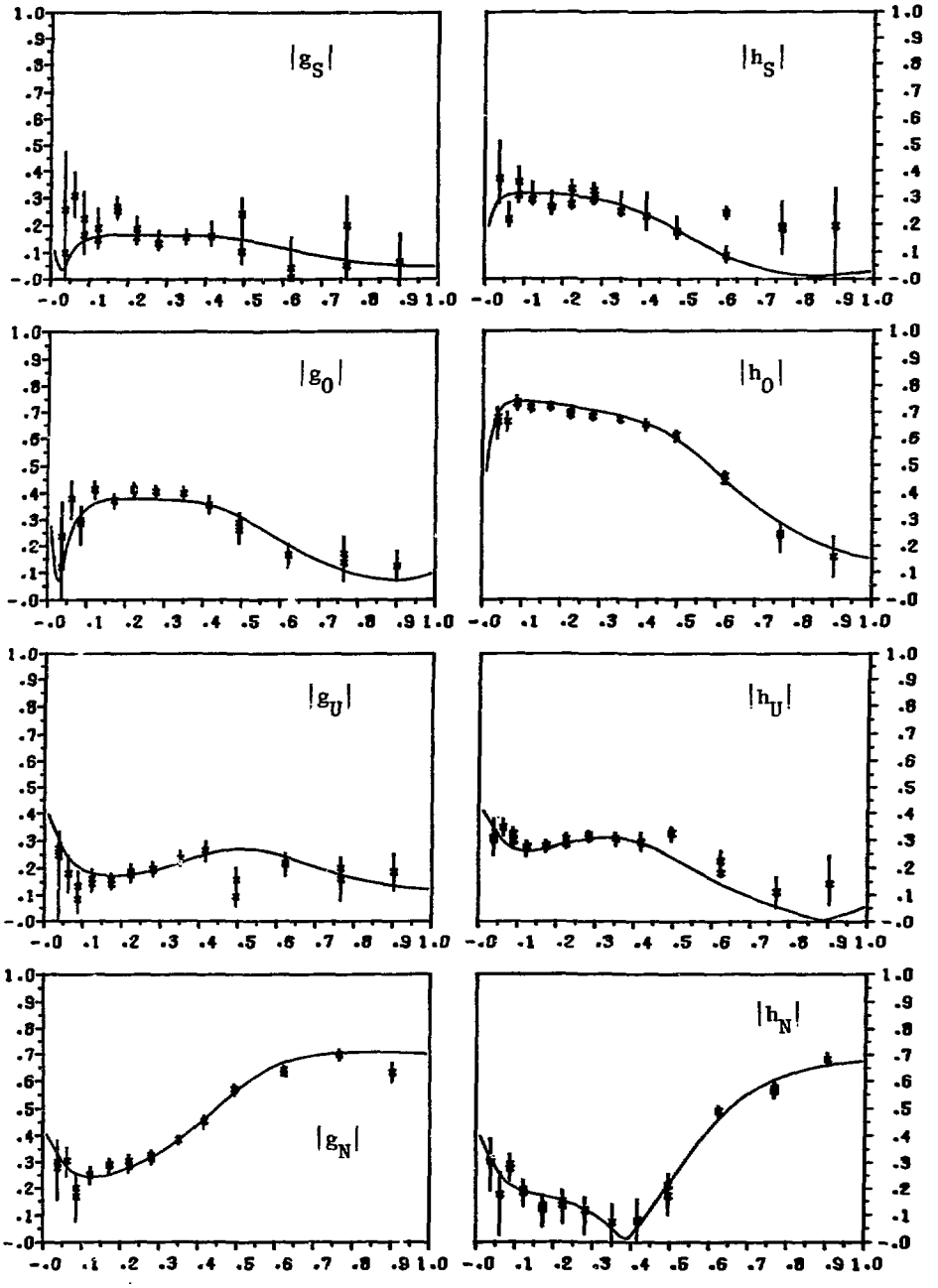

Fig. VI-26-a Agreement of the model with the magnitudes of the transversity amplitudes.
.71< $m_{\pi\pi}$ < .83 GeV.

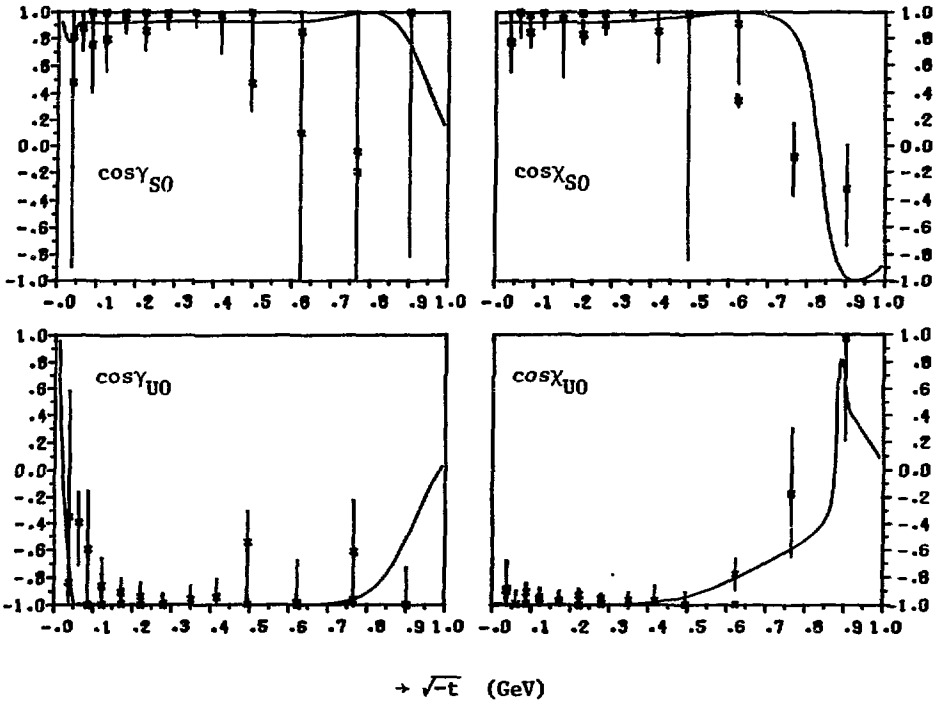

Fig VI-26-b Agreement of the model with the phases between the unnatural parity exchange transversity amplitudes. .71<$m_{\pi\pi}$<.83 GeV.

Kimel and Owens noticed the same problem in their analysis. In order to put additional constraints on the parameters of the A_1 and A_1-cut contributions they used preliminary hydrogen data at 6 GeV in their fit. The difference in the fitted parameters is also - partly - explained by Kimel and Owens' use of preliminary data from our experiment. For the present data the normalization of the polarization dependent moments has been determined properly. An important fact, however, is that the parameters of the π-exchange contributions seem to be rather independent of the changes in the parameters of the A_1 and A_1-cut contributions. This being so, a $\pi\pi$ phase shift analysis, based on a model like the one proposed by Kimel and Owens, could be envisaged.

VI-6 Consequences for $\pi\pi$ Phase Shift Analyses

The experiment was originally proposed to check, in a model independent way, the assumptions on which previous $\pi^+\pi^-$ phase shift analyses were based. These assumptions were the following:

a) Vanishing of the unnatural parity exchange s-channel helicity noflip amplitudes, i.e. no A_1 exchange.

b) Phase Coherence: The s-channel flip amplitudes for the same exchange naturality and the same $\pi^+\pi^-$ spin are in phase.

Phase shift analyses have been based on either the first or both of these assumptions. Estabrooks and Martin[13]) used only the supposed absence of A_1 exchange and show that in this case two ambiguous solutions are found below 1 GeV. One of these solutions was shown to be unphysical, this being the solution with a sizable deviation from phase coherence. Other analyses, using the method of Ochs and Wagner[12,17,21]) assume the absence of A_1 exchange as well as phase coherence. As we have demonstrated in the previous sections, a clear A_1 exchange contribution has been established while, at least in the low to medium t-range, no significant departure from phase coherence was found. The question that remains to be answered is to what extent the supposed absence of A_1 exchange amplitudes led to systematic errors, if any, in the published $\pi\pi$ phase shifts. In answering this question we will assume that phase coherence is not violated and that the unnatural flip and noflip amplitudes are proportional. For $\pi^+\pi^-$ masses between 0.6 and 0.9 GeV, and for the low to medium t-values which were typically used for phase shift analyses, both assumptions are supported

(though not proved) by our experiment. We will furthermore assume that the proportionality constant between flip and noflip amplitudes varies little with t and $m_{\pi\pi}$. Here we remark that, while our data suggests that the ratio of noflip to flip amplitudes is nearly independent of t, this ratio must be t-dependent at very low t because of the different t-behaviour of flip and noflip amplitudes near t_{min} [11]). A statistically significant anomaly in the π-exchange intensity at very low t was in fact observed in the hydrogen experiment[2]). At the time, without any further supporting evidence, this was not interpreted as an A_1 exchange signal however.

First we will consider the method of Estabrooks and Martin. As usual we shall restrict our argument to the region of the $\pi\pi$ mass spectrum which is clearly dominated by s and p wave production, i.e. $m_{\pi\pi} < 0.9$ GeV. Estabrooks and Martin carry out an amplitude analysis based on the assumption of vanishing A_1 exchange contributions. As a result, the three unnatural parity exchange amplitudes (one s-wave and two p-wave amplitudes) are contaminated with an A_1 exchange signal. If we assume that unnatural flip and noflip amplitudes are proportional i.e. n = c f, A exchange contributes a fraction $|c|.(1 + |c|^2)^{-\frac{1}{2}}$. In Estabrooks and Martins' analysis, the helicity 0 p-wave amplitude is parametrized as a π-exchange amplitude and fitted to the data as a function of t and $m_{\pi\pi}$. One overall normalization constant is adjusted such that the p-wave phase shift goes smoothly through the resonance. Therefore, if the flip and noflip amplitudes are proportional and this ratio is independent of $m_{\pi\pi}$ and t, no effect on the resulting phase shifts is expected, since in that case the A_1 exchange contamination of the amplitudes is absorbed in the overall normalization constant. The fact that for very small t the noflip/flip ratio must be t-dependent is probably of minor importance since it concerns only a small region in t, while the parametrization was fitted typically over a t-range from near t_{min} to $t=-0.2$ GeV^2 [11]).

An alternative method to extract the $\pi\pi$ phase shifts from the data was used by Ochs and Wagner[12,17,21]). Based also on the 17 GeV CERN-Munich(MPI) data, their method consisted essentially of a determination of the density matrix elements from moments integrated over a small t-range. In order to obtain the density matrix elements, both spin coherence and the absence of A_1 exchange contribution were necessary assumptions. As was already pointed out by Ochs recently[22]), the method

used is in fact more general than was stated originally. It appears that Ochs and Wagner's method gives identical results if the assumption of vanishing A_1 exchange contributions is replaced by the following:

c) The unnatural parity exchange s-channel flip and noflip amplitudes are proportional, i.e. $n_i = c\, f_i$, and c is independent of the $\pi^+\pi^-$ invariant mass.

Similar to Estabrooks and Martin's method, the A_1 exchange contamination of the π exchange amplitudes is absorbed in the overall normalization.

In conclusion we can say that, in the $\pi^+\pi^-$ invariant mass range between .6 and .9 GeV, we found no evidence for systematic errors in the published $\pi\pi$ phase shifts. We were not able, however, to prove that the published $\pi\pi$ phase shifts are free of systematic errors due to A_1-exchange contributions. A more definite answer to this question can be given by performing a new phase shift analysis taking full advantage of our polarization data.

REFERENCES (Chapter VI)

1) B.Gottschalk, unpublished.

2) G.Grayer, B.Hyams, C.Jones, P.Schlein, P.Weilhammer, W.Blum, H.Dietl, W.Koch, E.Lorenz, G.Lütjens, W.Männer, J.Meissburger, W.Ochs and U.Stierlin, Nucl. Physics B75 (1974) 189.

3) F.Udo, private communication.

4) Particle Data Group, "Review of Particle Properties" 1976.

5) J.D.Kimel and E.Reya, Int. Conf. on $\pi\pi$ Scattering and Associated Topics, Tallahassee, 1973. (eds. P.K.Willaims and V.Hagopian), AIP Conf. Proc. 13 New York, (1973) p.274.

6) F.James and M.Roos: "MINUIT A System for Function Minimization and Analysis of the parameter Errors and Correlations" Comp. Phys. Comm. 10 (1975) 343-367.

7) B.R.Martin, D.Morgan and G.Shaw, "Pion Pion Interaction in Particle Physics", Academic Press, New York, 1976
and:
J.L.Petersen: "The $\pi\pi$ Interaction", CERN Yellow Report, 77-04.

8) K.Gottfried and J.D.Jackson, Nuovo Cimento 34 (1964) 735
and:
F.S.Heney, G.L.Kane, J.Pumplin and M.Ross, Phys. Rev. 182 (1969) 1579.

9) P.K.Williams, Phys. Rev. D1 (1970) 1312
and:
G.C.Fox, Proc. Cal. Tech. Conference on Phenomenology in Particle Physics, Pasadena, 1971.

10) B.Sadoulet, Nucl. Phys. B53 (1973) 135.

11) P.Estabrooks, A.D.Martin, G.Grayer, B.Hyams, C.Jones, P.Weilhammer, W.Blum, H.Dietl, W.Koch, E.Lorenz, G.Lütjens, W.Männer, J.Meissburger and U.Stierlin, Int. Conf. on $\pi\pi$ Scattering and Associated Topics, Tallahassee, 1973 (eds. P.W.Williams and V.Hagopian) AIP conf. Proc. 13 New York (1973) p.37.

12) W.Ochs: "Die Bestimmung von $\pi\pi$ Streuphasen auf der Grundlage einer Amplitudenanalyse der Reaktion $\pi^- p \to \pi^- \pi^+ n$ bei 17 GeV/c Primärimpuls" Ph.D. Thesis, University of Munich, 1973.

13) P.Estabrooks and A.D.Martin, Phys. Lett 41B (1972) 350
and:
P.Estabrooks and A.D.Martin, "$\pi\pi$ Partial Waves from 0.6 to 1.8 GeV", University of Durham Preprint
and see also ref.11.

14) W.D.Apel, J.S.Ausländer, H.Müller, G.Sigurdsson, H.M.Standenmaier, U.Stier, E.Bertolucci, I.Manelli, G.Purazzini, P.Rehali, A.Scribano, F.Sergiampietri and M.L.Vincelli, Phys. Lett. B41 (1973) 542.

15) W.T.Eadie, D.Drijard, F.E.James, M.Roos and B.Sadoulet: "Statistical Methods in Experimental Physics", North Holland, Amsterdam, 1971.

16) G.Grayer, B.Hyams, C.Jones, P.Weilhammer, W.Blum, H.Dietl, W.Koch, E.Lorenz, G.Lütjens, W.Männer, J.Meissburger, W.Ochs and U.Stierlin, Nucl. Phys. B50 (1972) 29.

17) W.Ochs, Nuovo Cimento, 12A (1972) 724.

18) H.Becker, W.Blum, V.Chabaud, J.de Groot, H.Dietl, J.Gallivan, B.Gottschalk, G.Hentschel, B.Hyams, E.Lorenz, G.Lütjens, G.Lutz, W.Männer, B.Niczyporuk, D.Notz, T.Papadopoulou, R.Richter, K.Rybicki, U.Stierlin, B.Stringfellow, M.Turala, P.Weilhammer and A.Zalewska, Paper submitted to the 18th Int. Conf. on High Energy Physics, Tbilisi, July 1976.

19) J.D.Kimel and J.F.Owens, Nucl. Phys. B122(1977) 464-484.

20) D.S.Ayres, R.Diebold, A.F.Greene, S.L.Kramer, A.J.Pawlicki and A.B.Wicklund, Int. Conf. on $\pi\pi$ Scattering and Associated Topics, Tallahassee 1973 (eds. P.K.Williams and V.Hagopian) AIP Conf. Proc. 13 New York, (1973) 284.

21) B.Hyams, C.Jones, P.Weilahmmer, W.Blum, H.Dietl, G.Grayer, W.Koch, E.Lorenz, G.Lütjens, W.Männer, J.Meissburger, W.Ochs, U.Stierlin and F.Wagner, Nucl. Phys. B64 (1973) 134-162.

22) W.Ochs: "Results on $\pi\pi$ Scattering". Invited talk at the IInd International Conference on Nucleon Nucleon Interaction, Vancouver, B.C., Canada, June 1977.

SUMMARY

This thesis describes an experiment to study the reaction

$$\pi^- p \rightarrow \pi^- \pi^+ n \qquad \text{--- 1}$$

at 17.2 GeV beam momentum, using a transversely polarized butanol target. Many $\pi\pi$ phase shift analyses have been carried out in the past, based on measurements of the reaction 1. In the absence of polarization measurements however, it was necessary in these analyses to make some assumptions about the production mechanism of the reaction. The purpose of this experiment was to study the production mechanism of the reaction 1 in greater detail using the extra information which can be obtained from a polarization measurement. The new information regarding the production mechanism then affords an independent check for earlier assumptions about the production mechanism.

In the first chapter the physics interest in the reaction 1 is briefly discussed. The usual kinematical quantities are defined.

Chapter II gives a description of the elements of the CERN-Munich (MPI) Spectrometer which was used for the experiment. A short description is given of the technique which was used for the polarized target.

Chapter III briefly describes some aspects of the geometrical and kinematical analysis of the recorded events. A number of toplogy dependent corrections is determined.

Chapter IV gives an extensive description of the method which was used to correct the measured $\pi^+\pi^-$ angular distribution for the limited geometrical acceptance of the experimental apparatus. It is shown that the polarization dependent part of the $\pi^+\pi^-$ angular distribution can be isolated without contamination due to the unpolarized background.

In chapter V it is derived that the measurements of this experiment, combined with the results of an earlier experiment using a hydrogen target, supplies sufficient information for a model independent amplitude analysis. The relations which are needed for this analysis between the moments of the $\pi^+\pi^-$ angular distribution and the unknown amplitudes are derived for the case where the $\pi^+\pi^-$ system is in a spin 0 or 1 state.

In the last chapter the results of the experiment are described. Results are given almost exclusively for the case that the $\pi^+\pi^-$ invariant mass is smaller than 900 MeV. In this mass interval it can be assumed that

only $\pi^+\pi^-$ spin 0 and 1 states contribute. Using the distributions of some uncorrected quantities it is shown that, contrary to expectations, significant polarization effects are observed. From the corrected moments of the $\pi^+\pi^-$ angular distribution it is concluded directly that, in addition to π- and A_2 exchange, the exchange of an object with the quantum numbers of the A_1 ("A_1 exchange") contributes to the production of the $\pi^+\pi^-$ system. Next, the results of an amplitude analysis are described. Transversity amplitudes (and relative phases) are given as function of $\pi^+\pi^-$ invariant mass and four momentum transfer. From this it is derived that a model for the description of the production mechanism of the reaction 1 should include amplitudes for π, A_2 and A_1 exchange, while absorptive effects ("cuts") should be taken into account. The results of a Regge model fit are presented. This model includes amplitudes for π, A_2 and A_1 exchange plus contributions from absorbed π and A_1 exchange. It turns out that the model is able to describe the measurements accurately, both the polarization signal and the polarization dependent part. Finally the question what will be the impact of these results on the published $\pi^+\pi^-$ phase shifts is briefly discussed. It is concluded that no evidence has been found for systematic errors in the published $\pi\pi$ phase shifts for $m_{\pi\pi} < .9$ GeV.

SAMENVATTING

Dit proefschrift beschrijft een experiment ter bestudering van de reactie

$$\pi^- p \rightarrow \pi^- \pi^+ n \qquad \text{-------} \ 1$$

bij 17,2 GeV bundelimpuls, gebruik makend van een transversaal gepolarizeerd target. In het verleden zijn, gebazeerd op metingen van de reactie 1, veelvuldig $\pi\pi$ faseverschuivingsanalysen uitgevoerd. Bij gebrek aan polarizatiemetingen was het daarbij echter noodzakelijk om aannamen te maken omtrent het productiemechanisme van de reactie 1. Doel van dit experiment was om, gebruik makend van de extra informatie die kan worden verkregen uit een polarizatiemeting, het productiemechanisme van de reactie 1 nader te bestuderen. Gegeven deze nieuwe informatie kunnen dan de aannamen omtrent het productiemechanisme aan een onafhankelijk onderzoek worden onderworpen.

In het eerste hoofdstuk wordt kort ingegaan op het fysisch belang van de reactie 1, en worden de gebruikelijke kinematische grootheden gedefinieerd.

Hoofdstuk II geeft een beschrijving van de elementen vam de CERN-München (MPI) Spectrometer opstelling die voor het experiment werd gebruikt. Een korte beschrijving wordt gegeven van de techniek die werd gebruikt voor het polarizeren van de target protonen.

In hoofdstuk III wordt kort ingegaan op enkele aspecten van de geometrische en kinematische analyse van de verkregen gebeurtenissen. Een aantal topologie afhankelijke correcties wordt bepaald.

Hoofdstuk IV geeft een uitvoerige beschrijving van de metode die werd gebruikt om de gemeten $\pi^+\pi^-$ hoekverdeling te corrigeren voor de beperkte geometrische acceptantie van de experimentele opstelling. Daarbij wordt aangetoond dat het polarizatie afhankelijke deel van de $\pi^+\pi^-$ hoekverdeling kan worden geisoleerd zonder contaminatie ten gevolge van de ongepolarizeerde achtergrond.

In hoofdstuk V wordt afgeleid dat de metingen van dit experiment, tezamen met de resultaten van een eerder experiment gebruik makend van een waterstof target, voldoende informatie leveren voor een model onafhankelijke amplitude analyse. De daarvoor benodigde relaties tussen

de momenten van de $\pi^+\pi^-$ hoekverdeling en de onbekende amplituden worden afgeleid voor het geval dat het $\pi^+\pi^-$ systeem zich in een toestand met spin 0 of 1 bevindt.

In het laatste hoofdstuk worden de resultaten van het experiment beschreven. Vrijwel zonder uitzondering gaat het hierbij om resultaten voor het geval dat de invariante massa van het $\pi^+\pi^-$ systeem kleiner is dan 900 MeV. In dit massagebied mag worden aangenomen dat alleen $\pi^+\pi^-$ toestanden met spin 0 en 1 bijdragen. Aan de hand van de verdeling van enkele ongecorrigeerde grootheden wordt aangetoond dat, in tegenstelling tot de verwachtingen, significante polarizatie effecten worden waargenomen. Uit de gecorrigeerde momenten van de $\pi^+\pi^-$ hoekverdeling wordt direct de conclusie getrokken dat, naast π- en A_2-uitwisseling, de uitwisseling van een object met de quantum getallen van de A_1 ("A_1-uitwisseling") bijdraagt aan de productie van het $\pi^+\pi^-$ systeem. Vervolgens worden de resultaten van een amplitude analyse beschreven. Transversiteits amplituden (plus onderlinge fasen) worden gegeven als functie van de $\pi^+\pi^-$ invariante massa en de vierimpuls overdracht. Hieruit wordt afgeleid dat een model voor de beschrijving van het productiemechanisme van de reactie 1 amplituden moet bevatten voor π, A_2 en A_1-uitwisseling, terwijl absorptie effecten mee in rekening moeten worden gebracht. De resultaten van een Regge model fit worden gepresenteerd. Dit model omvat amplituden voor π, A_2 en A_1-uitwisseling alsmede bijdragen van geabsorbeerde π- en A_1-uitwisseling. Het blijkt dat het model in staat is de metingen (het polarizatie afhankelijke en het polarizatie onafhankelijke signaal) nauwkeurig te beschrijven. Tenslotte wordt kort ingegaan op de vraag welke invloed deze nieuwe resultaten zullen hebben op de gepubliceerde $\pi^+\pi^-$ faseverschuivingen. De conclusie daavan is dat geen aanwijzingen zijn gevonden voor systematische fouten in de gepubliceerde $\pi\pi$ faseverschuivingen voor $m_{\pi\pi} < 900$ MeV.

ACKNOWLEDGEMENTS

The data taking for the experiment which is described in this thesis took place over a period of almost two years. During this time, some 1300 data tapes were written. In a subsequent period of again about two years, this massive amount of data was gradually reduced and analyzed. It needs therefore no lengthy explanation to see that the succes of the experiment is the result of the joint effort of many people, each of them contributing her or his particular skills.

Now that I have completed my thesis, I wish to express my appreciation to the members of the CERN-Munich(MPI) Group. During my four year stay in the group I learned very much.

Specifically I want to thank Dr. G. Lutz who, leading the work for this experiment, influenced my work greatly. His expert comments and advice were invaluable.

I thank Dr. W. Hoogland for his help and many discussions. This work improved both in form and substance as a result of his critical remarks.

I thank my promotor Prof. Dr. A.G. Tenner for his support ever since I finished my studies. His critical reading of the manuscript resulted in numurous improvements and clarifications.

Thanks are also due to Dr. J. Gallivan, Dr. W. Männer, Dr. W. Ochs, Dr. F. Wagner and Dr. K. Rybicki for fruitful discussions and help, especially in more theoretical matters.

My special thanks go to Mrs. C. Ponting who not only volunteered to type this thesis, but also made many of the drawings.

Finally, thanks to all, mentioned here or not, who contributed in any way to the completion of this work.